CBCT IMAGE QUALITY ASSESSMENT TESTING CLINICALLY RELEVANT VOLUME ORIENTATION AND POSITION

Brittany L Kurzweg

A thesis submitted to the faculty at the University of North Carolina at Chapel Hill in partial fulfillment of the requirements for the degree of Masters of Science in the School of Dentistry (Oral and Maxillofacial Radiology).

Chapel Hill
2017

Approved by:

André Mol

John B. Ludlow

Marija Ivanovic

ABSTRACT

Brittany L Kurzweg: CBCT Image Quality Assessment Testing Clinically Relevant Volume Orientation and Position
(Under the direction of André Mol)

Introduction and Objectives: Some physical measures of CBCT image quality correlate well with diagnostic image quality. Traditionally, these measures have been assessed in the center in a standard orientation. The purpose of this study was to test whether measures of image quality vary as a function of test tool location, orientation and dose. The second purpose was to determine if there was an association between objective and subjective image quality.

Methods: CBCT objective image quality was assessed with one standard and three modified phantoms using five fields of view. The test tool was located at the center of the phantom (standard), at the periphery (Mod1), angled and at the center (Mod2), or angled plane and at the periphery (Mod3). Phantoms were imaged with a Carestream CS 9300 CBCT scanner (Carestream, Rochester, NY), using SDSR (180-250µm voxel/90kVp/64mAs) and LDLR (400µm voxel/85kVp/14.5mAs) for each field-of-view. Contrast-to-noise ratio (CNR) and 10% modulation transfer function (MTF) were assessed in three repeated volumes. Data were analyzed using ANOVA and Tukey's HSD. Subjective image quality was assessed with a pairwise comparison of anatomical landmarks corresponding to the test tool locations and orientations. Data were analyzed using logistic regression.

CNR differed by phantom (p<0.0001) and dose (p<0.0001) for the 8x8 and 17x11 cm FOVs. Mod3 displayed significantly greater CNR than other phantoms. Low dose protocol provided higher CNR. MTF differed only by dose (p<0.0001) for the 8x8, 17x6, and 17x11 cm FOVs. SDSR provided higher MTF. Dose protocol was statistically significant for subjective image quality. Observers preferred images with higher MTF rather than higher CNR. Mod3 was negatively associated with observer preference. The 17x6cm FOV was positively associated with observer preference.

Conclusions: CNR improved for a peripherally positioned angled test tool (Mod3). Reduced kVp and larger voxels appear to counteract the effect of reduced mAs producing improved CNR at LDLR. Thus, image quality parameters are different at the center of a CBCT volume when compared to the periphery, depend on the orientation of the object, and vary as a function of kVp and voxel size. Observers preferred images with a higher MTF rather than higher CNR.

To my husband and mentors. Thank you for all of your support along the way.

TABLE OF CONTENTS

LIST OF FIGURES ix

LIST OF TABLES xii

LIST OF ABBREVIATIONS AND SYMBOLS xiv

INTRODUCTION..... 1

METHODS AND MATERIALS AIM ONE 8

Objective Image Quality……...8

RESULTS AIM ONE.....18

CNR……...20

MTF……...30

DISCUSSION AIM ONE.....42

CNR……...42

MTF……..46

METHODS AND MATERIALS AIM TWO.....49

Subjective Image Quality (Aim Two)…..……...…...49

HUMAN SUBJECTS……...…...56

RESULTS AIM TWO.....57

DISCUSSION AIM TWO.....76

Subjective Image Quality……....76

CONCLUSION 81

APPENDIX 82

REFERENCES 170

LIST OF FIGURES

Figure 1 Design of Quart phantom....2

Figure 2 Standard Quart phantom....8

Figure 3 Quart phantom modification one (test tool in the center of the phantom and angled with respect to the axial plane)....9

Figure 4 Quart phantom modification two (test tool at the periphery and parallel to axial plane)....9

Figure 5 Quart phantom modification three (test tool at the periphery of the phantom and angled with respect to the axial plane)....10

Figure 6 Quart phantom position....11

Figure 7 CNR region of interest selection....12

Figure 8 MTF region of interest selection....13

Figure 9 Homogeneity ROI selection....14

Figure 10 Automatic software display of image quality parameters....15

Figure 11 Image quality parameter test results....15

Figure 12 Modification one Quart phantom at the 8 x 8 cm FOV, SDSR, prior to reorientation....16

Figure 13 Modification one Quart phantom at the 8 x 8 cm FOV, SDSR, after reorientation....17

Figure 14 CNR of each phantom and dose protocol at the 8 x 8 cm FOV....21

Figure 15 CNR of each phantom and dose protocol at the 10 x 5 cm FOV....22

Figure 16 CNR of each phantom and dose protocol at the 10 x 10 cm FOV....23

Figure 17 CNR of each phantom and dose protocol at the 17 x 6 cm FOV....24

Figure 18 CNR of each phantom and dose protocol at the 17 x 11 cm FOV....25

Figure 19 MTF 10% of each phantom and dose protocol at the 8 x 8 cm FOV....33

Figure 20 MTF 10% of each phantom and dose protocol at the 10 x 5 cm FOV....34

Figure 21 MTF 10% of each phantom and dose protocol at the 10 x 10 cm FOV.....35

Figure 22 MTF 10% of each phantom and dose protocol at the 17 x 6 cm FOV.....36

Figure 23 MTF 10% of each phantom and dose protocol at the 17 x 11 cm FOV.....37

Figure 24 RANDO phantom.....51

Figure 25 Hard palate in the coronal view simulating the test tool location and orientation of the standard Quart phantom at the 17 x 11 cm FOV, SDSR.....52

Figure 26 Hard palate in the sagittal view simulating the test tool location and orientation of the Mod1 Quart phantom at the 17 x 11 cm FOV, SDSR.....53

Figure 27 Lateral pterygoid plate in the axial view simulating the test tool location and orientation of the Mod2 Quart phantom at the 17 x 11 cm FOV, SDSR.....53

Figure 28 Mental foramen in the coronal view simulating the test tool location and orientation of the Mod3 Quart phantom at the 17 x 11 cm FOV, SDSR.....54

Figure 29 Sum preference scores of both observers for each phantom at the 8 x 8 cm FOV.....61

Figure 30 Sum preference scores of both observers for each phantom at the 10 x 5 cm FOV.....62

Figure 31 Sum preference scores of both observers for each phantom at the 10 x 10 cm FOV.....63

Figure 32 Sum preference scores of both observers for each phantom at the 17 x 6 cm FOV.....64

Figure 33 Sum preference scores of both observers for each phantom at the 17 x 11 cm FOV.....65

Figure 34 CNR image quality scores at each FOV.....68

Figure 35 CNR image quality scores of phantom and dose protocol.....69

Figure 36 MTF image quality score at each FOV.....71

Figure 37 MTF image quality score of phantom and dose protocol.....72

Figure 38 Phantom and agreement distribution.....75

Figure 39 FOV and agreement distribution per phantom.....77

LIST OF TABLES

Table 1 Dose protocols per FOV for all phantoms.....18

Table 2 Data summary. SDSR and LDLR refer to the protocols.....19

Table 3 Mean CNR, standard error (SE) and 95% confidence intervals (CIs) for each phantom and dose setting at the 8 x 8 cm FOV.....26

Table 4 *p* values, difference in means, and 95% CIs for statistically significant interactions between phantoms and dose at the 8 x 8 cm FOV…..…..26

Table 5 Mean CNR, SE and 95% CIs for each phantom and dose setting at the 17 x 11 cm FOV……..27

Table 6 *p* values, difference in means, and 95% CIs for statistically significant interactions between phantoms and dose at the 17 x 11 cm FOV…….28

Table 7 Mean CNR values for three FOVS at SDSR and LDLR regardless of phantom type……....29

Table 8 Mean CNR values for the phantoms at three FOVs without dose taken into account, SE, and CIs…….29

Table 9 *p* values, difference in means, and 95% CIs for statistically significant interactions between phantoms regardless of dose at three FOVs……....30

Table 10 Mean MTF values and standard deviations (SD) for each dose protocol, phantom modifications and field of view…….……..…30

Table 11 Mean MTF, SE and 95% CIs for each phantom and dose setting at the 8 x 8 cm FOV…….37

Table 12 *p* values, difference in mean MTF value, and 95% CIs for interactions between phantoms and dose at the 8 x 8 cm FOV……...38

Table 13 Mean MTF, SE, and 95% CI for each phantom and dose setting at the 17 x 6 cm FOV……..39

Table 14 *p* values, difference in mean MTF, and 95% CIs for interactions between phantoms and dose at the 17 x 6 cm FOV…….……...39

Table 15 Mean MTF, SE, and 95% CIs for each phantom and dose setting at the 17 x 11 cm FOV…….……...40

Table 16 *p* values, difference in mean MTF, and 95% CIs for interactions between phantoms and dose at the 17 x 11 cm FOV…….40

Table 17 Mean MTF values for two FOVS SDSR and LDLR regardless of phantom type……....41

Table 18 Coding system for the RANDO phantom observer sessions…….54

Table 19 Coding sequence for pairwise comparison……....54

Table 20 Summary of observer preference score, CNR score, MTF score…….…….57

Table 21 Highest three scores for combined observer preferences…….…….58

Table 22 Lowest three scores for combined observer preferences…….……..64

Table 23 Phantom, FOV, and dose estimates as predictors of observer preference..….....64

Table 24 Prediction of observer preference.....64

Table 25 CNR influence on observer preference.....65

Table 26 MTF influence on observer preference.....68

Table 27 Stepwise selection method analysis effects eligible for entry.....71

Table 28 Summary of stepwise selection method.....71

Table 29 Stepwise analysis of effects.....72

Table 30 Phantom as a predictor of observer agreement.....72

Table 31 Number of agreement/disagreement between observers.....73

Table 32 FOV as a predictor of agreement.....74

LIST OF ABBREVIATIONS AND SYMBOLS

CBCT	Cone-beam computed tomography
QA	Quality assurance
ALARA	As low as reasonably achievable
MTF	Modulation transfer function
CNR	Contrast-to-noise ratio
FOV	Field of view
kV	Kilo-voltage
kVp	Kilo-voltage-potential
Stand	Standard (Quart phantom)
Mod1/M1	Modification One (of the Quart phantom)
Mod2/M2	Modification Two (of the Quart phantom)
Mod3/M3	Modification Three (of the Quart phantom)
CI/CL	Confidence interval/Confidence level
SE/SD	Standard error/Standard deviation
FPD	Flat panel detector
cm	centimeter
ROI/ROIs	Region(s) of interest
QUART	Quality assurance in radiographic technologies
PDF	Portable document format
JPG/JPEG	Joint photographic experts group
ANOVA	Analysis of variance
SDSR	Standard dose standard resolution

LDLR	Low dose low resolution
DIN	Deutsches Institut für Normang' – (German regulations)
mA	Milliampere
DVTec	Test phantom for digital 3D X-ray (In german it is Prüfkorper für Digitales 3d-Rontgen
mAs	Milliampere-seconds
CS	Care Stream
PMMA	Polymethylmethacrylate
DICOM	Digital imaging and communications in Medicine
PVC	Polyvinyl Chloride

INTRODUCTION AND OBJECTIVES

Some physical measures of image quality have been shown to correlate well with diagnostic image quality. Traditionally, these objective measures have been assessed in the center of the volume in a standard orientation. The design of cone beam computed tomography (CBCT) scanners may result in altered quality of the peripheral aspect of the volume compared to the central aspect. Also, the orientation of structures relative to the scanning direction may impact image quality. Volumes are frequently reoriented in order to make orthogonal sections to best display anatomy of interest. The first purpose of this study was to test whether objective measures of image quality vary as a function of test tool location, test tool orientation, and dose. The test tool is also referred to as a test object and is located inside an image quality phantom. The phantom is made of polymethylmethacrylate (PMMA) surrounding the test tool and is 16 cm in width. The test tool consists of two discs which are 2 cm thick for a total of 4 cm (Figure 1).The tissue equivalents that the test tool simulates provide easily reproducible densities with which to measure contrast and noise [1]. The second purpose of this study was to test whether objective image quality correlates with subjective image quality.

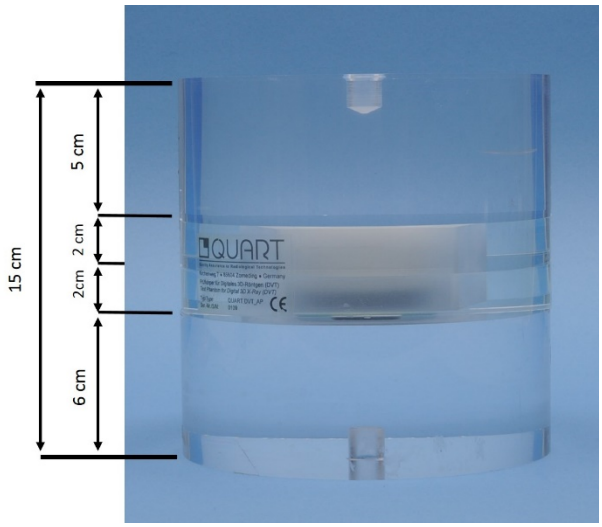

Figure 1: Design of Quart phantom

Cone beam computed tomography is a type of three-dimensional imaging technology. Indications for use of CBCT are broad and include, but are not limited to diagnosis and treatment planning in oral surgery, trauma, TMJ, orthodontics, pathology, implants, and forensic dentistry [2-4]. The use and availability of CBCT has increased since its introduction to the market nearly two decades ago [5, 6] . CBCT has been shown to improve diagnosis and treatment planning when compared with conventional two-dimensional radiographs for certain diagnostic tasks; however, the effective dose is usually higher than for two-dimensional transmission radiographs [7]. Effective dose varies significantly between fields of view, kVp and mAs selection, and CBCT units. Effective dose can also vary within CBCT units [8]. While data is available regarding effective dose of CBCT in the head and neck region, there is limited information on how radiation dose relates to image quality of CBCT [9-11].

Quality assurance (QA) programs are designed to produce images of high diagnostic quality and follow the ALARA (As Low As Reasonably Achievable) principle [12]. Image quality assessment by standardized and clinically relevant methods is important in a quality assurance program to keep radiation doses low while maintaining optimal image quality [13].

The purpose of a quality assurance phantom is to assess image quality objectively, quantitatively, and reproducibly. QA phantoms are useful because they measure image quality control parameters, allow for standardization, and devices can be compared [6]. QA programs measure image quality parameters. The image quality parameters for CBCT relevant to this study include spatial resolution, contrast resolution, homogeneity, noise and contrast-to-noise ratio (CNR) [13-15].

Spatial resolution is the ability to distinguish between two adjacent structures as they become smaller and closer together. This is measured by various units, including the Nyquist frequency and the modulation transfer function (MTF). Spatial resolution is sometimes referred to as sharpness or as the amount of detail the image depicts[16]. Nyquist frequency is a sampling frequency which represents the limit of spatial resolution [17]. The modulation transfer function measures the accuracy of an image compared to the original object using a scale of 0.0–1.0 [18]. The measurement can vary depending upon the size of the object and is sometimes referred to as the fidelity or trueness of the image. A value of 1.0 is a perfectly recorded image while a value of 0.0 means there is no signal and therefore no image [19]. The MTF curve shows the relationship between spatial frequency and contrast transfer. The higher the MTF curve at a specific spatial frequency, the higher the spatial resolution (Fig 7). MTF is commonly reported as MTF 10% or MTF 50%, which both refer to perceived sharpness. For example, if an image correctly rendered alternating black and white stripes exactly as they are in an object, the MTF would be 100%. As the black and white stripes get closer together, the contrast would decrease progressively. Eventually, the edges of the black and white stripes would blend into each other. MTF 50% refers to the frequency reached when the contrast has decreased by 50%. MTF 10% is used in

this study because this better corresponds to the clinical resolution and is where the line pairs visually become indistinguishable.

Contrast in a digital image is the difference between shades of gray. Contrast resolution is the ability of an imaging modality to record and display differences in x-ray attenuation. Contrast is necessary for tissue differentiation as anatomical structures of interest can only be visualized when sufficiently large differences in image intensities exist. The higher the contrast, the more differentiation between structures and the lower the contrast, the less differentiation. The level of desired contrast can vary depending upon the diagnostic task. For example, caries detection usually requires a high level of contrast (fewer shades of gray or short gray scale or a larger difference between dark and light structures) and detection of periodontal disease requires a low level of contrast (more shades of gray or long gray scale or a smaller difference between the dark and light structures). Caries detection is a high contrast diagnostic task due to the different attenuation characteristics of enamel (high attenuation) and decalcified or carious tissue (low attenuation) [20, 21]. Periodontal disease shows less change in attenuation characteristics and there is less differentiation between the attenuation characteristics of the tissues [22, 23]. A higher contrast image will have more tissue differentiation while a low contrast image will have less tissue differentiation. The primary controlling factor for contrast on the x-ray generator is kilovoltage potential (kVp). Higher kVp settings within the range of kVps used for dental diagnostic imaging result in a decrease in the differential attenuation between the various tissues and thus lowers contrast [17]. In addition, x-ray production efficiency is increased at higher kVp settings, which requires a reduction in mAs to maintain the exposure to the receptor. [24]. A second important factor determining contrast resolution is the receptor. Variations in the ability of a receptor to record differences in photon count impact image contrast. Finally, image

processing algorithms of the reconstructed image data applied prior to the display also have a profound effect on image contrast.

Another important factor affecting image quality is image noise. Noise can be defined as variations in image intensities that are not related to the object being imaged. Potential sources of noise are the x-ray source (quantum noise), the receptor, and the electronics involved in generating the image. Quantum noise can be minimized by using higher milliamperage-seconds (mAs), which would increase the amount of photons reaching the receptor. Noise generated by the receptor and imaging system is generally inherent to the system and cannot be changed by the operator[25]. Noise is directly measured and used to calculate the CNR. Each CBCT unit's settings, and reconstruction algorithms affect the image noise [26]. Scatter radiation is a main cause of decrease in contrast in a CBCT volume and scatter can be up to 15 times higher when compared to medical CT [27].

Homogeneity is a measure of the uniformity of gray levels. Theoretically, in a uniform object, gray levels should be the same in every part of the image representing the object. This does not always occur and gray levels have been shown to differ in certain quality assurance phantoms [28]. Due to a uniform gray level rarely occurring in dental imaging of human subjects with CBCT, image homogeneity was not included as a measure of image quality in this study [8].

Diagnostic quality is a clinician's ultimate interest. Using indicators of image quality that are representative of diagnostic quality are valuable for selecting exposure factors that are as low as possible while still providing reliable interpretation. Indicators of image quality are particularly valuable when they can be used to predict diagnostic accuracy. Assessing the relationship between objective measures of image quality and subjective perception of image

quality can be accomplished by comparing images acquired with systematically varied image quality parameters.

In a CBCT volume with a large field of view (FOV), a number of important anatomic landmarks are located towards the periphery of the volume. This is especially true for anatomical landmarks associated with the maxilla and the mandible where the dentoalveolar ridge forms a horseshoe shaped curve. If the FOV is smaller, the anatomy of interest may be centered in the volume, however, the volume itself is peripheral to the patient's anatomic center [29]. The quality of the image volume at the periphery may be different than the quality of the volume in the center as a result of the projection geometry, the presence of a more limited number of projections for peripheral structures, and slightly reduced photon flux [30]. Using a modified phantom where the test tool (element for measuring image quality) is shifted to the periphery could be useful for evaluating differences between image quality measurements from the standard phantom.

Images acquired with CBCT are reconstructed from raw image data [31]. The raw data consists of basis projections that are subsequently reconstructed into a volume from which other images can be derived [32]. CBCT utilizes isotropic voxels [33, 34]. Therefore, there are no constraints on measuring image quality in the original reconstruction plane (axial). Information limited to the axial planes of the primary reconstruction of the CBCT volume is of limited value to end users of the CBCT volume. Clinicians frequently utilize axial, coronal, sagittal, and oblique planes to accomplish the diagnostic task as well as reorientation of the volume to the occlusal plane (or Frankfort plane). Reconstruction is one of several factors affecting image quality. Some studies have shown that reorientation of a volume can result in inaccurate evaluation of bone dimensions in rotated teeth [35]. The effect of reformatting is important to

image quality and may have an influence on subjective perception of image quality [36]. A modified phantom where the test tool is angled with respect to the image acquisition planes could be utilized to test if reformatting does affect image quality.

Anatomy of interest is commonly located at the periphery of the volume and at an angle to the image acquisition plane [37]. A modified phantom where the test tool is angled with respect to the image acquisition plane and at the periphery could be utilized to test if reformatting affects image quality and if there are any differences between image quality measurements from the standard phantom.

The first purpose of this study was to test whether objective measures of image quality vary as a function of test tool location, test tool orientation, and dose protocol. The second purpose of this study was to test whether objective image quality correlates with subjective image quality.

AIM ONE METHODS AND MATERIALS

Objective Image Quality (Aim One)

The standard Quart phantom (Quart GmbH, Zorneding, Germany) (Figure 2) was constructed for routine quality assurance purposes with CBCT volumes. This phantom is a cylinder approximately 16 cm in diameter, 15 cm in height and consists of a test object (test tool) in the center of a polyvinyl chloride (PVC) acrylic cylinder. The test tool appears as the block of material with an open square in the center and is made of polymethylmethacrylate (PMMA), air and PVC. The cylinder and test tool simulate the attenuation characteristics of free air, soft tissue, and bone. There is a built-in positioning tool that consists of a bubble level that is important for positioning the phantom properly. The quality assurance phantom can be used to evaluate image quality for field sizes 4 x 4 cm to large FOVS.

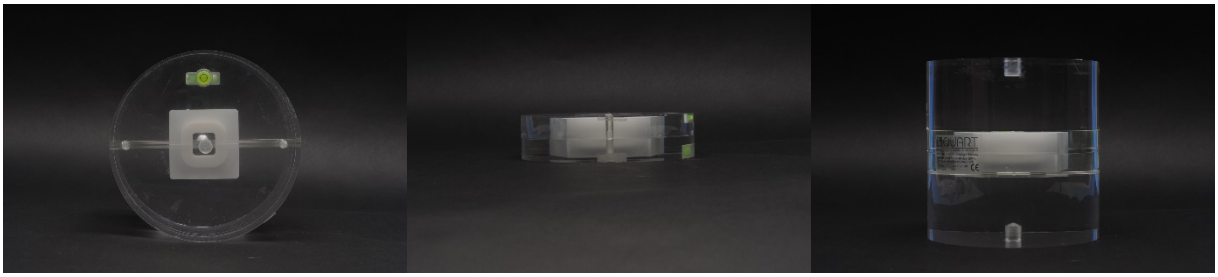

Figure 2: Standard Quart phantom. The standard Quart phantom consists of a test tool in the center of the phantom that is parallel to the axial plane.

The standard Quart phantom was compared to three modified Quart phantoms as described below. Modification one (Mod1) of the Quart phantom consisted of the test tool centered and oriented 30º to the axial plane (Figure 3). This modification was used to measure image quality parameters where the elements for measuring image quality were located at the center and angled with respect to the image acquisition plane at varying FOVs and dose protocols.

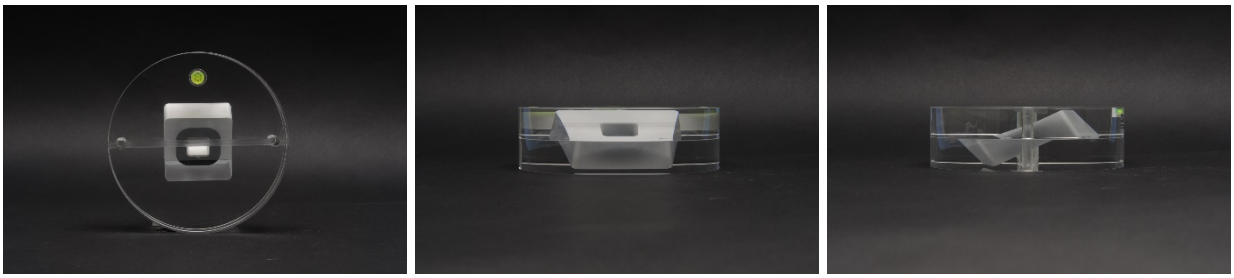

Figure 3: Quart phantom Mod1. This figure shows the test tool in the center of the phantom and angled with respect to the axial plane.

Modification two of the Quart phantom (Mod2) consisted of the test tool displaced to the periphery of the acrylic slab and parallel to the axial plane (Figure 4). This modification was utilized to measure image quality parameters where the elements for measuring image quality are at the periphery instead of the center of the phantom at varying FOVs and dose protocols.

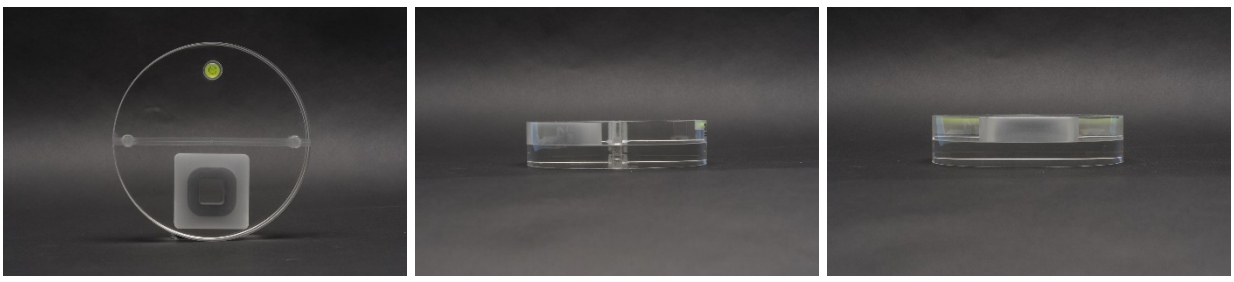

Figure 4: Quart phantom Mod2. This figure shows the test tool at the periphery of the phantom and parallel to the axial plane.

Modification three of the Quart phantom (Mod3) consisted of the test tool displaced to the periphery of the acrylic slab and oriented 30° to the axial plane (Figure 5). This modification

was used to measure image quality parameters where the elements for measuring image quality were located at the periphery instead of the center and angled with respect to the axial plane at varying FOVs and dose.

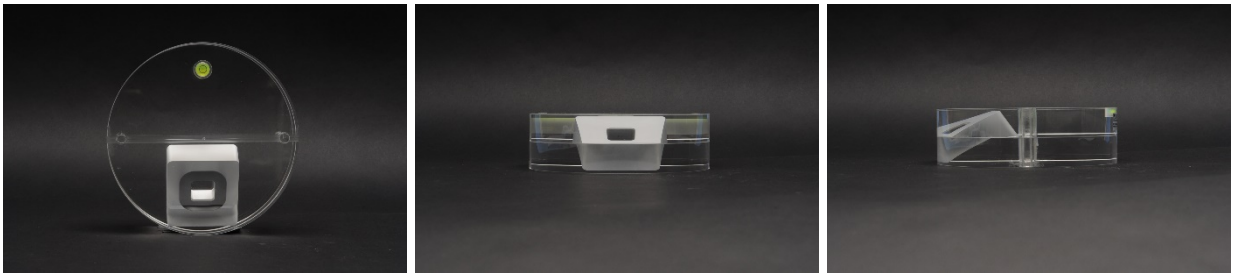

Figure 5: Quart phantom Mod3. This figure shows the central element at the periphery of the phantom and angled with respect to the axial plane.

Each modified Quart phantom was compared to the standard Quart phantom and to each other. All CBCT volumes were acquired on the Carestream (CS) 9300 CBCT unit using different FOVs. The two large FOVs used were 17 x 11 cm and 17 x 6 cm. The two medium FOVs were 10 x 10 cm and 10 x 5 cm. The one small FOV was 8 x 8 cm. The five FOVs were used because they were large enough to image the entire Quart phantom test tool. Two dose protocols were used per FOV. These included a standard acquisition mode and feather acquisition mode. The standard acquisition mode is called regular dose from the manufacturer. In this study, the regular dose mode is abbreviated standard dose, standard resolution (SDSR). The feather acquisition mode is a low dose protocol and abbreviated as low dose, low resolution (LDLR) in this study. When compared to the standard acquisition mode, the LDLR mode acquired images at about 80% lower dose for this study although it can range depending up on the CBCT unit [38]. This was due to different exposure settings. Reduction in exposure settings (kVp and mAs) while maintaining contrast and controlling noise is facilitated by increasing voxel size. However, the increase in voxel size does reduce resolution. The imaging parameters are listed in Table 1. The phantoms were positioned using the same tripod (SLK PRO 700DX) and the alignment laser

beams of the CS 9300 CBCT unit to center the phantom (Figure 6). The tripod stand had a built in leveling device in the sagittal and coronal planes. The Quart phantoms had a built in leveling device in the axial plane (bubble level). The alignment laser beams of the CS 9300 CBCT unit were used to confirm the proper position of the Quart phantoms, with the air segment of the test tool centered within the FOV. A scout image was then acquired to confirm the orientation and position of the Quart phantom before image acquisition.

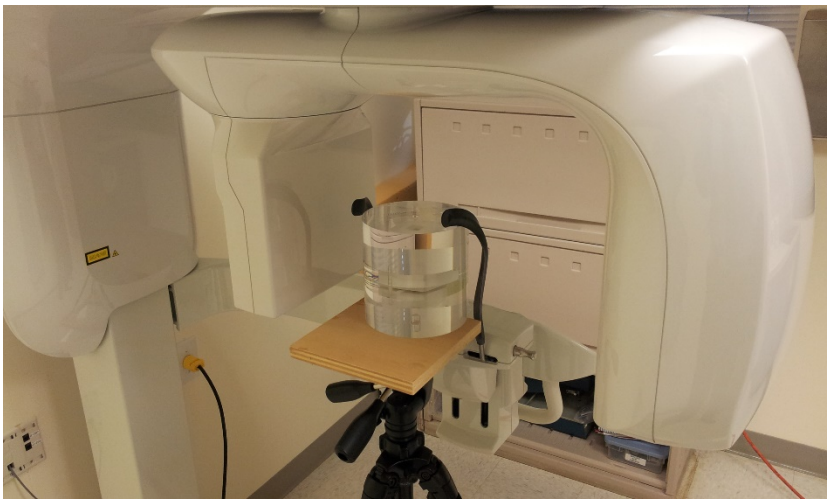

Figure 6: Quart phantom positioning. The Quart phantom will be centered in the FOV of the CS9300 CBCT unit using the positioning lights as a guide. The same tripod and platform were used for all phantoms.

Each phantom was imaged three times at each FOV and each dose protocol. The volume data were exported from the CS 9300 CBCT unit software as uncompressed digital imaging and communication in medicine (DICOM) data. The DICOM data were imported into the Quart phantom image assessment software (DVTec) for image quality parameter calculation. MTF was automatically calculated by the software from the spatial resolution test tool. Both contrast and noise were measured through the software and used to calculate the contrast-to-noise ratio (CNR) using the German Institute of Standardization (DIN) standard 868-161. All measurements were calculated using the Quart software.

Alternative (more detailed explanation of CNR calculation) In order to calculate the CNR, a rectangular region of interest (ROI) was selected between the PMMA and PVC sections of the phantom (Figure 7). The CNR was determined as the difference in mean voxel valuaes of the PMMA and PVC materials divided by the standard deviation for the PMMA material.

Alternative (more detailed explanation of MTF calculation) First, a rectangular region of interest (ROI) was selected for postprocessing of the voxels with dimensions parallel and perpendicular to the edge (Figure 8). The software computed a row-by-row averaging of voxel profiles parallel to the PVC-air interface to acquire the edge spread function (ESF). Using the ESF profile, the line spread function (LSF) was calculated [39]. A Fourier-transformation of the LSF was used to calculate the MTF. MTF50% and MTF10% were determined from the MTF curve, which allowed for characterizing the spatial resolution.

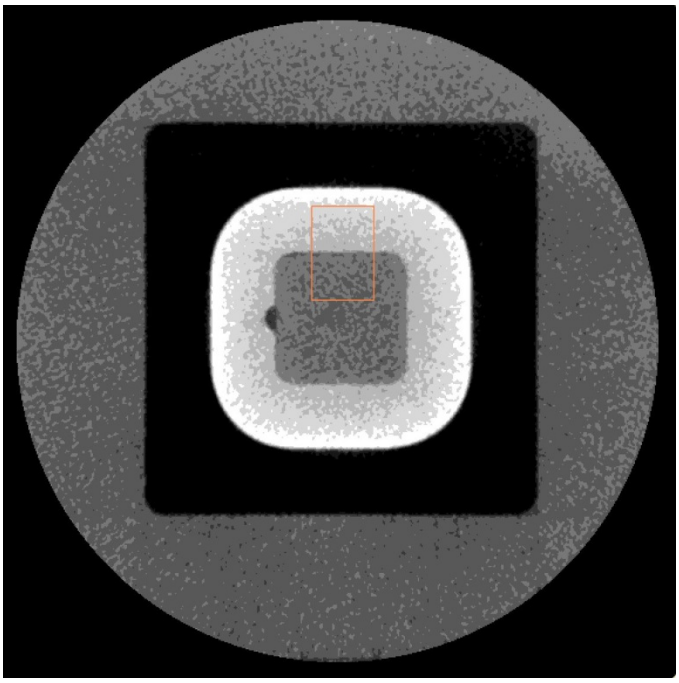

Figure 7: CNR region of interest selection

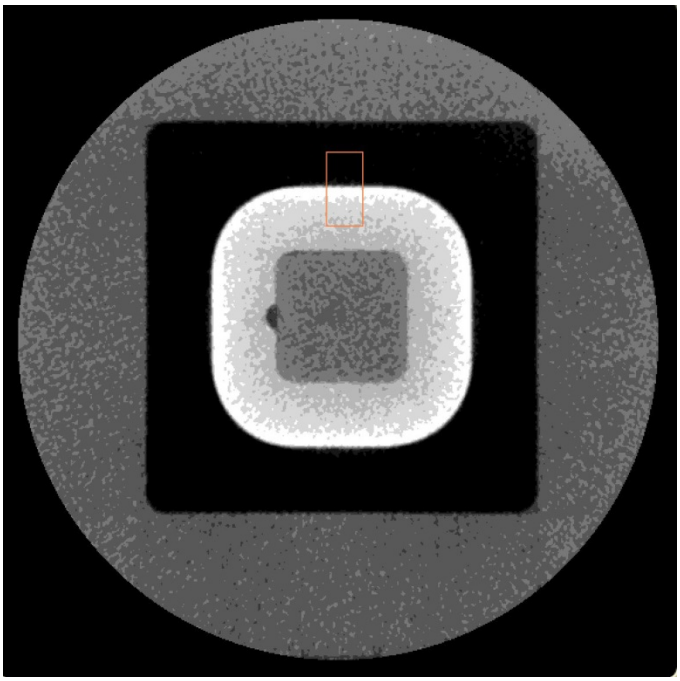

Figure 8: MTF region of interest selection

In order for the software to calculate the image quality parameters, an image slice where the open block segment of the test tool produced a range of gray levels was imported. The slice of the test tool was selected by the lowest slice (closest to the most inferior surface) that was fully visible within the software for standardization of slice selection. All possible regions of interest (ROIs) were automatically displayed and could be manually adjusted. The ROI was defined by manually clicking and drawing a square or rectangle over the test tool within the loaded slice selection. The test result for Nyquist Frequency, contrast, noise, contrast-to-noise ratio, modulation transfer function 10%, and modulation transfer function 50% were automatically displayed. An example is shown in Figure 10. The homogeneity test was completed by selecting a second test slice that consisted only of the acrylic cylinder (Figure 9). The software automatically selected five ROIs and automatically calculated the parameter. The test results were previewed and printed in Adobe PDF files (Figure 11). This evaluation process was performed three times for each volume for a total of nine evaluations per FOV and dose

protocol. Two researchers performed the analysis and recorded the data on an excel spreadsheet. The researchers were standardized for slice selection, ROI selection, and there were no significant differences in the researcher's calculations. Each data point was cross-checked for each researcher and Adobe PDF file of the test result to ensure accuracy and reliability of data recording.

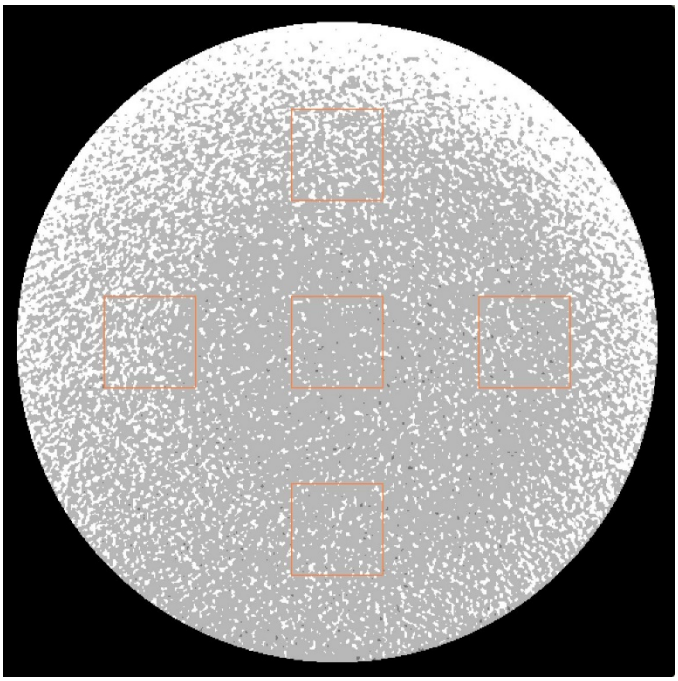

Figure 9: Homogeneity ROI selection

Parameter	Tol.	1	2	3
Dose	-	???	???	???
Acceptance Indicator		0.000	0.000	0.000
PMMA Voxel		988.972	988.972	988.972
PMMA Noise		75.385	75.385	75.385
Homogeneity	>5	24	25	25
Contrast		661.981	673.463	670.333
CNR	20%	9.478	9.621	9.599
MTF 10%	>1	1.218	1.193	1.252
MTF 50%		0.604	0.596	0.610
Nyquist Frequency	5%	2.750	2.750	2.750

Figure 10: Automatic software display of image quality parameters.

Test results

Test variable	Tol.	1	2	3	4	5	Average
Acceptance Indicatator		0.000	0.000	0.000			0.000
Homogeneity	>5	24	25	25			24.667
CNR	20%	9.478	9.621	9.599			9.566
$V_{10\%}$ [LP/mm]	>1	1.218	1.193	1.252			1.221
$V_{50\%}$ [LP/mm]		0.604	0.596	0.610			0.603
Nyquistfrequency	5%	2.750	2.750	2.750			2.750

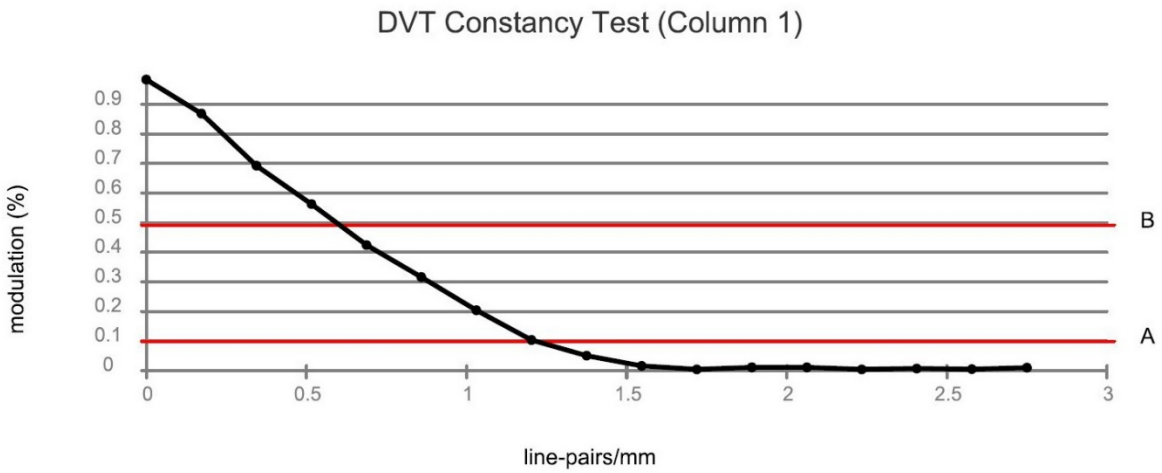

Figure 11: Image quality parameter test results in PDF format.

Mod1 and Mod3 volumes needed to be reoriented so that the test tool was in the axial plane before Quart DVTec image analysis. Dolphin Imaging Version 11.8.06.22 Premium was used to reorient the volumes without any loss of image quality. Figure 12 shows an example of modification one at the 8 x 8 cm FOV, SDSR prior to reorientation. Figure 13 shows modification one at the 8 x 8 cm FOV, SDSR after reorientation.

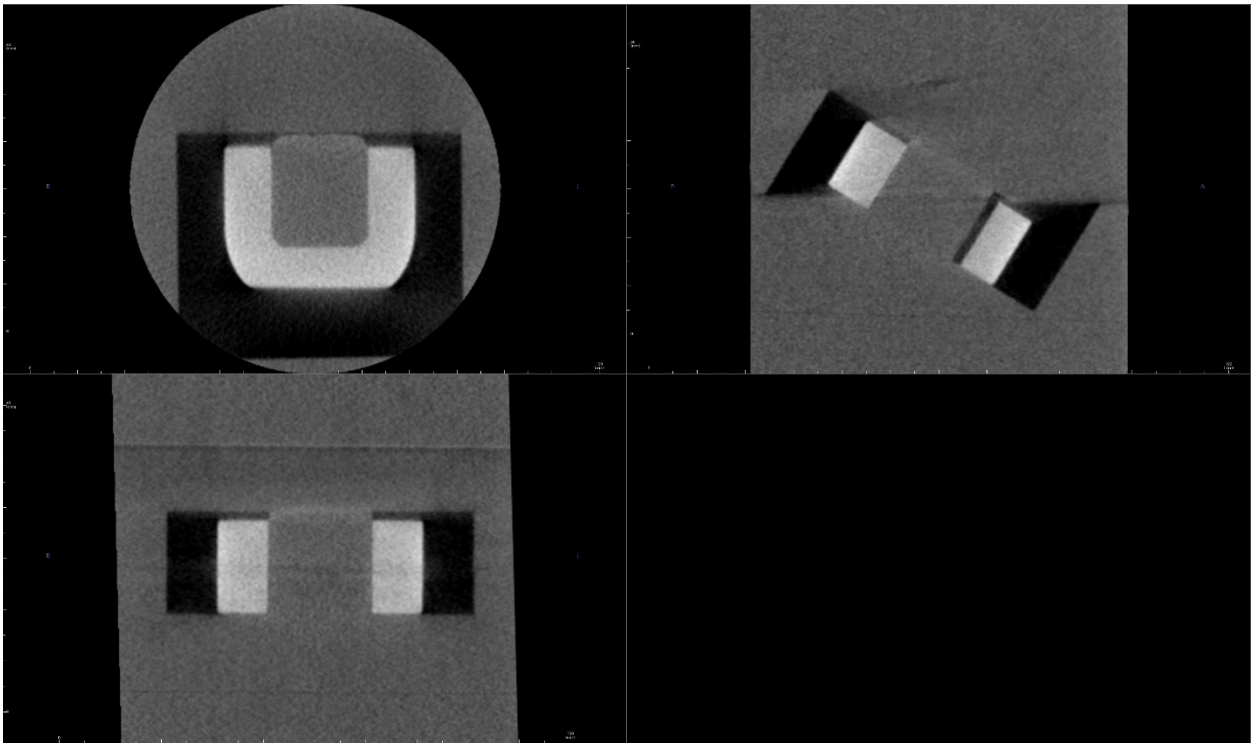

Figure 12: Mod1 Quart phantom at the 8 x 8cm FOV, SDSR prior to reorientation

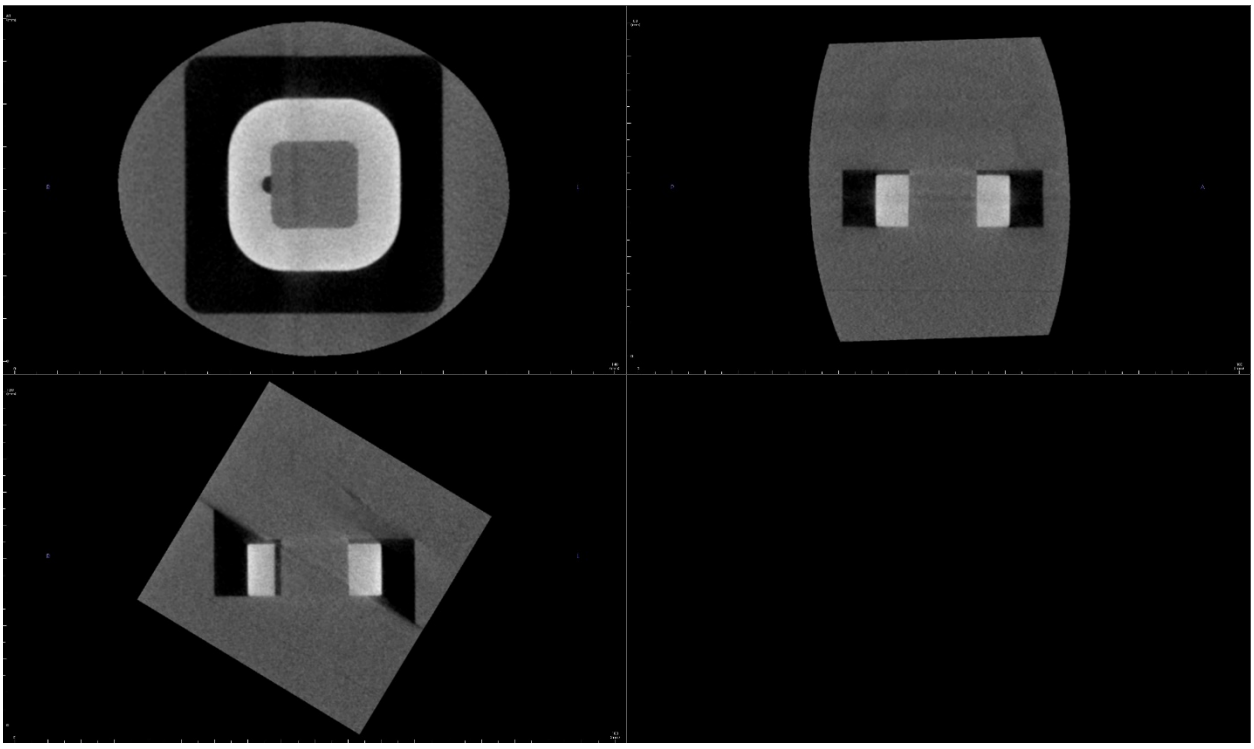

Figure 13: Mod1 phantom at the 8 x 8 cm FOV, SDSR after reorientation

Statistical analysis consisted of analysis of variance (ANOVA) for aim one, assessing the relationship between image quality parameters and image quality phantoms, in order to determine if any significant differences existed between the MTF and CNR at the five different FOVs and two dose protocols both within and between the Quart phantoms. MTF and CNR were chosen to represent the image quality measures because they encompass spatial resolution, contrast, and noise for the calculations. ANOVA was considered for aim one because the data structure was mixed, the explanatory variables were nominal, and the outcome variables were continuous and predicted to be normally distributed.

RESULTS AIM ONE

Objective measures of image quality were recorded and analyzed for each phantom, FOV, and dose protocol. The mean CNR, MTF, and standard deviations (SD) are summarized in Table 1.

Table 1: Dose protocols per FOV for all phantoms

	SDSR			LDLR		
FOV (cm)	Voxel Size (µm)	kVp	mAs	Voxel Size (µm)	kVp	mAs
8x8	180	90	64	400	85	14.8
10x5	180	90	64	400	85	14.8
10x10	180	90	64	400	85	14.8
17x6	200	90	50.4	400	85	14.8
17x11	250	85	64.9	400	85	12

Table 2: Data summary. SDSR and LDLR refer to the dose protocols.

Stand	SDSR		LDLR		SDSR		LDLR	
FOV (cm)	CNR Mean	SD	CNR Mean	SD	MTF Mean	SD	MTF Mean	SD
8x8	9.9	0.324	15.5	0.342	1.20	0.022	1.06	0.005
10x5	8.8	0.015	14.0	0.089	1.26	0.005	0.93	0.022
10x10	9.4	0.144	14.2	0.008	1.31	0.018	1.19	0.042
17x6	8.7	0.085	15.2	0.666	1.27	0.017	1.04	0.018
17x11	4.8	0.014	12.3	0.164	1.46	0.012	1.05	0.063
Mod1	SDSR		LDLR		SDSR		LDLR	
FOV (cm)	CNR Mean	SD	CNR Mean	SD	MTF Mean	SD	MTF Mean	SD
8x8	9.8	0.203	22.6	0.203	1.25	0.022	0.93	0.008
10x5	9.3	0.178	21.3	0.911	1.29	0.011	0.94	0.013
10x10	10.6	0.134	15.6	0.089	1.27	0.016	1.10	0.039
17x6	12.2	0.194	16.9	0.782	1.16	0.009	0.80	0.006
17x11	10.9	0.104	12.0	0.223	1.28	0.012	1.13	0.033
Mod2	SDSR		LDLR		SDSR		LDLR	
FOV (cm)	CNR Mean	SD	CNR Mean	SD	MTF Mean	SD	MTF Mean	SD
8x8	8.1	0.197	24.8	1.158	1.22	0.008	0.97	0.049
10x5	12.8	0.459	19.6	0.957	1.26	0.010	0.96	0.015
10x10	12.9	0.197	20.1	2.022	1.34	0.014	1.01	0.064
17x6	13.0	0.125	16.9	0.991	1.31	0.531	1.20	0.246
17x11	12.0	0.014	15.8	0.036	1.30	0.008	1.04	0.047
Mod3	SDSR		LDLR		SDSR		LDLR	
FOV (cm)	CNR Mean	SD	CNR Mean	SD	MTF Mean	SD	MTF Mean	SD

8x8	19.9	0.084	30.9	0.333	1.27	0.010	0.91	0.004
10x5	20.4	0.582	26.6	0.111	1.36	0.002	0.90	0.010
10x10	21.7	0.153	35.8	0.296	1.53	0.020	0.87	0.003
17x6	18.8	0.831	26.3	1.444	1.44	0.017	1.08	0.032
17x11	19.7	0.653	30.5	2.947	1.45	0.018	0.99	0.014

CNR

A three-way ANOVA was conducted to determine the effects of dose protocol, phantom, and FOV on CNR. There was a statistically significant three-way interaction between dose protocol, phantom, and FOV, $p < 0.001$. Because of the three-way interaction, a two-way ANOVA was performed to assess the effect of phantom (the primary explanatory variable) and dose protocol separately for each FOV. Statistical significance was set at an alpha level of 0.05 level. There was not a statistically significant simple two-way interaction between phantom and dose for the 10 x 5 cm FOV, ($p = .1637$), or for the 10 x 10 cm FOV, ($p = .0978$), or for the 17 x 6 cm FOV($p = .6975$). There was a statistically significant simple two-way interaction between phantom and dose for the 8 x 8cm FOV ($p = .0145$), and for the 17 x 11 cm FOV ($p < .001$). Therefore, an analysis of all possible pairwise comparisons was performed using a Bonferroni correction adjustment for statistical significance. The mean CNR values for each phantom and dose protocol are illustrated for each FOV in Figures 14–18.

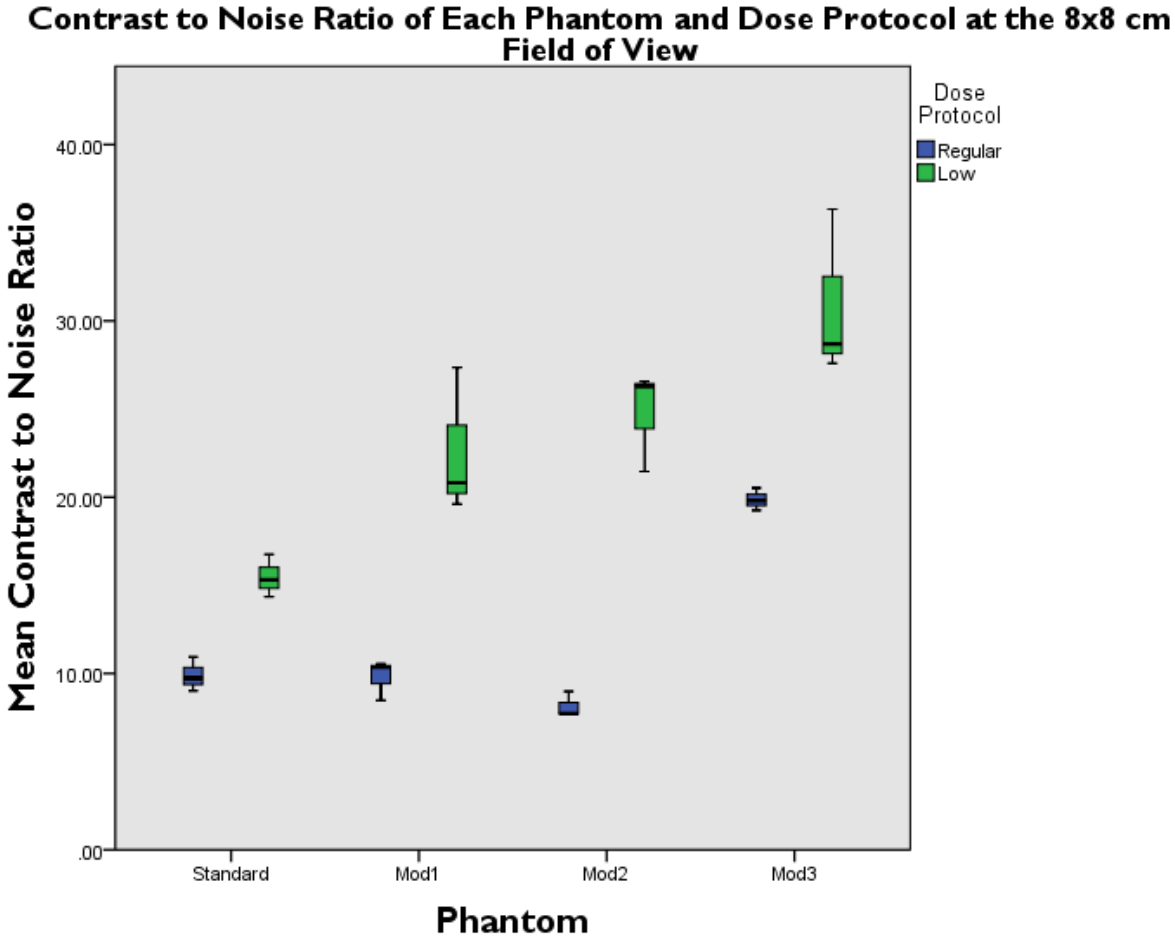

Figure 14: CNR of each phantom and dose protocol at the 8 x 8 cm FOV

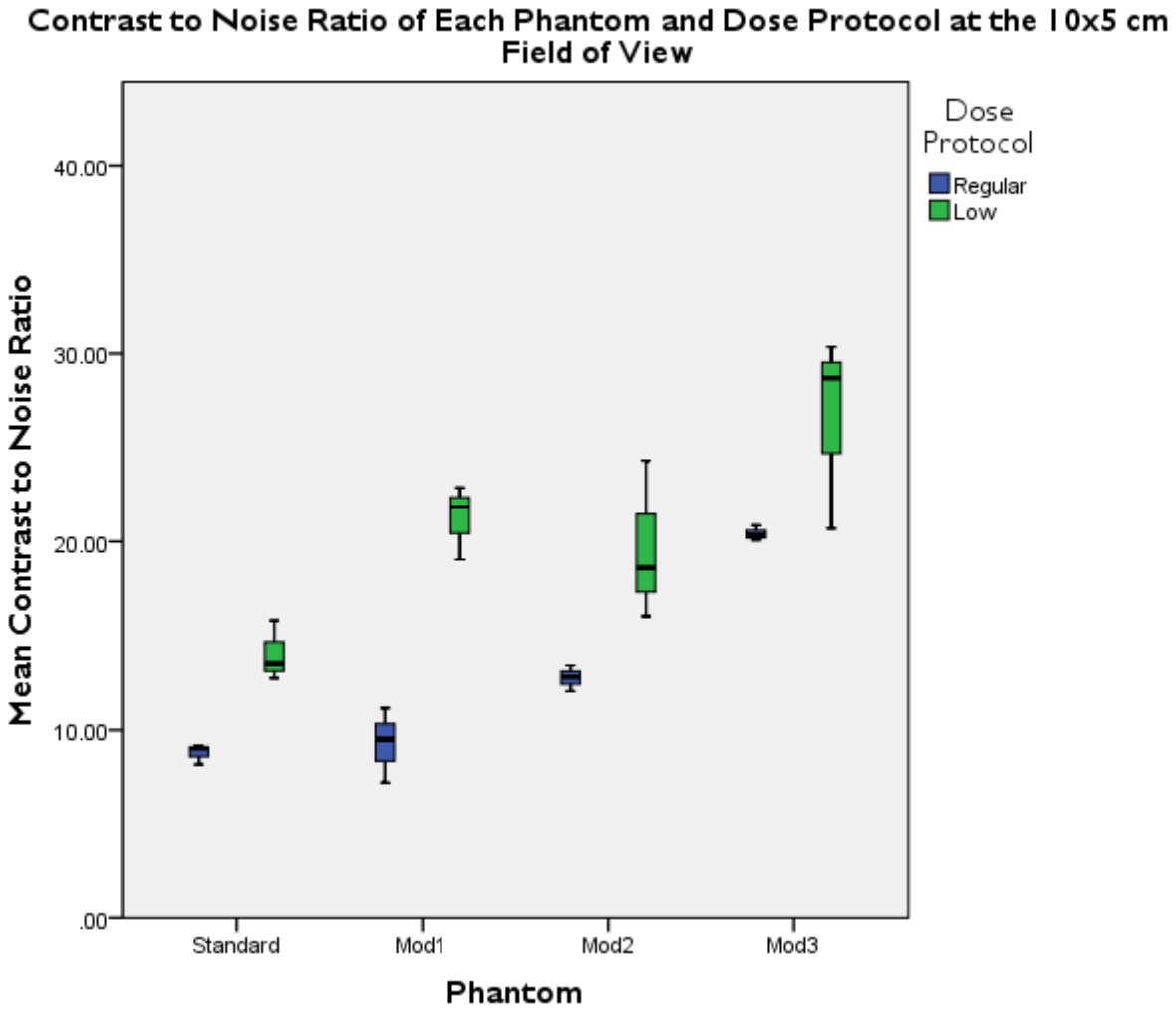

Figure 15: CNR of each phantom and dose protocol at the 10 x 5 cm FOV

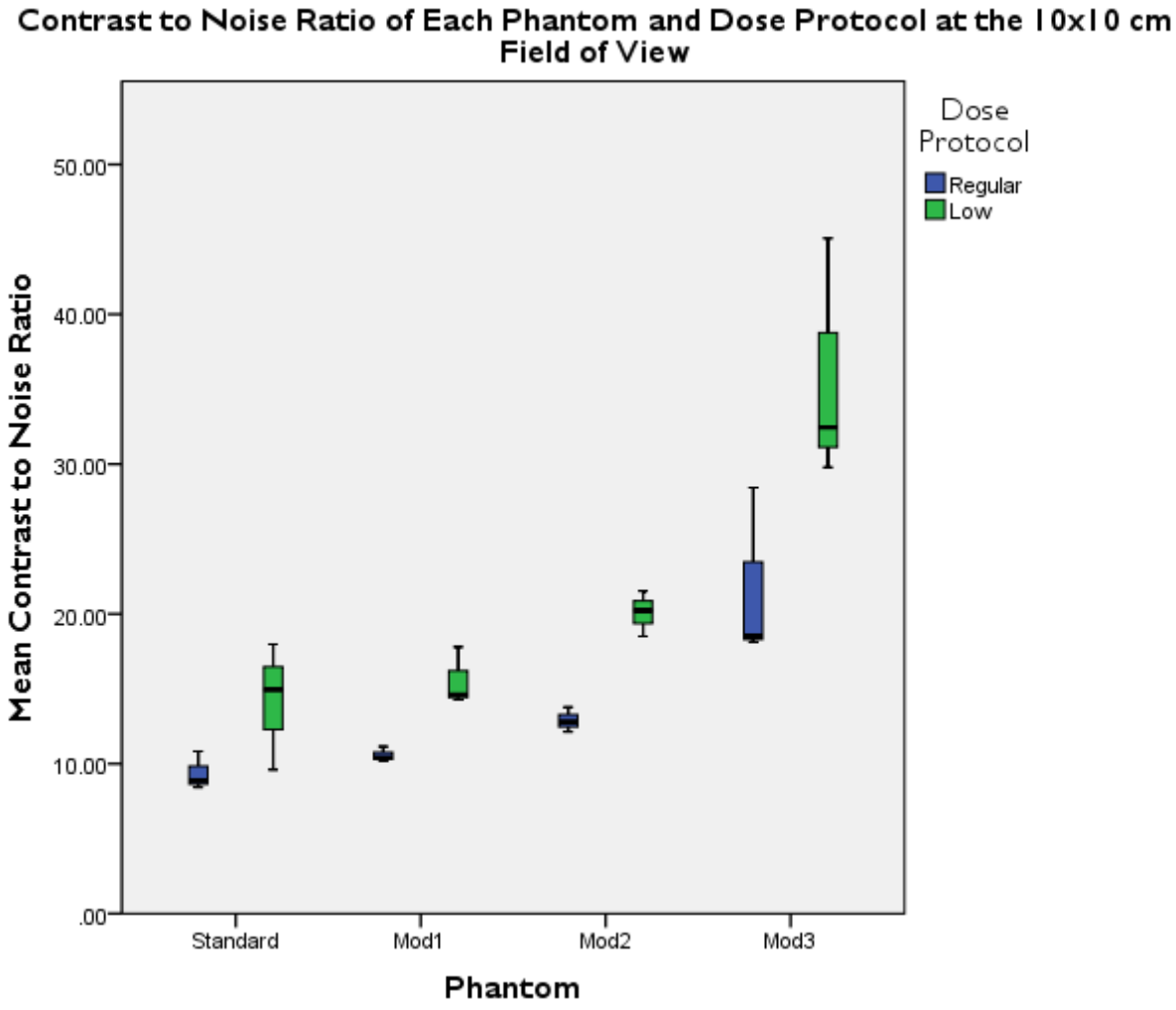

Figure 16: CNR of each phantom and dose protocol at the 10 x 10 cm FOV

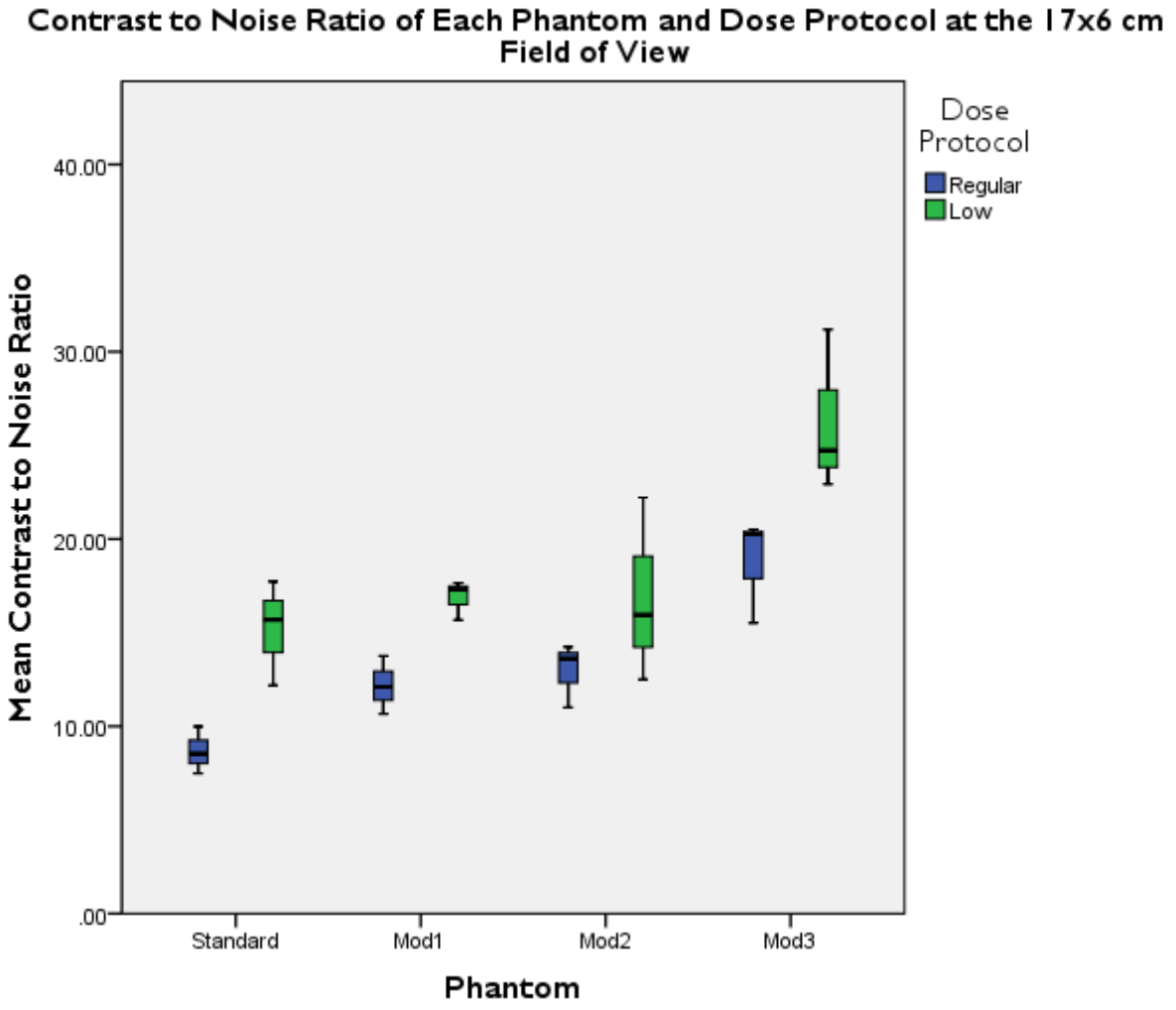

Figure 17: CNR of each phantom and dose protocol at the 17 x 6 cm FOV

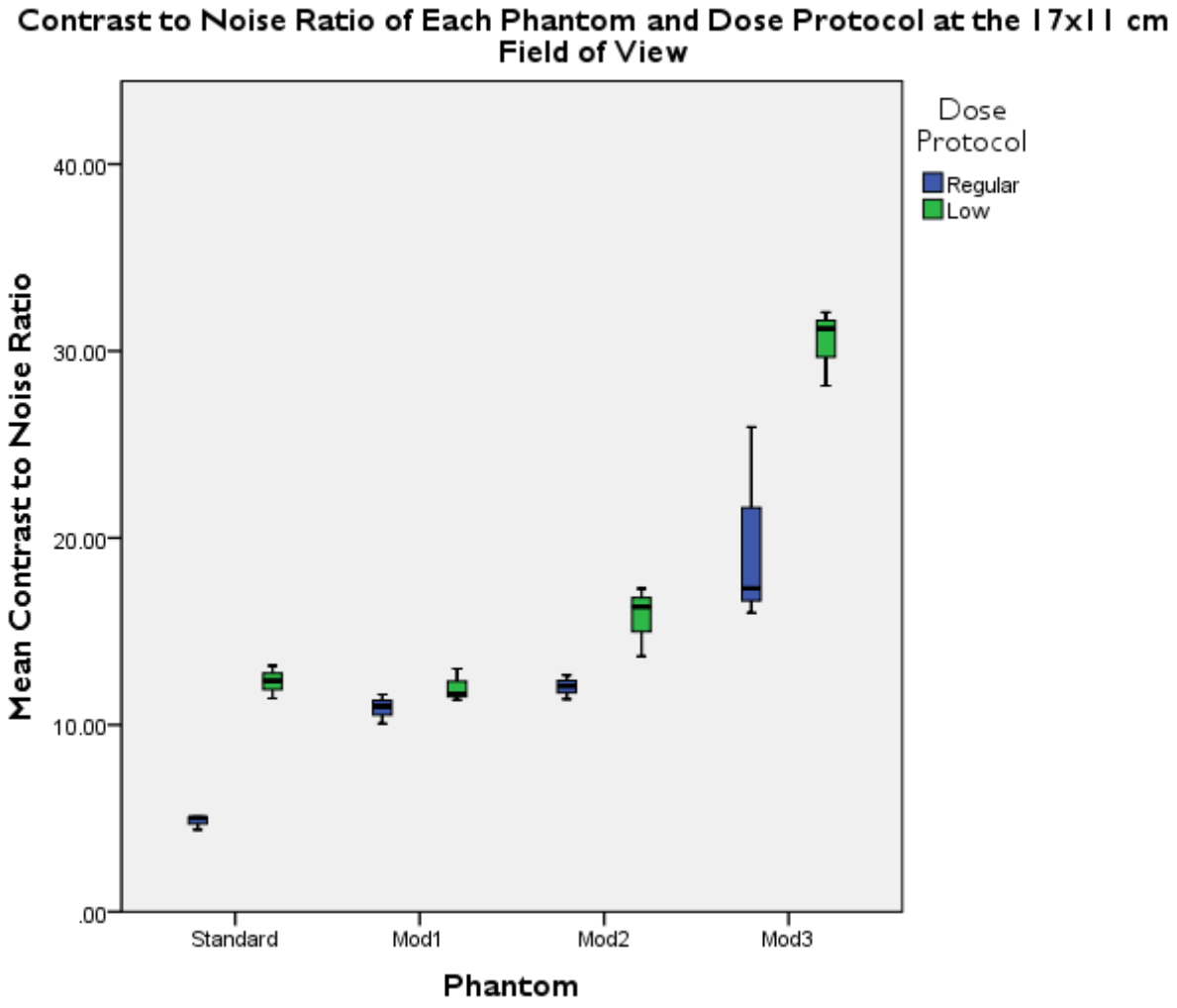

Figure 18: CNR of each phantom and dose protocol at the 17 x 11 cm FOV

At the 8 x 8cm FOV, modification three at SDSR had a statistically significantly higher mean CNR value than all other phantoms at SDSR. However, at the 8 x 8 cm FOV, modification three at SDSR had a statistically significant lower mean CNR than modification one and three phantoms at LDLR. At LDLR and the 8 x 8cm FOV, modification three phantom had a statistically significantly higher CNR than all other phantoms at SDSR or LDLR. Mean CNR values for each phantom at each dose for the 8 x 8 cm FOV are listed in Table 3.

Table 3: Mean CNR, standard error (SE) and 95% confidence intervals (CIs) for each phantom and dose setting at the 8 x 8 cm FOV

Phantom	Dose Protocol	Mean CNR	SE	CI1	CI2
Standard	SDSR	9.9	0.570	6.743	13.044
Standard	LDLR	15.5	0.324	12.321	18.623
Mod1	SDSR	9.8	0.075	6.641	12.943
Mod1	LDLR	22.6	0.203	19.444	25.745
Mod2	SDSR	8.1	0.221	4.992	11.293
Mod2	LDLR	24.8	0.197	21.629	27.930
Mod3	SDSR	19.9	0.302	16.709	23.011
Mod3	LDLR	30.9	0.084	27.727	34.028

At the 8 x 8 cm FOV, modification three at SDSR had a statistically significantly higher mean CNR value than the standard phantom at SDSR, and modification one at SDSR. The mean CNR, standard error (SE), and 95% confidence intervals (CI1 and CI2) for each phantom and dose setting at the 8 x 8 cm FOV are listed in Table 3.

At the 8 x 8 cm FOV, modification two at LDLR had a statistically significantly higher mean CNR value than the standard phantom at both SDSR and LDLR, modification one at SDSR and modification two at SDSR. At the 8 x 8 cm FOV, modification one at LDLR had a statistically significantly higher mean CNR value than modification one at SDSR and modification two at SDSR. The difference in means, confidence intervals, and the difference in the means are listed in Table 4.

Table 4: *p* values, difference in means, and 95% CIs for statistically significant interactions between phantoms and dose at the 8 x 8 cm FOV

Phantom Dose Protocol	Phantom Dose Protocol	*p* value	Difference in means	95% CI1	95% CI2
Std-Reg	M1-Low	<0.001	-12.70	-19.978	-5.424
Std-Reg	M2-Low	<0.001	-14.89	-22.163	-7.609
Std-Reg	M3-Reg	0.004	-9.97	-17.243	-2.689
Std-Reg	M3-Low	<0.001	-20.98	-28.261	-13.707
Std-Low	M2-Reg	0.0477	7.33	0.052	14.606
Std-Low	M2-Low	0.0078	-9.31	-16.584	-2.030
Std-Low	M3-Low	<0.001	-15.41	-22.683	-8.129
M1-Reg	M1-Low	0.003	-12.80	-20.079	-5.525

M1-Reg	M2-Low	<0.001	-14.99	-22.264	-7.710
M1-Reg	M3-Reg	0.0038	-10.07	-17.345	-2.791
M1-Reg	M3-Low	<0.001	-21.09	-28.362	-13.809
M1-Low	M2-Reg	<0.001	14.45	7.175	21.729
M1-Low	M3-Low	0.0201	-8.28	-15.560	-1.006
M2-Reg	M2-Low	<0.001	-16.64	-23.914	-9.360
M2-Reg	M3-Reg	<0.001	-11.72	-18.994	-4.440
M2-Reg	M3-Low	<0.001	-22.74	-30.012	-15.458
M3-Reg	M3-Low	0.0016	-11.02	-18.295	-3.741

At the 17 x 11 cm FOV, modification three at SDSR and LDLR had a statistically significantly different mean CNR value than all other phantoms at SDSR and LDLR. Additionally, at the 17 x 11 cm FOV, modification three at SDSR had a statistically significantly different mean CNR value than modification three at LDLR. Mean CNR values for each phantom at each dose for the 17 x 11 cm FOV are listed in Table 5. The difference in means, confidence intervals, and the difference in the means are listed in Table 6.

Table 5: Mean CNR, SE and 95% CIs for each phantom and dose setting at the 17 x 11 cm FOV

Phantom	Dose Protocol	Mean CNR	SE	95% CI1	95% CI2
Standard	SDSR	4.8	0.666	2.108	7.557
Standard	LDLR	12.3	0.014	9.589	15.038
Mod1	SDSR	10.9	0.782	8.175	13.624
Mod1	LDLR	12.0	0.104	9.279	14.728
Mod2	SDSR	12.0	0.991	9.312	14.761
Mod2	LDLR	15.8	0.531	13.034	18.483
Mod3	SDSR	19.7	1.444	17.019	22.468
Mod3	LDLR	30.5	0.653	27.747	33.196

Table 6: *p* values, difference in means, and 95% CIs for statistically significant interactions between phantoms and dose at the 17 x 11 cm FOV

Phantom-Dose Protocol	Phantom-Dose Protocol	*p* Value	Difference in means	95% CI1	95% CI2
Std-Reg	Std-Low	0.0143	-7.48	-13.774	-1.188
Std-Reg	M1-Low	0.0199	-7.17	-13.463	-0.878
Std-Reg	M2-Reg	0.0192	-7.20	-13.496	-0.911
Std-Reg	M2-Low	<.001	-10.93	-17.218	-4.633
Std-Reg	M3-Reg	<.001	-14.91	-21.203	-8.618
Std-Reg	M3-Low	<.001	-25.64	-31.931	-19.346
Std-Low	M3-Reg	0.0151	-7.43	-13.722	-1.137
Std-Low	M3-Low	<.001	-18.16	-24.450	-11.865
M1-Reg	M3-Reg	0.0033	-8.84	-15.137	-2.551
M1-Reg	M3-Low	<.001	-19.57	-25.865	-13.279
M1-Low	M3-Reg	0.0101	-7.74	-14.032	-1.447
M1-Low	M3-Low	<.001	-18.47	-24.760	-12.175
M2-Reg	M3-Reg	0.0112	-7.71	-14.000	-1.414
M2-Reg	M3-Low	<.001	-18.43	-24.728	-12.142
M2-Low	M3-Low	<.001	-14.71	-21.005	-8.420
M3-Reg	M3-Low	<.001	-10.73	-17.021	-4.435

All simple pairwise comparisons were run for phantom modifications regardless of phantom type and regardless of dose for the 10 x 5 cm, 10 x 10 cm and 17 x 6 cm FOVs with a Bonferroni adjustment applied. Mean CNR values for these three FOVs adjusted for phantom type are listed in Table 7. There was a statistically significant difference in CNR values between SDSR and LDLR regardless of phantom type for the 10 x 5cm FOV, ($p < 0.001$), 10 x 10 cm FOV ($p = 0.0037$), and 17 x 6 cm FOV ($p < 0.001$), with the mean CNR for LDLR was statistically significantly higher than the mean CNR for the SDSR for each FOV.

Table 7: Mean CNR values for the 10 x 5, 10 x 10, and 17 x 6 cm FOVS at SDSR and LDLR regardless of phantom type

FOV (cm)	Dose Protocol	Mean CNR
10x5	Regular	12.8
10x5	Low	20.4
10x10	SDSR	13.6
10x10	Low	21.4
17x6	SDSR	13.1
17x6	Low	18.8

Mean CNR values for these three FOVS adjusted for dose are listed in Table 8. There was a statically significant difference in mean CNR values between the phantoms regardless of dose for the 10 x 5 cm FOV ($p < 0.001$), 10x10 cm FOV ($p = 0.0089$), and the 17 x 6 cm FOV ($p < 0.001$) with the mean CNR for Mod3 being higher than the other phantom modifcations. The *p* values, difference in means, and 95% confidence intervals for statistically significant interactions between phantoms regardless of dose at the 10 x 5 cm, 10 x 10 cm and 17 x 6 cm FOVs are listed in Table 9.

Table 8: Mean CNR values for the phantoms at three FOVs without dose taken into account, SE, and CIs

Phantom	FOV (cm)	CNR Mean	SE	95% CI1	95% CI2
Standard	10x5	11.4	0.052	8.984	13.831
Mod1	10x5	15.3	0.545	12.850	17.697
Mod2	10x5	16.2	1.415	13.787	18.634
Mod3	10x5	23.5	0.347	21.073	25.920
Standard	10x10	11.8	0.076	3.438	20.114
Mod1	10x10	13.1	0.112	4.731	21.407
Mod2	10x10	16.5	1.110	18.984	35.659
Mod3	10x10	28.7	0.225	20.389	37.065
Standard	17x6	11.9	0.376	9.568	14.306
Mod1	17x6	14.5	0.488	12.162	16.900
Mod2	17x6	14.9	0.558	12.553	17.291
Mod3	17x6	22.5	1.137	20.155	24.892

Table 9: *p* values, difference in means, and 95% CIs for statistically significant interactions between phantoms regardless of dose at three FOVs

Phantom	Phantom	FOV (cm)	*p* value	Difference in means	95% CI1	95% CI2
Std	M2	10x5	0.039	-4.80	-9.408	-0.199
Std	M3	10x5	<.001	-12.09	-16.694	-7.485
M1	M3	10x5	<.001	-8.22	-12.828	-3.619
M2	M3	10x5	0.0014	-7.29	-11.891	-2.682
Std	M3	10x10	0.0334	-16.95	-32.792	-1.110
Std	M3	17x6	<.001	-10.59	-15.087	-6.086
M1	M3	17x6	<.001	-7.99	-12.493	-3.492
M2	M3	17x6	<.001	-7.60	-12.103	-3.101

At the 10 x 5 cm FOV, modification three had a statistically significantly higher mean CNR than all other phantoms, regardless of dose. Additionally, at the 10 x 5cm FOV, modification two had a statistically significantly higher mean CNR than the standard phantom, regardless of dose. At the 10 x 10 cm FOV, modification three had a statistically significantly higher mean CNR than the standard phantom, regardless of dose. At the 17 x 6 cm FOV, modification three had a statistically significantly higher mean CNR than all other phantoms, regardless of dose.

In summary, CNR significantly differed by phantom and dose protocol for the 8x8 and 17x11 cm FOV. CNR was higher on average for the LDLR and Mod3.

MTF

Table 10: Mean MTF 10% values and standard deviations (SD) for each dose protocol (SDSR and LDLR), phantom modifications and field of view.

Stand	SDSR		LDLR	
FOV (cm)	MTF Mean	SD	MTF Mean	SD
8x8	1.20	0.022	1.06	0.005
10x5	1.26	0.005	0.93	0.022
10x10	1.31	0.018	1.19	0.042

17x6	1.27	0.017	1.04	0.018
17x11	1.46	0.012	1.05	0.063
Mod1	SDSR		LDLR	
FOV (cm)	MTF Mean	SD	MTF Mean	SD
8x8	1.25	0.022	0.93	0.008
10x5	1.29	0.011	0.94	0.013
10x10	1.27	0.016	1.10	0.039
17x6	1.16	0.009	0.80	0.006
17x11	1.28	0.012	1.13	0.033
Mod2	SDSR		LDLR	
FOV (cm)	MTF Mean	SD	MTF Mean	SD
8x8	1.22	0.008	0.97	0.049
10x5	1.26	0.010	0.96	0.015
10x10	1.34	0.014	1.01	0.064
17x6	1.31	0.531	1.20	0.246
17x11	1.30	0.008	1.04	0.047
Mod3	SDSR		LDLR	
FOV (cm)	MTF Mean	SD	MTF Mean	SD
8x8	1.27	0.010	0.91	0.004
10x5	1.36	0.002	0.90	0.010
10x10	1.53	0.020	0.87	0.003
17x6	1.44	0.017	1.08	0.032
17x11	1.45	0.018	0.99	0.014

A three-way ANOVA was conducted to determine the effects of dose, phantom and FOV on modulation transfer function 10%. There was a statistically significant three-way interaction between dose protocol, phantom and FOV ($p < 0.001$). Because of the three way interaction, a two-way ANOVA was performed to assess the effect of phantom (the primary explanatory variable) and dose protocol separately for each FOV. Statistical significance was set at the $p < 0.05$ level. Mean MTF values were higher at SDSR than at LDLR for all FOVs. The mean MTF values for each phantom and dose protocol are illustrated for each FOV in Figures 19–23.

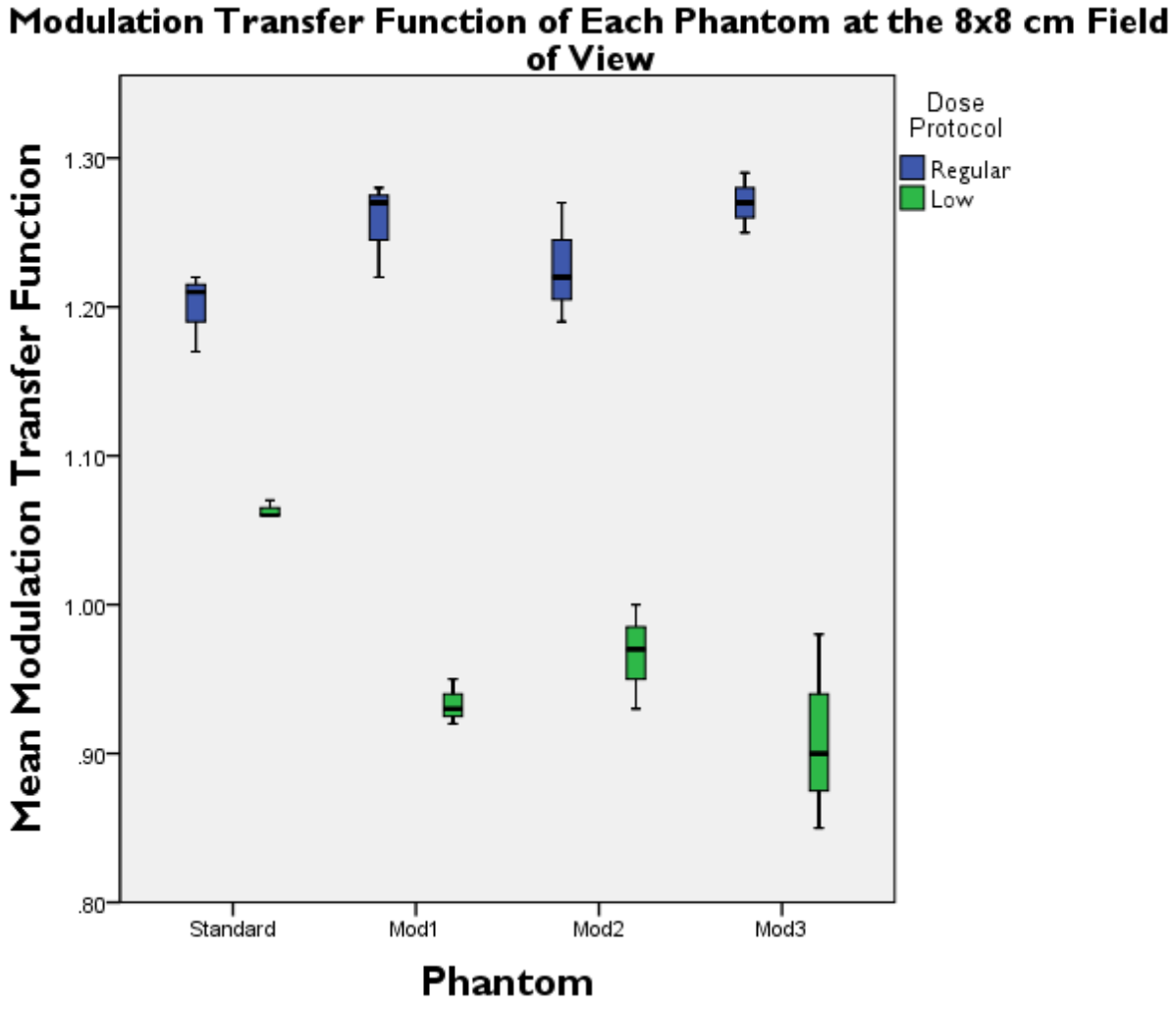

Figure 19: MTF 10% of each phantom and dose protocol at the 8 x 8 cm FOV

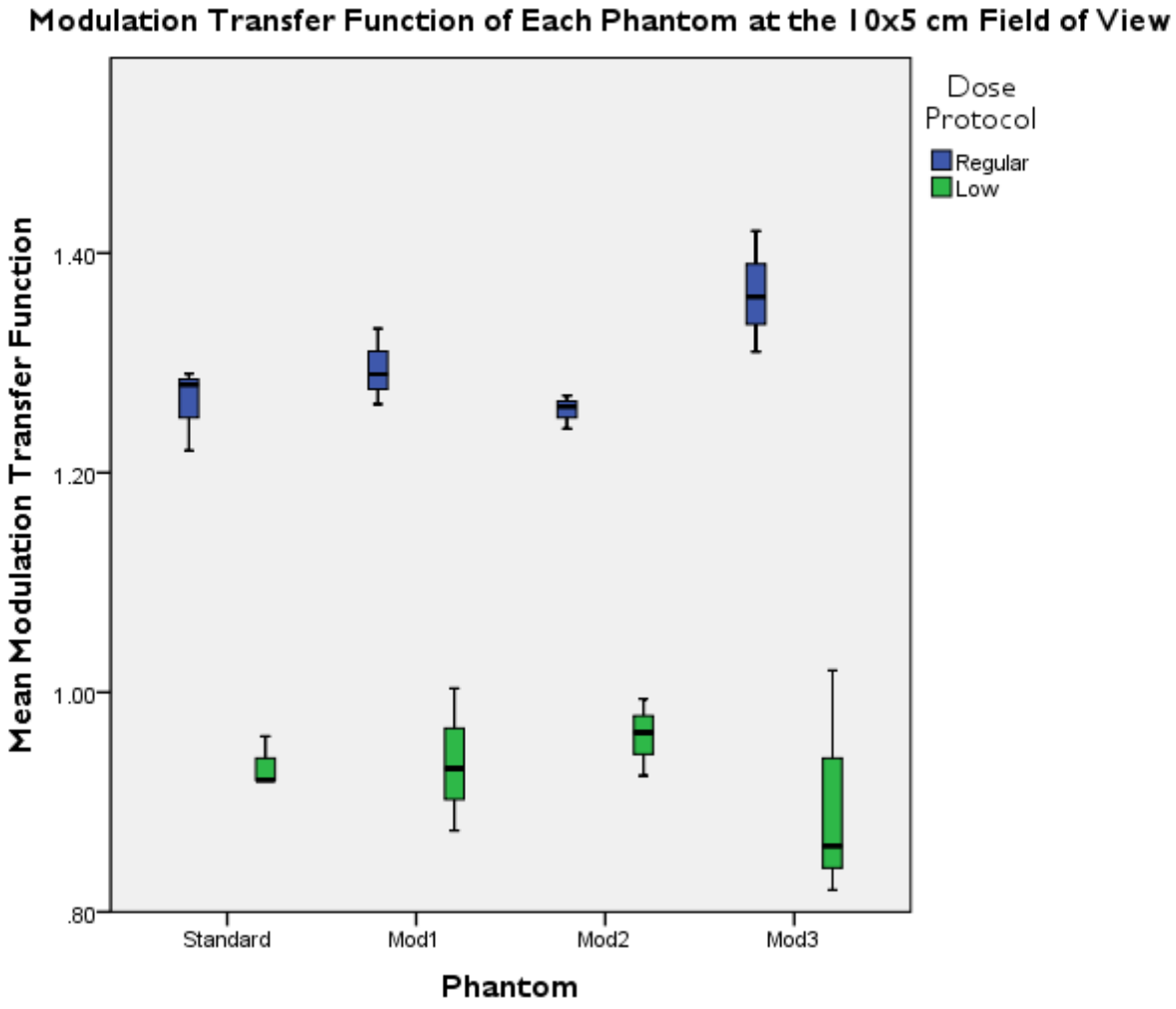

Figure 20: MTF 10% of each phantom and dose protocol at the 10 x 5 cm FOV

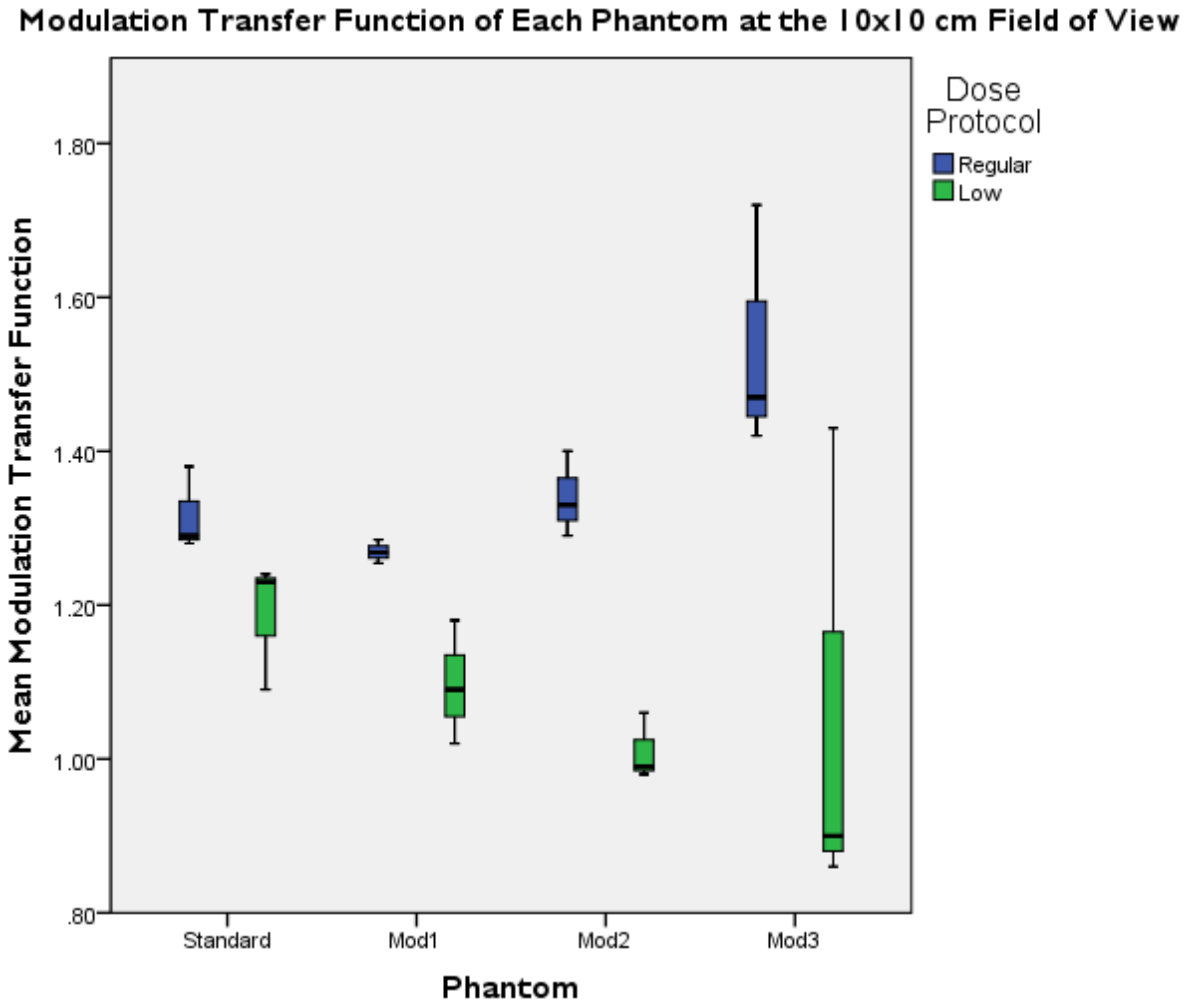

Figure 21: MTF 10% of each phantom and dose protocol at the 10 x 10 cm FOV

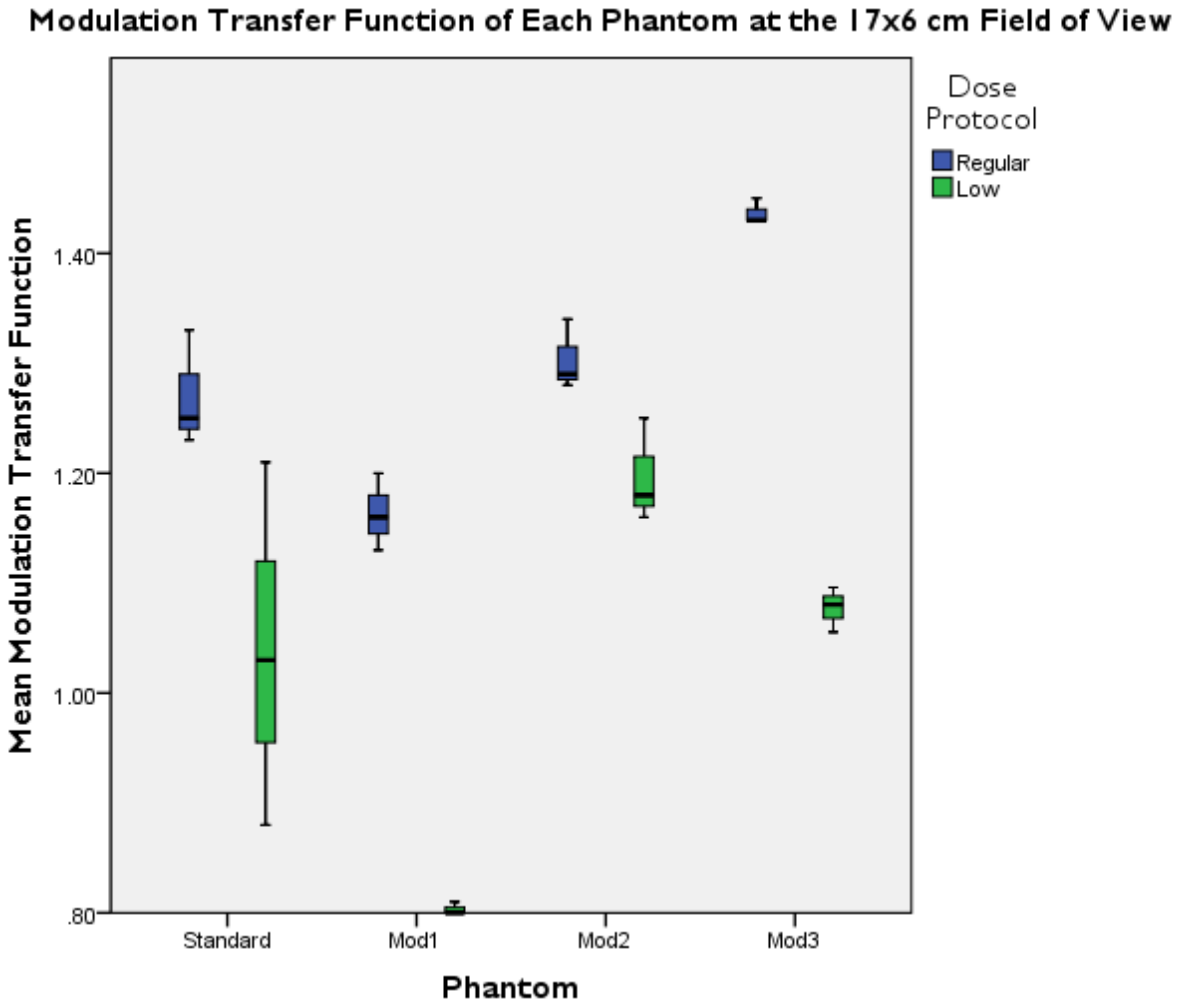

Figure 22: MTF 10% of each phantom and dose protocol at the 17 x 6 cm FOV

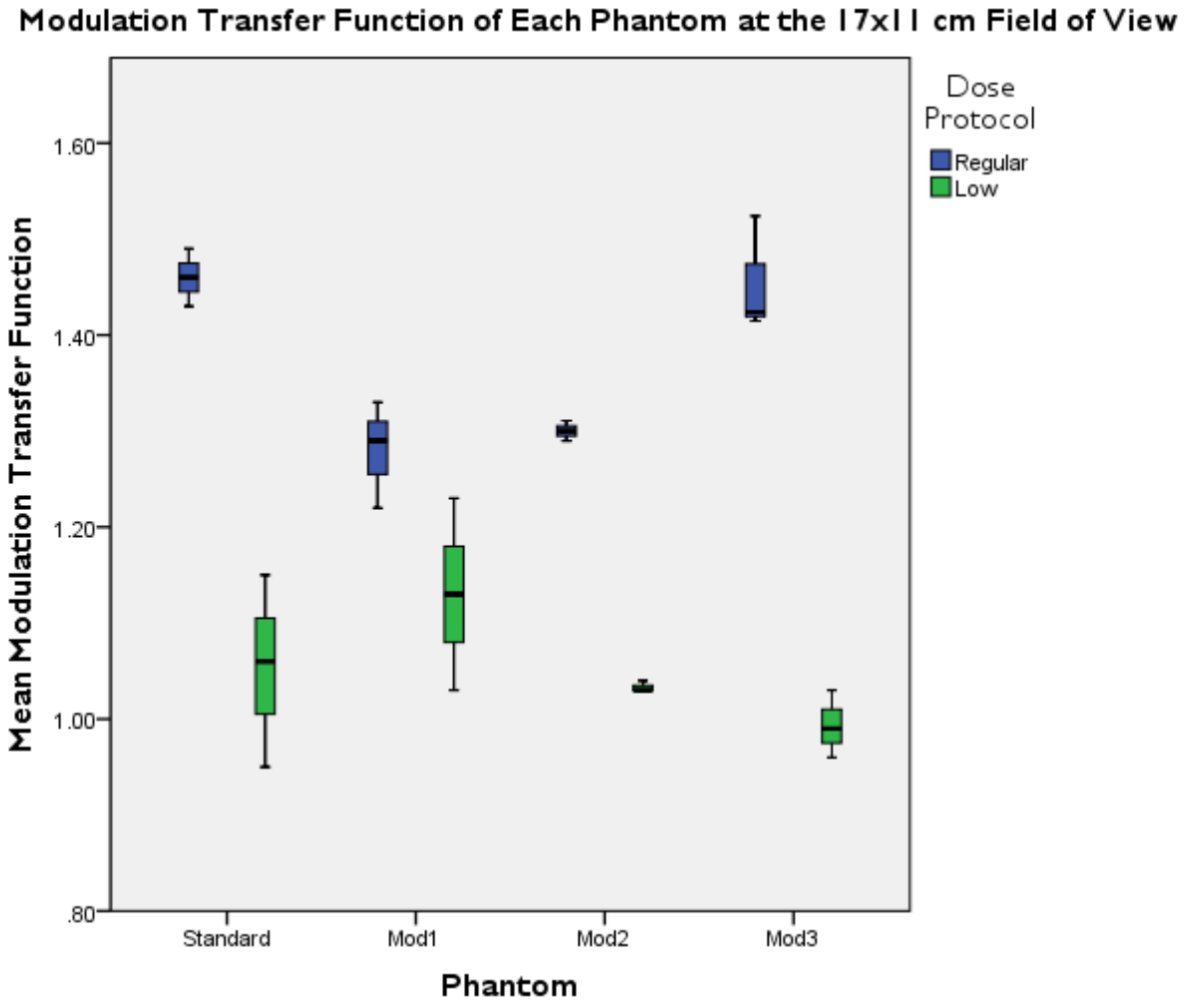

Figure 23: MTF 10% of each phantom and dose protocol at the 17 x 11 cm FOV

There was not a statistically significant simple two-way interaction between phantom and dose for the 10x5cm FOV ($p = 0.0921$), or for the 10 x 10cm FOV ($p = 0.1512$). There was a statistically significant simple two-way interaction between phantom and dose for the 8 x 8cm FOV ($p = 0.0003$), for the 17 x 6cm FOV ($p = 0.0116$) and for the 17 x 11cm FOV ($p < 0.0014$). Therefore, an analysis of all possible pairwise comparisons was performed using a Bonferroni adjustment for statistical significance.

Mean MTF values for each phantom at each dose for the 8x8cm FOV are listed in Table 11. At the 8 x 8cm FOV, modification three at SDSR had a statistically significantly lower mean MTF value than the standard phantom at SDSR ($p < 0.001$), the standard phantom at LDLR ($p = 0.0017$), modification one at SDSR ($p < 0.001$), modification two at SDSR ($p < 0.001$), and modification three at SDSR ($p < 0.001$).

Table 11: Mean MTF, SE and 95% CIs for each phantom and dose setting at the 8 x 8 cm FOV

Phantom	Dose Protocol	MTF Mean	SE	95% CI1	95% CI2
Standard	SDSR	1.20	0.022	1.157	1.243
Standard	Low	1.06	0.005	1.018	1.103
Mod1	SDSR	1.25	0.022	1.211	1.297
Mod1	Low	0.93	0.008	0.892	0.978
Mod2	SDSR	1.22	0.008	1.181	1.267
Mod2	Low	0.97	0.049	0.923	1.009
Mod3	SDSR	1.27	0.010	1.228	1.313
Mod3	Low	0.91	0.004	0.869	0.955

At the 8 x 8 cm FOV, modification three at LDLR had a statistically significantly higher mean MTF value than the standard phantom at LDLR ($p < 0.001$), modification one at SDSR ($p < 0.001$), and modification two at LDLR ($p < 0.001$).

At the 8 x 8 cm FOV, modification two at SDSR had a statistically significantly higher mean MTF value than the standard phantom at LDLR and modification one at LDLR. At the 8 x 8 cm FOV, modification two at LDLR had a statistically significantly lower mean MTF value than the standard phantom at SDSR. At the 8 x 8 cm FOV, modification one at SDSR had a statistically significantly higher mean MTF value than the standard phantom at LDLR and modification one at LDLR. The difference in means, confidence intervals, and the *p* values for the 8x8 cm FOV are listed in Table 12.

Table 12: *p* values, difference in mean MTF value, and 95% CIs for interactions between phantoms and dose at the 8 x 8 cm FOV

Phantom-Dose Protocol	Phantom-Dose Protocol	*p* value	Difference in mean MTF	95% CI1	95% CI2
Std-Reg	Std-Low	0.0033	0.14	0.040	0.238
Std-Reg	M1-Reg	0.5462	-0.05	-0.154	0.044
Std-Reg	M1-Low	<0.001	0.26	0.166	0.364
Std-Reg	M2-Reg	0.987	-0.02	-0.123	0.075
Std-Reg	M2-Low	<0.001	0.23	0.135	0.333
Std-Reg	M3-Reg	0.2719	-0.07	-0.170	0.028
Std-Reg	M3-Low	<0.001	0.29	0.189	0.387
Std-Low	M1-Reg	<0.001	-0.19	-0.293	-0.095
Std-Low	M1-Low	0.0082	0.13	0.027	0.225
Std-Low	M2-Reg	0.007	-0.16	-0.262	-0.064
Std-Low	M2-Low	0.0661	0.09	-0.004	0.194
Std-Low	M3-Reg	<0.001	-0.21	-0.309	-0.111
Std-Low	M3-Low	0.0017	0.15	0.050	0.248
M1-Reg	M1-Low	<0.001	0.32	0.220	0.418
M1-Reg	M2-Reg	0.9563	0.03	-0.069	0.129
M1-Reg	M2-Low	<0.001	0.29	0.189	0.387
M1-Reg	M3-Reg	0.9989	-0.02	-0.115	0.083
M1-Reg	M3-Low	<0.001	0.34	0.243	0.441
M1-Low	M2-Reg	<0.001	-0.29	-0.388	-0.190
M1-Low	M2-Low	0.9503	-0.03	-0.130	0.068
M1-Low	M3-Reg	<0.001	-0.34	-0.435	-0.237
M1-Low	M3-Low	0.9903	0.02	-0.076	0.122
M2-Reg	M2-Low	<0.001	0.26	0.159	0.357
M2-Reg	M3-Reg	0.7281	-0.05	-0.146	0.052
M2-Reg	M3-Low	<0.001	0.31	0.213	0.411
M2-Low	M3-Reg	<0.001	-0.30	-0.404	-0.206
M2-Low	M3-Low	0.5734	0.05	-0.045	0.153
M3-Reg	M3-Low	<0.001	0.36	0.260	0.458

At the 17 x 6 cm FOV, modification three at LDLR had a statistically significantly different mean MTF value than all other phantoms at SDSR and LDLR except for modifications 1 and 2 at LDLR. Mean MTF values for each phantom at each dose for the 17 x 6 cm FOV are listed in Table 13. The difference in means, confidence intervals and *p* values are listed in Table 14.

Table 13: Mean MTF, SE, and 95% CI for each phantom and dose setting at the 17 x 6 cm FOV

Phantom	Dose Protocol	MTF Mean	SE	95% CL1	95% CL2
Standard	SDSR	1.27	0.017	1.193	1.355
Standard	Low	1.04	0.018	0.957	1.120
Mod1	SDSR	1.16	0.009	1.083	1.246
Mod1	Low	0.80	0.006	0.717	0.879
Mod2	SDSR	1.31	0.014	1.224	1.387
Mod2	Low	1.20	0.036	1.116	1.279
Mod3	SDSR	1.44	0.017	1.357	1.519
Mod3	Low	1.08	0.032	0.996	1.158

Table 14: *p* values, difference in mean MTF, and 95% CIs for interactions between phantoms and dose at the 17 x 6 cm FOV

Phantom-Dose Protocol	Phantom-Dose Protocol	*p* value	Difference in mean MTF	95% CI1	95% CI2
Std-Reg	Std-Low	0.0091	0.24	0.048	0.423
Std-Reg	M1-Reg	0.4956	0.11	-0.078	0.297
Std-Reg	M1-Low	<0.001	0.48	0.288	0.663
Std-Reg	M2-Reg	0.9987	-0.03	-0.219	0.156
Std-Reg	M2-Low	0.8379	0.08	-0.111	0.264
Std-Reg	M3-Reg	0.112	-0.16	-0.351	0.024
Std-Reg	M3-Low	0.0362	0.20	0.009	0.384
Std-Low	M1-Reg	0.3389	-0.13	-0.313	0.062
Std-Low	M1-Low	0.0077	0.24	0.053	0.428
Std-Low	M2-Reg	0.0029	-0.27	-0.455	-0.080
Std-Low	M2-Low	0.1296	-0.16	-0.347	0.029
Std-Low	M3-Reg	<0.001	-0.40	-0.587	-0.212
Std-Low	M3-Low	0.9952	-0.04	-0.226	0.149
M1-Reg	M1-Low	<0.001	0.37	0.179	0.554
M1-Reg	M2-Reg	0.2227	-0.14	-0.329	0.046
M1-Reg	M2-Low	0.9982	-0.03	-0.221	0.154
M1-Reg	M3-Reg	0.0023	-0.27	-0.461	-0.086
M1-Reg	M3-Low	0.7398	0.09	-0.100	0.275
M1-Low	M2-Reg	<0.001	-0.51	-0.695	-0.320
M1-Low	M2-Low	<0.001	-0.40	-0.587	-0.212
M1-Low	M3-Reg	<0.001	-0.64	-0.827	-0.452
M1-Low	M3-Low	0.0019	-0.28	-0.467	-0.091
M2-Reg	M2-Low	0.5134	0.11	-0.079	0.296
M2-Reg	M3-Reg	0.2858	-0.13	-0.320	0.055
M2-Reg	M3-Low	0.0118	0.23	0.041	0.416
M2-Low	M3-Reg	0.0076	-0.24	-0.428	-0.053
M2-Low	M3-Low	0.3905	0.12	-0.067	0.308
M3-Reg	M3-Low	<0.001	0.36	0.173	0.548

At the 17 x 11 cm FOV, modification three at LDLR had a statistically significantly different mean MTF value than all other phantoms at SDSR. Mean MTF values for each phantom at each dose for the 17x11cm FOV are listed in Table 15. The difference in means, confidence intervals, and *P* values are listed in Table 16.

Table 15: Mean MTF, SE, and 95% CIs for each phantom and dose setting at the 17 x 11 cm FOV

Phantom	Dose Protocol	MTF Mean	SE	95% CI1	95% CI2
Standard	SDSR	1.46	0.012	1.390	1.537
Standard	Low	1.05	0.063	0.979	1.126
Mod1	SDSR	1.28	0.012	1.208	1.355
Mod1	Low	1.13	0.033	1.058	1.205
Mod2	SDSR	1.30	0.008	1.227	1.374
Mod2	Low	1.04	0.047	0.962	1.109
Mod3	SDSR	1.45	0.018	1.381	1.528
Mod3	Low	0.99	0.014	0.919	1.066

Table 16: *p* values, difference in mean MTF, and 95% CIs for interactions between phantoms and dose at the 17 x 11 cm FOV

Phantom-Dose Protocol	Phantom-Dose Protocol	*p* value	Difference in mean MTF	95% CI1	95% CI2
Std-Reg	Std-Low	<0.001	0.41	0.241	0.580
Std-Reg	M1-Reg	0.0313	0.18	0.012	0.351
Std-Reg	M1-Low	<0.001	0.33	0.162	0.501
Std-Reg	M2-Reg	0.0641	0.16	-0.007	0.333
Std-Reg	M2-Low	<0.001	0.43	0.258	0.598
Std-Reg	M3-Reg	1	0.01	-0.161	0.179
Std-Reg	M3-Low	<0.001	0.47	0.301	0.640
Std-Low	M1-Reg	0.0049	-0.23	-0.398	-0.059
Std-Low	M1-Low	0.7387	-0.08	-0.249	0.091
Std-Low	M2-Reg	0.0023	-0.25	-0.417	-0.078
Std-Low	M2-Low	0.9999	0.02	0.152	0.187
Std-Low	M3-Reg	<0.001	-0.40	-0.571	-0.232
Std-Low	M3-Low	0.9136	0.06	-0.110	0.230
M1-Reg	M1-Low	0.1048	0.15	-0.020	0.319
M1-Reg	M2-Reg	0.9999	-0.02	-0.188	0.151
M1-Reg	M2-Low	0.0024	0.25	0.077	0.416
M1-Reg	M3-Reg	0.0444	-0.17	-0.342	-0.003
M1-Reg	M3-Low	0.0005	0.29	0.119	0.458
M1-Low	M2-Reg	0.0524	-0.17	-0.338	0.001
M1-Low	M2-Low	0.528	0.10	-0.073	0.266

M1-Low	M3-Reg	<0.001	-0.32	-0.492	-0.153
M1-Low	M3-Low	0.1544	0.14	-0.031	0.308
M2-Reg	M2-Low	0.0012	0.27	0.095	0.435
M2-Reg	M3-Reg	0.0896	-0.15	-0.324	0.016
M2-Reg	M3-Low	0.0002	0.31	0.138	0.477
M2-Low	M3-Reg	<0.001	-0.42	-0.589	-0.249
M2-Low	M3-Low	0.9857	0.04	-0.127	0.212
M3-Reg	M3-Low	<0.001	0.46	0.292	0.631

All simple pairwise comparisons were ran for phantom modifications regardless of phantom type and regardless of dose for the 10 x 5 cm and 10 x 10 cm with a Tukey adjustment applied. Mean MTF values for these two FOVS adjusted for phantom type are listed in Table 17. There was a statistically significant difference in MTF values regardless of phantom type for the 10 x 5 cm FOV ($p < 0.001$) and the 10x10cm FOV ($p = 0.0002$) with the mean MTF for SDSR statistically significantly higher than the mean MTF for the LDLR for each FOV. There was not a statically significant difference in mean MTF values regardless of dose for the 10x5cm FOV ($p = 0.7898$) or the 10x10 cm FOV ($p = 0.98$).

Table 17: Mean MTF values for the 10 x 5 and 10 x 10 cm FOVs at SDSR and LDLR regardless of phantom type

FOV (cm)	Dose Protocol	Mean MTF
10x5	SDSR	1.30
10x5	Low	0.93
10x10	SDSR	1.36
10x10	Low	1.04

In summary, MTF significantly differed only by dose for the 8x8 cm, 17x6 cm and 17x11 cm FOVs. MTF was higher on average for the SDSR.

DISCUSSION AIM ONE

CNR

Voxel size, kVp, and mAs impacted the CNR (Table 3). The kVp, mA, and time were all higher for the standard dose protocol when compared to LDLR. Additionally, the voxel size for the LDLR was larger than the standard dose protocol at all FOVs. There was a statistically significant interaction between phantom and dose protocol at the 8 x 8 cm and 17 x 11 cm FOV. The mean CNR values for LDLR were higher than SDSR for each phantom. All mean CNR values for LDLR were higher than all CNR values for SDSR regardless of phantom; an exception was the mean CNR value at the 8 x 8 cm FOV for the modification three phantom at SDSR was higher than the mean CNR of the standard phantom at LDLR. However, this was not statistically significant. Usually, a SDSR would result in a higher CNR value than a LDLR due to the effect of more noise for the LDLR. However, this study found that the LDLR resulted in higher CNR. The results suggest that the larger voxel size of the LDLR counteracted the effect of reduced mAs producing an improved CNR. The opposite was found in another study by Elkhateeb and co-workers where the CNR was lower with LDLR. This difference was accounted for by keeping the FOV and voxel size constant [40]. All SDSRs had a higher kVp than the LDLR by about 5 kVp. One would expect that there would be increased contrast with decreased kVp. However, the small increase of 5 kVp did not significantly affect the contrast.

The LDLR had lower kVp and lower mAs than the SDSR. The expected results were less signal (due to lower mAs and lower kVp) and more noise if the voxel size was the same. However, voxelvolume was 4-11 times larger in LDLRs and thus had a larger signal and lower noise which counteracted the expected decrease in signal due to lower mAs and kVp. The most plausible explanation for the observation of a higher CNR on average for the LDLR when compared to the SDSR is that the difference in voxel size had more effect on the noise reduction than mAs had on signal.

The LDLR used a larger voxel size than the SDSR for all FOVs. Reduced kVp can increase contrast [41]. However, a lower kVp can also result in less signal as a result of a lower x-ray production efficiency, thus creating more noise. Elkhateeb and co-workers found that by keeping all exposure parameters the same, except kVp, that the LDLR had lower CNR [40]. Our study had multiple exposure parameters change which accounts for the different results. The large voxel size resulted in an increase in signal and counteracted the effect of a decrease in signal due to reduced mAs. CBCT uses isotropic voxels (cuboidal voxel). The matrix and pixel size of the detector determine voxel size in CBCT. If CBCT units have smaller voxels, the dose is usually increased to achieve a reasonable signal-to-noise ratio. The voxel size for the standard dose was smaller than the voxel size of the LDLR at all FOVs. Standard dose voxel sizes ranged from 180 to 250 um. LDLR voxel size was 400 um for all FOVs. The average noise of the LDLR was significantly lower than the average noise for the standard dose.

The modification three phantom was constructed with a tilted test tool at the periphery. The modification three phantom at SDSR had a statistically significant higher mean CNR value than the other phantoms at SDSR. The modification 3 phantom at LDLR had a statistically significant higher mean CNR value than all of the other phantoms at SDSR and LDLR.

However, there was no statistically significant difference in CNR between modification one phantom and the standard or modification two phantoms regardless of dose at the 10 x 5, 10 x 10 or 17 x 6 cm FOVs.

Due to CBCT image acquisition techniques, there is a potential source of artifact at the periphery of the volume. This is called cone beam artifact and is caused by the divergence of the x-ray beam as it rotates around the patient in an axial plane [33]. Structures at the top and bottom of the image field are exposed only when the x-ray source is on the opposite side of the patient. As a result, there is a potential for more noise and reduced contrast at the periphery of a CBCT volume. One would expect contrast to be the lowest and noise to be the highest. However, the CNR for Mod3 was found to be significantly larger than for any of the other phantoms. The reason for this finding is not well understood and speculative at this time. Possibly, the test tool was not far enough from the periphery or not rotated far enough out of the horizontal plane to see the cone beam effect. This would explain why CNR would not be decreased, but does not explain why it actually increased. Alternatively, CNR may have been higher because of image processing algorithms designed by the manufacturer. Communication with the Quart phantom manufactured indicated that edge enhancement may have been applied in peripheral aspects of the phantom. While this does not fully explain the findings of this study, it at least suggests that the software may have played a role.

The quality and quantity of the x-ray beam depend on tube voltage (kVp) , tube current (mA) and exposure time (s). These settings can be adjusted, however, fixed exposure settings (manufacturer recommendations) were used for each FOV and dose setting. As mAs increases, exposure increases proportionally. The mAs for standard dose was approximately four times higher than that of LDLR. Higher mAs resulted in more signal. One would expect for the LDLR

to have a slightly higher contrast due to lower kVp but much higher noise than the SDSR, resulting in a lower CNR (an increase in the numerator or a decrease in the denominator will result in an increase in the CNR ratio). When both the numerator and denominator are increased or reduced, whether the CNR ratio increases or decreases is determined by the respective changes in the both the numerator and denominator. This was not found to be true for the phantoms due to a larger voxel size for LDLR. Based upon the results, the difference in contrast was much less than the difference in noise due to the effect of larger voxel size in noise reduction.

Subject contrast is the result of differential attenuation based on characteristics of the object. Influencing factors of subject contrast include the subject's thickness, density, and atomic number. The atomic number and mass density were the same for each phantom. The thickness of the acrylic for modification one and modification three was greater than for the standard phantom and for modification two. The reason for this was the need to accommodate the angled test tool. The greater the thickness of the subject, the more scatter is produced, which could lower contrast. Because of this, the modification 1 and modification 3 phantoms should have had lower contrast than the standard and modification 2 phantoms. At SDSR, there was no statistical difference between the modification 1 phantom and the standard or the modification two phantom at the 8x8cm FOV. At LDLR, there was no statistical difference between the modification 1 phantom and the standard or the modification two phantom at the 8 x 8 cm FOV. Therefore, for the 8 x 8 cm FOV the small change in subject thickness did not have a significant effect on the mean difference in contrast between modification one phantom and the other phantoms.

MTF

Mean MTF values for the SDSR were higher than the mean MTF values for the LDLR for each field of view and for each phantom (Table 10). There was a statistically significant difference between the MTF values based upon dose protocols at the 8 x 8 cm, 17 x 6 cm, and 17 x 11 cm FOVs. There were no significant differences of the MTF values between the phantoms. Other studies have shown similar results in that the smaller the voxel size, the higher that spatial resolution [42, 43]. The combined effect of higher kVp, higher mAs, and smaller voxel size of the SDSR had a positive effect on MTF, when compared to LDLR. In contrast, a study by Elkhateeb et al shows that there was no difference between MTF and changing voxel size (180 um, 300 um, and 500 um) or FOV (5 x 10 cm or 17 x 13.5 cm) using the same CBCT unit (CS 9300) [13, 40]. Similar results of no effect on MTF with changing voxels sizes were found in other studies [44, 45].

Reducing the field of view to the region of interest (collimation) is known to improve image quality by reducing scattered radiation [46]. Therefore, the smaller FOVs should theoretically have had a higher MTF than the larger FOVs. However, this was not found consistently throughout the five fields of view used in this study. The results were consistent with other studies that failed to identify any effect of FOV on MTF [7, 13]. This may be due to similar attenuation characteristics throughout the image quality phantoms. Other studies have shown that scatter can have an effect on spatial resolution, especially for low contrast structures [34, 47].

Generally, the higher the kVp, the more the scatter due to the energy of the scatter angle increasing and the scatter oriented in a more forward direction (towards the receptor). Additional scatter results in less contrast. Noise degrades edges and makes structure differentiation difficult,

especially between low contrast structures. This affects spatial resolution. Spatial resolution is the ability to distinguish between two adjacent structures as they become smaller and closer together [48]. The higher the spatial resolution is, the finer the detail in an image. Unaided human vision can distinguish approximately 10 lines per mm. Factors affecting spatial resolution include noise, motion blur, focal spot size, source-to-object distance, object-to-image distance and number of basis images [49]. The exposure settings also affected the image noise in other studies with larger amounts of exposure (higher kVp and/or higher mAs) associated with lower noise in CS9300 CBCT units [13, 44].

Spatial resolution in a CBCT image is also determined by the voxel size. CBCT uses isotropic voxels (voxels that are equal size in all three dimensions). Matrix and pixel size of the detector are the main determinant of voxel size. If the number of photons remains the same, a larger voxel size allows more photons to be detected and results in less image noise [50]. However, larger voxel sizes lower the spatial resolution. Smaller voxel sizes (higher resolution) usually require higher doses to maintain a reasonable signal-to-noise ratio. However, depending upon the diagnostic task, sometimes this is necessary. For example, a higher spatial resolution was found to result in higher detection of internal resorption than low resolution CBCT images [51].

The use of the low-dose protocol resulted in a reduction in the MTF. The binning of the pixels for a larger voxel at the LDLR resulted in a significant impact on reducing spatial resolution (lowered spatial resolution). Other studies have found similar results with image noise decreasing with increasing voxel size [8, 43]. These studies also showed that an increase in voxel size decreased spatial resolution. However, the increased voxel size may be beneficial to use in the future due to the increase in voxel size allowing for a shorter scan time, lower dose, and

decreased reconstruction time. The shortened scan time has been shown to reduce motion artifact, which is frequently encountered in orthodontics [52].

METHODS AND MATERIALS AIM TWO

Subjective Image Quality (Aim Two)

The relationship of specific indicators of objective image quality to subjective measures of image quality of CBCT at varying FOVs and dose was evaluated. Two expert observers viewed images of a RANDO phantom (Figure 24) that were acquired with the CS 9300 CBCT unit utilizing the same image quality parameters, the same five FOVs and the two dose protocols used in the objective image quality study described previously. The RANDO phantom contains materials that simulates human tissue attenuation characteristics. Therefore, the RANDO phantom is suitable to be imaged for subjective image quality assessment.

Figure 24: RANDO phantom

Positioning of the RANDO phantom was accomplished by using the CS 9300 positioning devices (chin and forehead rest) and laser beam positioning lights. A scout image was acquired to ensure that the RANDO phantom was centered within the FOV. All FOVs were imaged on the same day and by moving the CBCT unit superior or inferior instead of moving the RANDO

phantom. This helped to ensure the same orientation throughout the different FOVs and dose protocols.

The CBCT volumes were exported from the CS software as uncompressed DICOM files. The volumes were imported into InVivoDental 5.0 (Anatomage Inc.) for landmark selection. The brightness and contrast settings were standardized for all FOVs, dose protocols, and landmarks in the center of the range in the software. The RANDO phantom was not repositioned or reoriented for any of the image reconstructions to maintain standardization. A Lenovo W540 laptop was used to make static images as JPG files of the selected images. The anatomic landmarks selected for the observer sessions were the hard palate in the coronal view (Figure 25), the hard palate in the sagittal view (Figure 26), the lateral pterygoid plates in the axial view (Figure 27), and the mental foramen in the coronal view (Figure 28).

Figure 25: Hard palate in the coronal view simulating the test tool location and orientation of the standard Quart phantom at the 17x11 cm FOV, SDSR.

Figure 26: Hard palate in the sagittal view simulating the test tool location and orientation of the Mod1 Quart phantom at the 17x11 cm FOV, SDSR.

Figure 27: Lateral pterygoid plate in the axial view simulating the test tool location and orientation of the Mod2 Quart phantom at the 17x11 cm FOV, SDSR.

Figure 28: Mental foramen in the coronal view simulating the test tool location and orientation of the Mod3 Quart phantom at the 17x11 cm FOV, SDSR.

The anatomical landmarks were selected for comparison based upon location, orientation, and visibility within the FOV. The anatomical landmarks were representative of central structures, peripheral structures, and structures angled in relation to the axial acquisition plane [53]. The hard palate in the coronal view is located in the center of the volume and parallel to the axial plane, similar to the test tool of the standard Quart phantom. The hard palate in the sagittal view is located in the center of the volume and angled with respect to the image acquisition plane, similar to the test tool of Mod1. The lateral pterygoid plates in the axial view are located at the periphery of the volume and parallel to the image acquisition plane, similar to Mod2. The mental foramen in the coronal view is located at the periphery of the volume and at an angle to the image acquisition plane, similar to Mod3. The static images were imported into Qualtrics for comparison.

Images were compared through pairwise comparison by two observers using Qualtrics. Expert observers were used for this study. Expert observers were defined as dentists with additional oral and maxillofacial radiology (OMR) training. Informed consent was obtained from each observer outlining the study steps and measures taken to ensure their confidentiality. There were 180 questions that took each observer approximately 90 minutes to complete. The expert observers viewed the images on a Lenovo W540 laptop in a quiet environment with low ambient lighting. They were not required to complete the survey in one session and had one week to complete all observations.

Each question asked the observer which image they preferred for identifying a specific landmark. For each anatomic landmark, at each FOV and dose level, the observers were asked to express their preference for one of the images or express no preference. The answers were compiled using a coding sequence (Table 18) in an Excel spreadsheet. If the observer preferred one image over the other, they selected that image. If the observer had no preference between the two images for identification of an anatomical landmark, the observer selected a no preference option. At the completion of each observer session, each image was scored based on the amount of times the image was preferred, not preferred, or if there was no preference between the two images (Table 19). If one image was preferred over the other, the image received 2 points. The image that was not preferred received 0 points. If there was no preference, each image received one point. The higher the points/score per image, the higher the score for the image, and therefore the higher the preference level of the observer for a specific set of conditions for that anatomical landmark.

Table 18: Coding system for the RANDO phantom observer sessions. The hard palate in the coronal view simulated the test tool location of the standard phantom. The hard palate in the sagittal view simulated the test tool of the Mod1 phantom. The lateral pterygoid plate in the axial view simulated the test tool of the Mod2 phantom. The mental foramen in the coronal view simulated the test tool of the Mod3 phantom.

RANDO Phantom Identifier	FOV (cm)	Protocol	Hard palate Coronal Plane	Hard palate Sagittal Plane	Lateral pterygoid plate Axial Plane	Mental foramen Coronal Plane
R2	17x11	SDSR	R2_1	R2_2	R2_3	R2_4
R3	17x11	Low	R3_1	R3_2	R3_3	R3_4
R4	17x6	SDSR	R4_1	R4_2	R4_3	R4_4
R5	17x6	Low	R5_1	R5_2	R5_3	R5_4
R6	10x10	SDSR	R6_1	R6_2	R6_3	R6_4
R7	10x10	Low	R7_1	R7_2	R7_3	R7_4
R8	10x5	SDSR	R8_1	R8_2	R8_3	R8_4
R9	10x5	Low	R9_1	R9_2	R9_3	R9_4
R10	8x8	SDSR	R10_1	R10_2	R10_3	R10_4
R11	8x8	Low	R11_1	R11_2	R11_3	R11_4

Table 19. Coding sequence for pairwise comparison

Point Value	**Preference Level of Image**
0	NOT Preferred
1	No Preference/Cannot Determine Difference
2	Preferred

For each pairwise comparison, CNR and MTF were compared and also given a score. If the CNR was higher for an image that was chosen, 2 points were given to the image's CNR score. The image not chosen received zero points. If there was no difference between the CNRs, each image was given one point for the CNR score. If the MTF was higher for an image that was chosen, 2 points were given to the image's MTF score. The image not chosen received zero points. If there was no difference between the MTFs, each image was given one point for the MTF score. Statistical analysis was based on assessing the relationship between objective image quality and subjective images quality and consisted of a correlation analysis using a nominal outcome variable and a point scale.

Three models with logistic regression were completed to analyze whether the phantom, FOV, or dose protocol were significant predictors of subjective image quality. These models included the total preference scores (of both observers combined), the preferences associated with images with higher CNRs, and the preferences associated with higher MTFs. A stepwise selection model and logistic regression were completed to analyze whether the phantom, FOV, or dose protocol were associated with the observer agreement. If the observers agreed on the preference for the image, a value of 1 was given. If the observers did not agree on the image, a value of 0 was given. In order to determine if the observers agreed or disagreed based upon the image preference, FOV, dose protocol, or outcome variables (CNR and MTF), a coding system using A and C were used in tables. The association of the observer choosing one of the FOVs (A or C), dose (A or C), or Phantom (A or C). A and C refer to the observer's choice. First, the variable phantom was selected into the model since it is the most significant variable among those to be chosen. Next, the variable FOV was added to the model since both phantom and FOV

remained significant. The null hypothesis was that no association existed between the predictors (phantom, FOV) and the response (agreement).

HUMAN SUBJECTS

This submission (IRB #15-1641) was reviewed by the University of North Carolina (UNC) Office of Human Research Ethics, and approved by UNC's Biomedical Institutional Review Board on 10/5/2016.

RESULTS AIM TWO

Subjective Image Quality

The responses of each expert observer were listed from most preferred to least preferred based upon a point system (Table 20). Figures 29–33 illustrate the sum preference scores of both observers for each field of view. The top three scores are listed in Table 21.

Table 20: Summary of observer preference score, CNR score, MTF score

Image Name	Phantom Comparison	FOV (cm)	Dose Protocol	Preference Score (points)	CNR Score (points)	MTF Score (points)
R2_1	Standard	17x11	SDSR	23	1	23
R2_2	Mod 1	17x11	SDSR	15	5	13
R2_3	Mod 2	17x11	SDSR	22	4	20
R2_4	Mod 3	17x11	SDSR	22	2	22
R3_1	Standard	17x11	Low	27	15	9
R3_2	Mod 1	17x11	Low	12	6	6
R3_3	Mod 2	17x11	Low	11	5	7
R3_4	Mod 3	17x11	Low	9	7	9
R4_1	Standard	17x6	SDSR	28	4	24
R4_2	Mod 1	17x6	SDSR	31	17	19
R4_3	Mod 2	17x6	SDSR	24	6	22
R4_4	Mod 3	17x6	SDSR	22	0	20
R5_1	Standard	17x6	Low	18	18	10
R5_2	Mod 1	17x6	Low	28	20	0
R5_3	Mod 2	17x6	Low	20	12	12
R5_4	Mod 3	17x6	Low	11	9	11
R6_1	Standard	10x10	SDSR	18	6	18
R6_2	Mod 1	10x10	SDSR	24	3	15
R6_3	Mod 2	10x10	SDSR	27	7	27
R6_4	Mod 3	10x10	SDSR	29	9	29

R7_1	Standard	10x10	Low	19	15	13
R7_2	Mod 1	10x10	Low	3	3	1
R7_3	Mod 2	10x10	Low	14	10	4
R7_4	Mod 3	10x10	Low	5	5	5
R8_1	Standard	10x5	SDSR	13	9	13
R8_2	Mod 1	10x5	SDSR	24	0	24
R8_3	Mod 2	10x5	SDSR	35	9	25
R8_4	Mod 3	10x5	SDSR	33	9	21
R9_1	Standard	10x5	Low	6	4	2
R9_2	Mod 1	10x5	Low	11	9	3
R9_3	Mod 2	10x5	Low	20	14	2
R9_4	Mod 3	10x5	Low	3	1	3
R10_1	Standard	8x8	SDSR	21	9	12
R10_2	Mod 1	8x8	SDSR	23	3	15
R10_3	Mod 2	8x8	SDSR	6	0	6
R10_4	Mod 3	8x8	SDSR	34	10	24
R11_1	Standard	8x8	Low	7	6	6
R11_2	Mod 1	8x8	Low	9	9	1
R11_3	Mod 2	8x8	Low	1	1	1
R11_4	Mod 3	8x8	Low	12	10	6

Table 21: Highest three scores for combined observer preferences

Score (points)	FOV (cm)	Dose Protocol	Anatomy	Imaging Plane	Simulated test tool location of phantom
35	10x5	SDSR	Lateral Pterygoid Plate	Axial	Mod2
34	8x8	SDSR	Mental Foramen	Coronal	Mod3
33	10x5	SDSR	Mental Foramen	Coronal	Mod3

Figure 29: Sum preference scores of both observers for each phantom at the 8 x 8 cm FOV

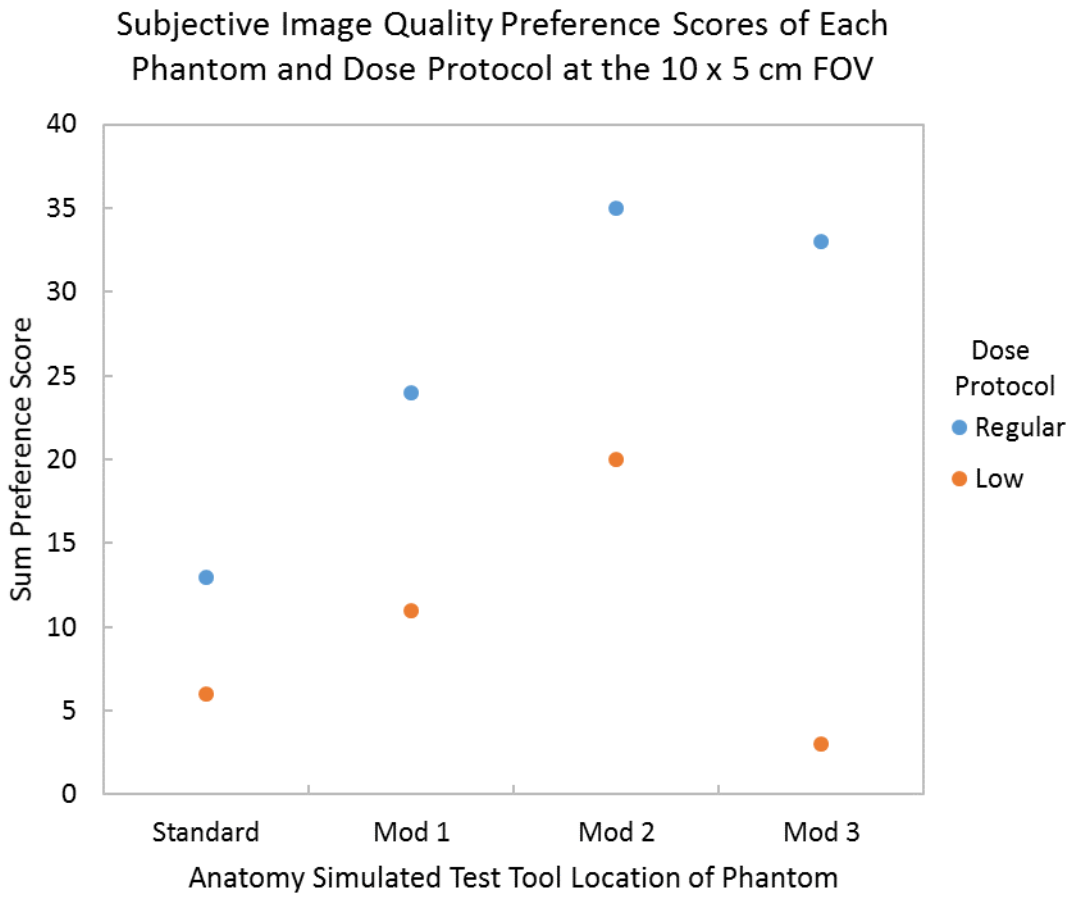

Figure 30: Sum preference scores of both observers for each phantom at the 10 x 5 cm FOV

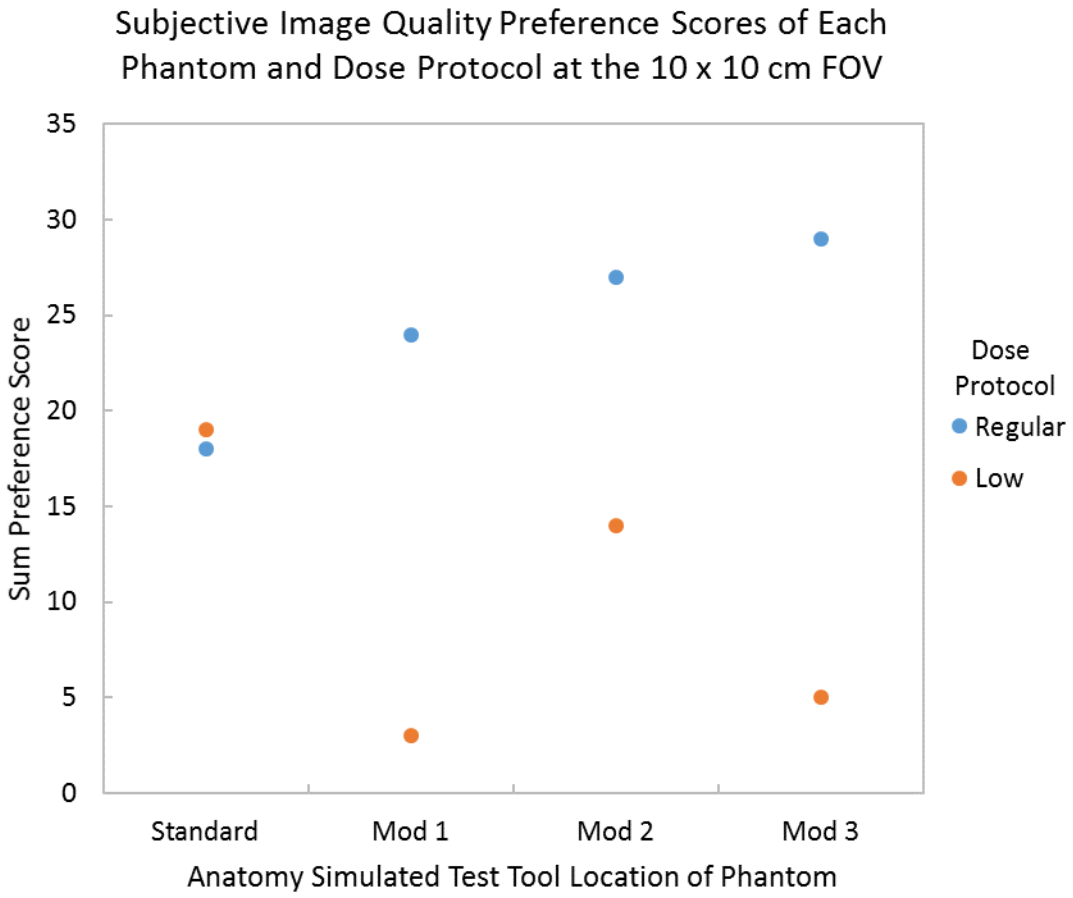

Figure 31: Sum preference scores of both observers for each phantom at the 10 x 10 cm FOV

Figure 32: Sum preference scores of both observers for each phantom at the 17 x 6 cm FOV

Figure 33: Sum preference scores of both observers for each phantom at the 17 x 11 cm FOV

The highest overall observer preference scores were for the two smallest fields of view (8 x 8 cm and 10 x 5 cm) at SDSR, however this was not significant. The lowest score with only one point was for the 8 x 8 cm FOV at LDLR. The three lowest scores are listed in Table 22. SDSR was preferred over LDLR for each phantom modification. The highest preference score was for the 10 x 5 cm FOV, SDSR, looking at the lateral pterygoid plate in the axial orientation (compared to modification two), however this was not significant.

Table 22: Lowest three scores for combined observer preferences

Score (points)	FOV (cm)	Dose Protocol	Anatomy	Imaging Plane	Simulated test tool location of phantom
1	8x8	Low	Lateral Pterygoid Plate	Axial	Mod2
3	10x5	Low	Mental Foramen	Coronal	Mod3
3	10x10	Low	Hard Palate	Sagittal	Mod1

Table 23: Phantom, FOV, and dose estimates as predictors of observer preference. A and C refer to the observer's choice of the pairwise comparison.

Effect	DF	Score Chi-Square	Pr > ChiSq
Phantom	3	3.0451	0.3847
FOV A	4	1.4717	0.8317
FOV C	4	1.0887	0.8961
Dose A	1	0.3574	0.5500
Dose C	1	1.1187	0.2902

Table 24: Prediction of observer preference
Analysis Of Maximum Likelihood Parameter Estimates

Parameter		DF	Estimate	Standard Error	Wald 95% Confidence Limits		Wald Chi-Square	Pr > ChiSq
Intercept		1	2.9230	0.1172	2.6933	3.1528	621.98	<0.0001
Phantom	Mod 1	1	-0.0000	0.1054	-0.2066	0.2066	0.00	1.0000
Phantom	Mod 2	1	0.0000	0.1054	-0.2066	0.2066	0.00	1.0000
Phantom	Mod 3	1	0.0000	0.1054	-0.2066	0.2066	0.00	1.0000
Phantom	Standard	0	0.0000	0.0000	0.0000	0.0000	.	.
FOV	10x10	1	0.2071	0.1267	-0.0412	0.4553	2.67	0.1021

FOV	10x5	1	0.2493	0.1255	0.0034	0.4953	3.95	0.0469
FOV	17x11	1	0.2214	0.1263	-0.0261	0.4688	3.07	0.0796
FOV	17x6	1	0.4766	0.1198	0.2419	0.7114	15.84	<0.0001
FOV	8x8	0	0.0000	0.0000	0.0000	0.0000	.	.
Dose	Low	1	-0.6559	0.0786	-0.8099	-0.5019	69.67	<0.0001
Dose	SDSR	0	0.0000	0.0000	0.0000	0.0000	.	.
Scale		0	1.0000	0.0000	1.0000	1.0000		

Dose has a significant effect on subjective image quality. LDLR has a negative correlation with the observer preference scores (estimates=-0.6559, *p* value < 0.0001). SDSR leads to higher preference scores. The total observer preference score tends to be higher in SDSR and lower in LDLR on average. The 17 x 6 cm FOV is also a significant predictor of preference scores. It is positively correlated with the response.

Table 25: CNR influence on observer preference

Parameter		DF	Estimate	Standard Error	Wald 95% Confidence Limits		Wald Chi-Square	Pr > ChiSq
Intercept		1	1.7110	0.1853	1.3479	2.0741	85.28	<0.0001
Phantom	Mod 1	1	-0.1484	0.1576	-0.4572	0.1604	0.89	0.3462
Phantom	Mod 2	1	-0.2464	0.1619	-0.5636	0.0708	2.32	0.1279
Phantom	Mod 3	1	-0.3388	0.1662	-0.6645	-0.0130	4.15	0.0415
Phantom	Standard	0	0.0000	0.0000	0.0000	0.0000	.	.

FOV	10x10	1	0.1892	0.1951	-0.1932	0.5717	0.94	0.3321
FOV	10x5	1	0.1361	0.1975	-0.2510	0.5233	0.47	0.4907
FOV	17x11	1	-0.0645	0.2075	-0.4712	0.3422	0.10	0.7558
FOV	17x6	1	0.5831	0.1802	0.2300	0.9363	10.48	0.0012
FOV	8x8	0	0.0000	0.0000	0.0000	0.0000	.	.
Dose	Low	1	0.4600	0.1202	0.2245	0.6955	14.66	0.0001
Dose	SDSR	0	0.0000	0.0000	0.0000	0.0000	.	.
Scale		0	1.0000	0.0000	1.0000	1.0000		

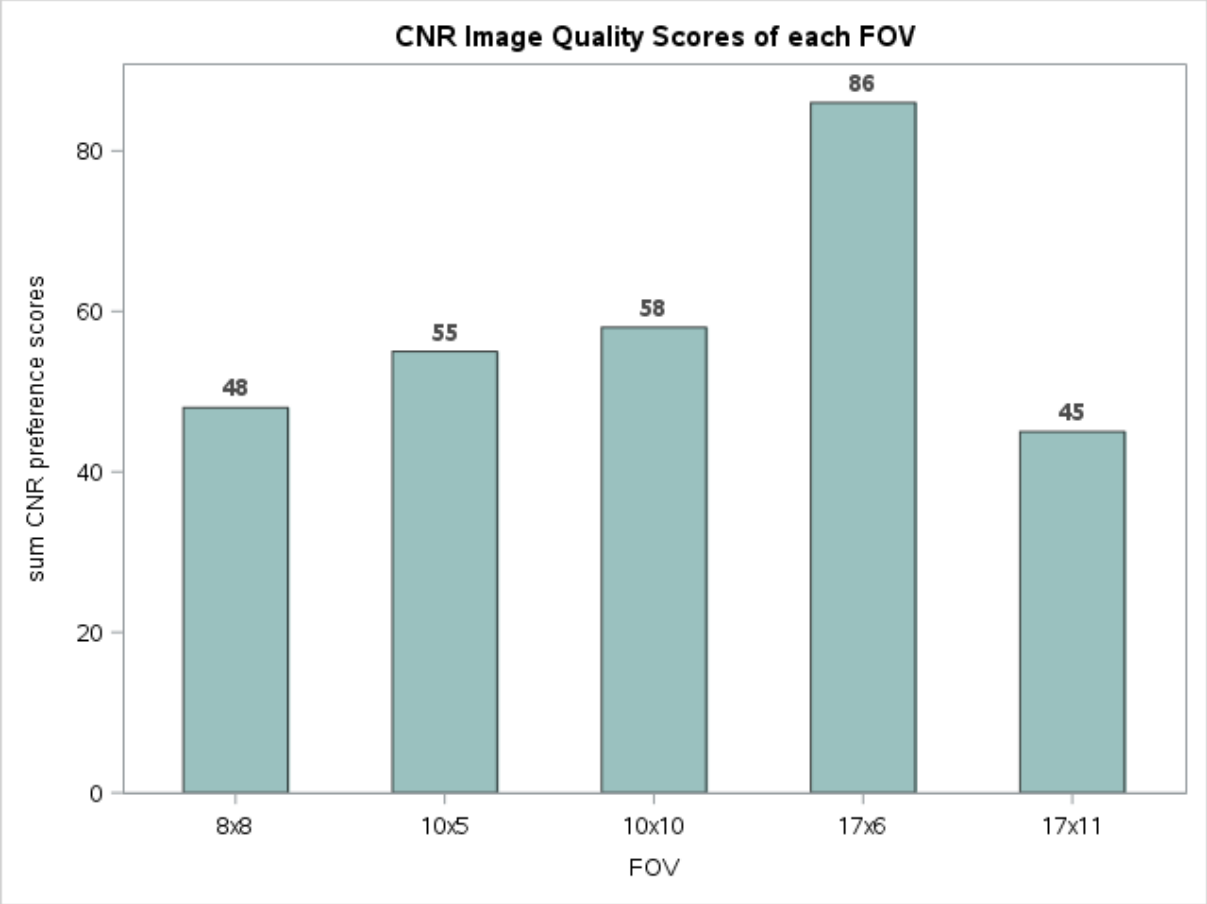

Figure 34: CNR image quality scores at each FOV

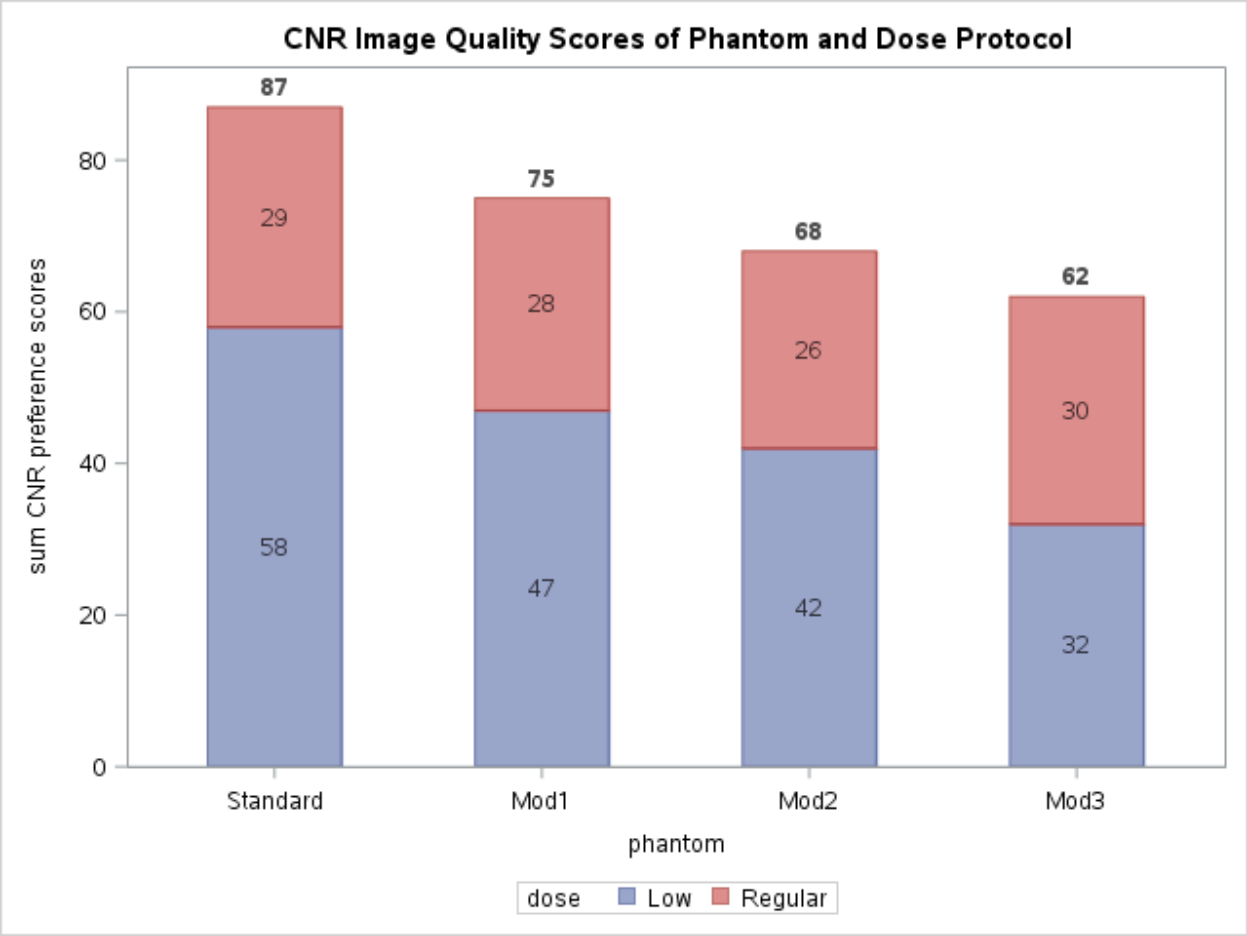

Figure 35: CNR image quality scores of phantom and dose protocol

Dose protocol is a highly significant predictor of CNR preference scores (p = 0.0001). LDLR resulted in higher CNR on average. Mod 3 has a negative correlation with the images that were preferred with higher CNR. At the 17 x 6 cm FOV, CNR is a highly significant predictor of response (estimates = 0.5831, *p* value = 0.0012).

Table 26: MTF influence on observer preference
Analysis Of Maximum Likelihood Parameter Estimates

Parameter		DF	Estimate	Standard Error	Wald 95% Confidence Limits		Wald Chi-Square	Pr > ChiSq
Intercept		1	2.6603	0.1427	2.3807	2.9399	347.74	<0.0001
Phantom	Mod 1	1	-0.2928	0.1342	-0.5558	-0.0299	4.76	0.0291
Phantom	Mod 2	1	-0.0313	0.1250	-0.2763	0.2138	0.06	0.8026
Phantom	Mod 3	1	0.1431	0.1198	-0.0918	0.3780	1.43	0.2324
Phantom	Standard	0	0.0000	0.0000	0.0000	0.0000	.	.
FOV	10x10	1	0.4558	0.1517	0.1585	0.7531	9.03	0.0027
FOV	10x5	1	0.2699	0.1576	-0.0390	0.5788	2.93	0.0868
FOV	17x11	1	0.4287	0.1525	0.1298	0.7276	7.90	0.0049
FOV	17x6	1	0.5080	0.1502	0.2136	0.8024	11.44	0.0007
FOV	8x8	0	0.0000	0.0000	0.0000	0.0000	.	.
Dose	Low	1	-1.2617	0.1075	-1.4725	-1.0510	137.71	0<.0001
Dose	SDSR	0	0.0000	0.0000	0.0000	0.0000	.	.
Scale		0	1.0000	0.0000	1.0000	1.0000		

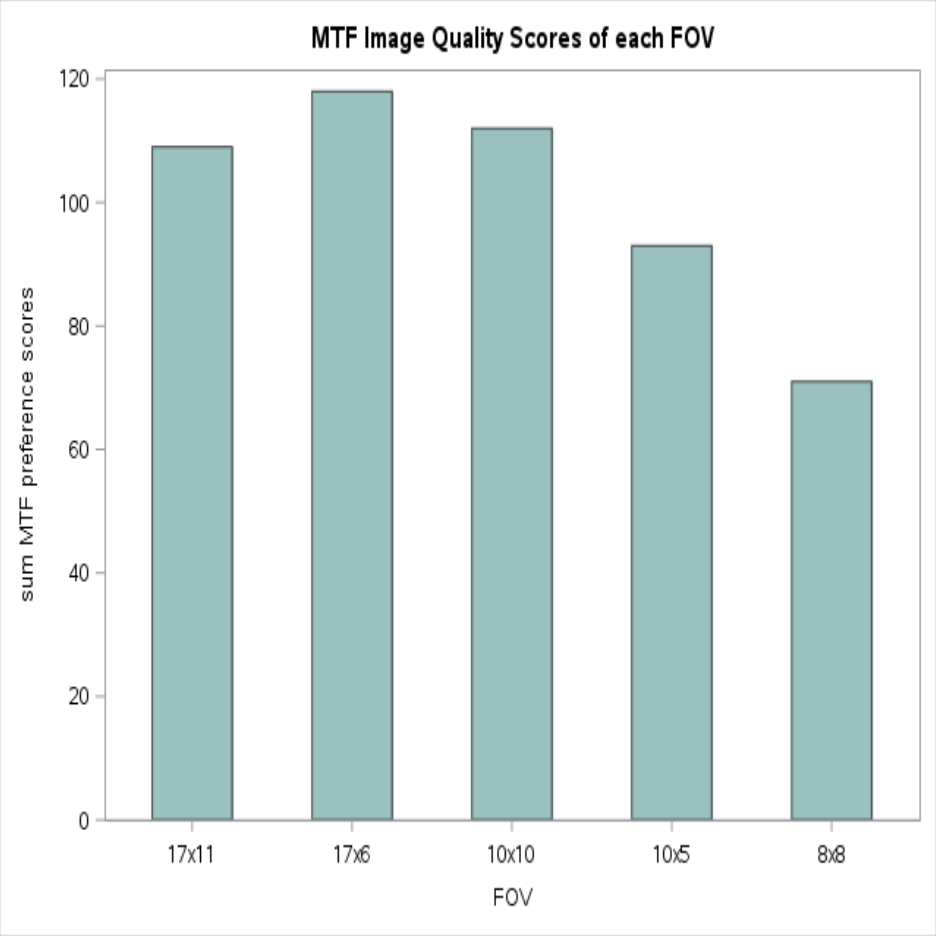

Figure 36: MTF image quality score at each FOV

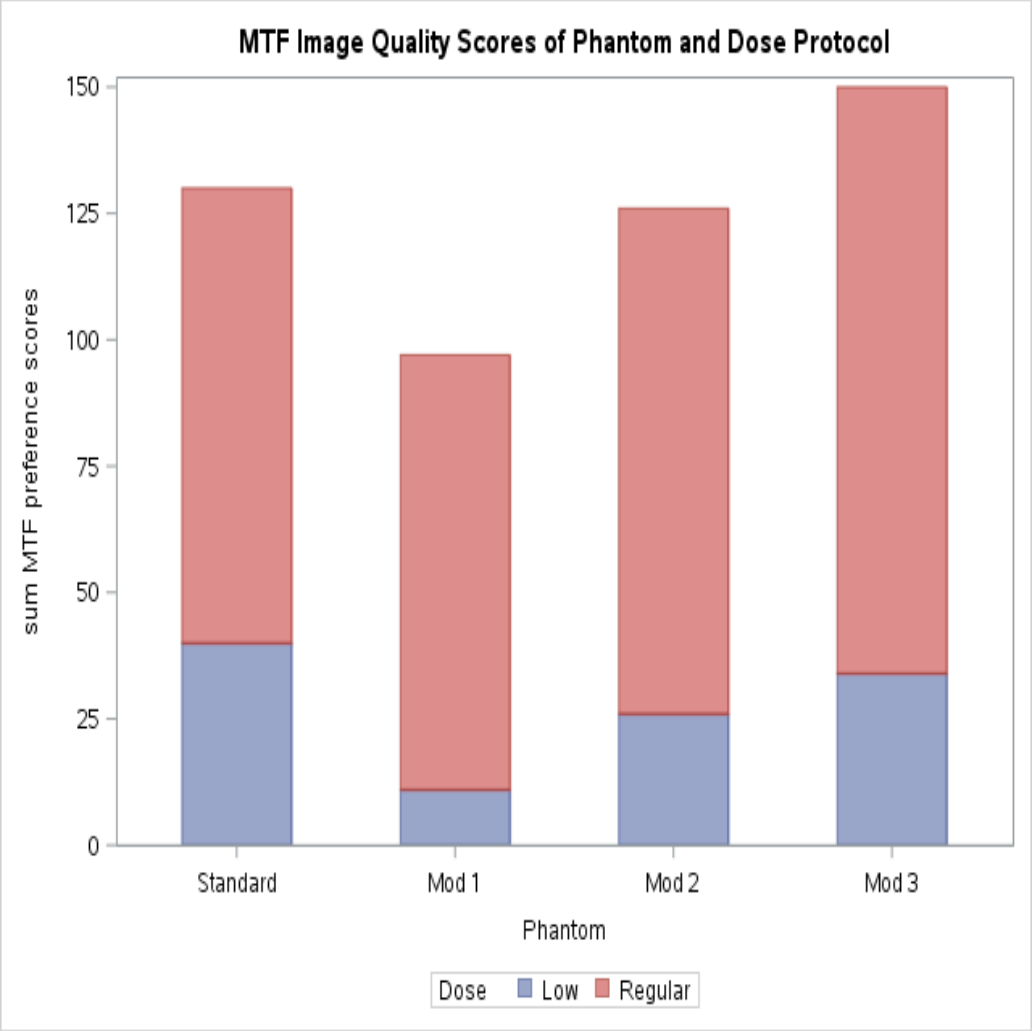

Figure 37: MTF image quality score of phantom and dose protocol

Dose protocol was a significant predictor of image quality preference associated with MTF. LDLR was negatively correlated with images that had a higher MTF. Of the phantom modifications, Mod 1 is negatively correlated with the MTF preference scores. The FOVs that were correlated with significant predictors of preference scores associated with higher MTF values were the 10 x 10, 17 x 6, 17 x 11 cm FOVs. All of the FOVS listed are positively correlated with the MTF scores

Table 27: Stepwise selection method analysis effects eligible for entry
Analysis of Effects Eligible for Entry

Effect	DF	Score Chi-Square	Pr > ChiSq
Phantom	3	16.11	0.0011
FOV	4	11.54	0.0211
Dose	1	0.09	0.76

A stepwise selection method was applied to remove any insignificant variables from the model before adding a significant variable to the model. Prior to the first step, the intercept-only model was fit and individual score statistics for the potential variables were evaluated.

Table 28: Summary of stepwise selection method

Step	Entered	Removed	DF	Number In	Score Chi-Square	Wald Chi-Square	Pr > ChiSq	Variable Label
1	phantom		3	1	16.1111		0.0011	Phantom
2	FOV_C		4	2	12.2533		0.0156	FOV C

In step 1, the variable phantom is selected into the model since it is the most significant variable among those to be chosen (p value = 0.0011). In step 2, the variable FOV_C is added to the model since both Phantom and FOV_C remains significant. There is no evidence that FOV_A, Dose_A and Dose_C is related to the agreement.

Table 29: Stepwise analysis of effects

Type 3 Analysis of Effects

Effect	DF	Wald Chi-Square	Pr > ChiSq
Phantom	3	16.11	0.0016
FOV	4	11.54	0.0195

The null hypothesis of what drives the agreement between the observers was that there was no association between the predictors (phantom, FOV) and the response (agreements). The type 3 analysis below shows that both phantom and FOV_c is significant. Therefore, we reject H_0. Phantom has a strong association with the agreement, FOV_c has some association with agreement. The null hypothesis was rejected because the phantom has a strong association with the agreement and the FOV has a strong association with the agreement.

Table 30: Phantom as a predictor of observer agreement
Analysis of Maximum Likelihood Estimates

Phantom	Standard Error	Wald Chi-Square	Pr > ChiSq
Standard	0.28	2.89	0.09
Mod 1	0.27	1.50	0.22
Mod 2	0.28	0.01	0.90
Mod 3	0.33	11.69	0.0006

Table 31: Number of agreement/disagreement between observers

Agreement

Phantom	Agree (*N*=108)	Disagree (*N*=72)	Total (*N*=180)
Standard	19 (42.2)	26 (57.8)	45 (25.0)
Mod 1	24 (53.3)	21 (46.7)	45 (25.0)
Mod 2	28 (62.2)	17 (37.8)	45 (25.0)
Mod 3	37 (82.2)	8 (17.8)	45 (25.0)

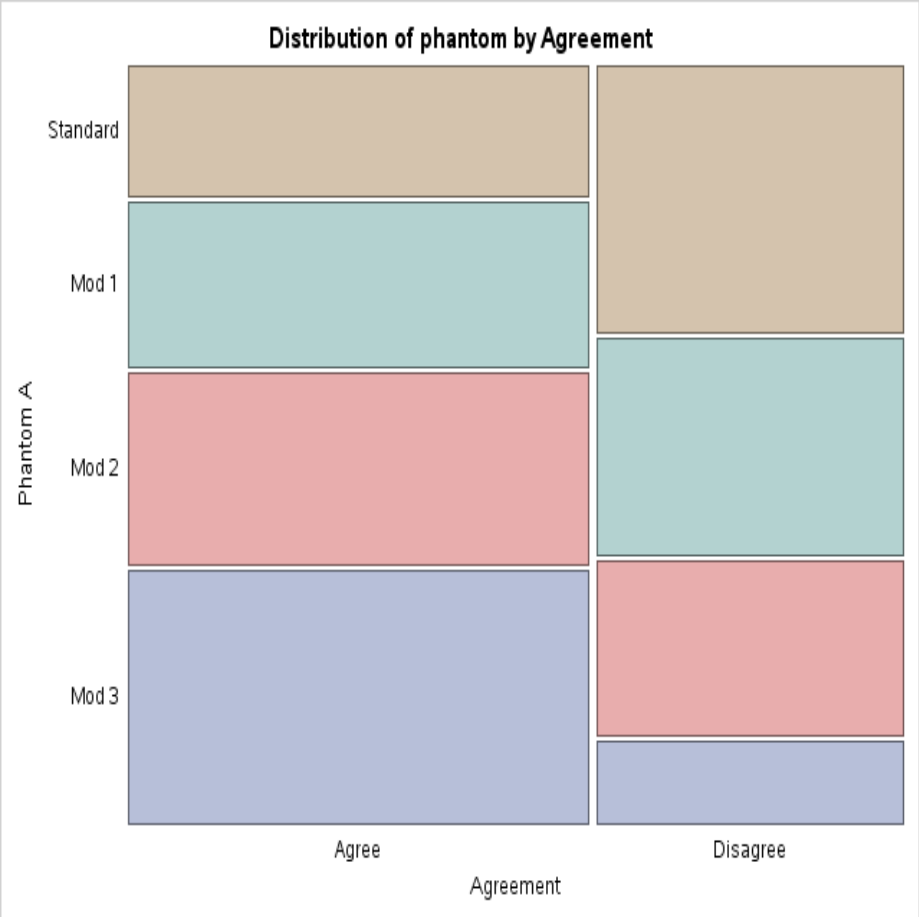

Figure 38: Phantom and agreement distribution

The estimated proportion for the agreement (agree) increases with the phantom. Modification 3 has the highest proportion with an 82.2% agreement between two observers.

Table 32: FOV as a predictor of agreement

FOV (cm)	DF	Standard Error	Wald Chi-Square	Pr > ChiSq
8x8	1	0.69	3.74	0.053
10x5	1	0.39	3.28	0.07
10x10	1	0.36	0.51	0.48
17x6	1	0.97	0.59	0.44
17x11	1	0.46	1	0.31

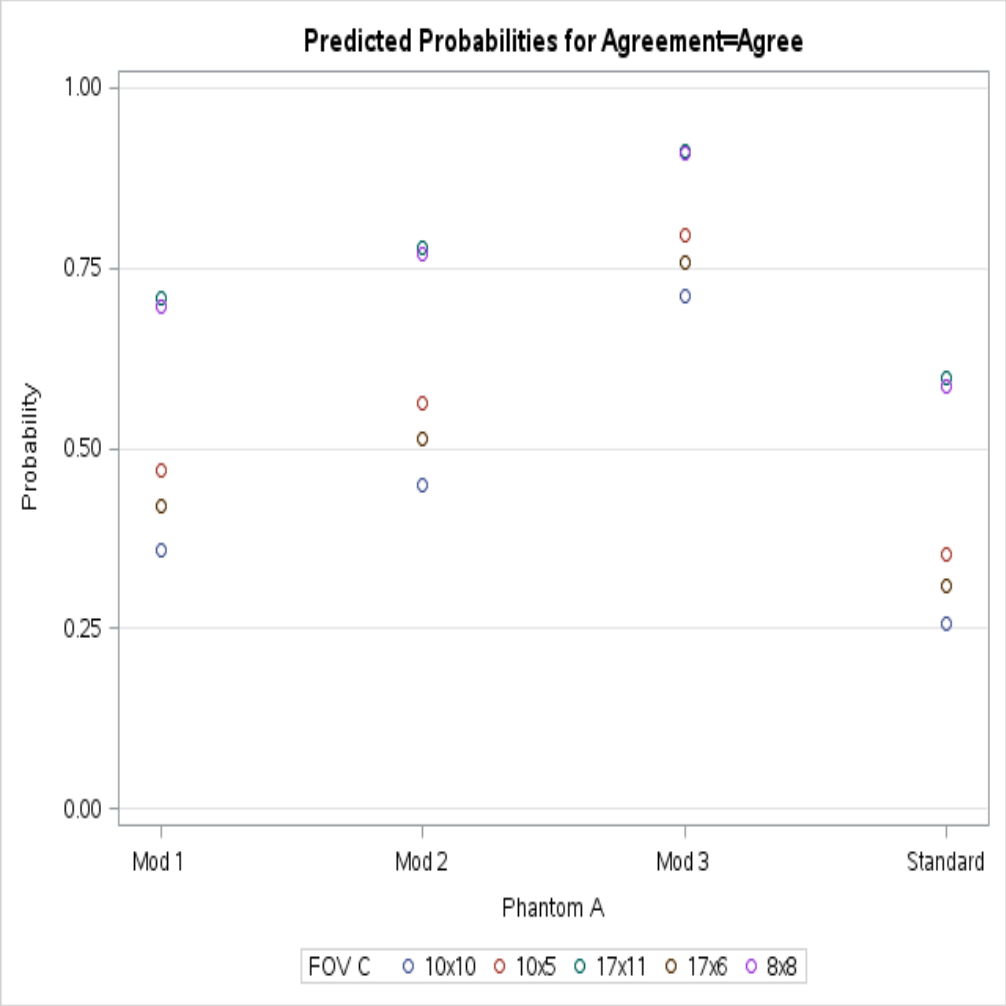

Figure 39: FOV and agreement distribution per phantom

The field of view was not a significant predictor of agreement between the two observers.

DISCUSSION AIM TWO

Subjective Image Quality

The SDSR used in this study was associated with higher observer preference scores. The SDSR had a higher kVp, mAs, and smaller voxel size when compared to the LDLR used in this study. Other studies show similar results. For example, a study by Kwong and co-workers showed that observers ranked the diagnostic quality of images more favorably with higher mAs and higher kVp settings [26]. While subjective perception of image quality of certain diagnostic tasks may show that diagnosticians refer images with higher dose settings, objective measures show that dose can be reduced without loss of diagnostic quality such as in evaluation of paranasal sinuses [54].

Noise is an important influencing factor for the ability to see contrast differences. The influence of noise is mostly seen when looking at anatomical structures with low contrast (low contrast structures like the brain or soft tissue in periodontal imaging) [55]. Bone is a high contrast structure. Diagnostic capabilities of CBCT are largely high contrast structures/high contrast imaging. Therefore, noise may affect CNR more than spatial resolution in CBCT imaging.

The modifications one and three image quality phantom volumes were reoriented prior to analysis. The anthropomorphic phantom volumes were not reoriented prior to observer sessions.

This may have affected the results. However, the images were acquired in the same orientation, and this may not have as much effect on the results as originally expected/anticipated.

The anatomic areas of interest simulate the location of the test tool location and orientation of the image quality phantoms. There was not statistically significant strength of preference when looking at the anatomic features for the images. This may be due to the anatomy being easy to identify in all images as this was evaluated preference and not a specific diagnostic task. The purpose of the scoring system was to get an overall estimate on what the observers preferred or did not prefer. However, this study did not specifically ask the observers to decide between anatomic structures. For example, the observers did not compare the lateral pterygoid plate to the mental foramen.

When the voxel size is larger than the size of the object being imaged, an artifact called partial volume averaging can occur. For example, partial volume averaging can be a limitation in resolution of small or thin structures in the temporal bone[56]. The anatomy that was selected for the observer sessions was large enough that partial volume averaging did not have much of an effect, if any at all. However, for specific diagnostic tasks, a smaller voxel size may be indicated [57-59]. Spatial resolution is reduced more commonly in regions where the surfaces change rapidly in the Z direction [30]. The Z direction is along the axis of the slice thickness direction, which in the case of CBCT is most likely in the axial plane. For the observer sessions, the anatomy that would have changed the most in the Z direction would have been the mental foramen, and the anatomy that would have changed the least would be the hard palate in the coronal view. The observer session scores do not reflect a significant change in the scores for these and that may have had little effect on the subjective image quality.

Cone beam artifact appears as a peripheral V-shaped artifact decreased capture of peripheral structures compared to structures in the center of the volume and in a horizontal plane [60]. The test tools of modifications two and three were at the periphery of the volume compared to the standard and modification one phantom. Modification three at LDLR had the lowest mean MTF for all FOVs. This was not true for the MTF of modification three at SDSR. If reducing the FOV to the ROI reduces cone-beam effect, one would expect the 8x8 cm FOV to have the highest MTF overall. However, the 17x6cm FOV modification three at SDSR had the highest MTF. This is suggestive that dose protocol had more effect on cone beam artifact than the FOV for this study on observer preference and that observer preference was associated with images with a higher MTF. Another study by et al compared different FOVs for specific imaging tasks. Smaller FOVs (3 x 4 cm) were associated with a higher decision level for implant planning while larger FOVs (6 x 6 cm) were associated with a higher decision level for periapical diagnosis [61]. All FOVs used in that study were smaller than the FOVs used in this study but do show that there could be an association between observer preference for imaging and the diagnostic task.

Additional sources of noise for CBCT imaging include inhomogeneity of the x-ray beam (quantum mottle) and electronic noise (added noise of detector system). Inhomogeneity of the x-ray beam depends upon the primary and scattered x-rays absorbed, the primary and scattered x-ray spectra incident on the detector, and the number of basis projections. Electronic noise is due to the inherent degradation of the detector system related to the x-ray absorption efficiency at the detector.

The CS9300 CBCT unit uses a flat panel detector (FPD). FPD is an indirect imaging system in which a solid-state sensor panel is coupled with an x-ray scintillator layer. Inherent FPD-based artifacts could have affected the image quality. Saturation (nonlinear pixel effects

above a certain exposure), dark current (charge that accumulates over time (with or without exposure), and bad pixels (pixels that do not react to exposure) contribute to nonlinearity. In addition, the sensitivity of different regions of the panel to radiation (pixel-to-pixel gain variation) may not be uniform over entire region [62]. The homogeneity differed both within and between phantoms, field of view, and dose. This may have been due to photon flux and inherent FPD-based artifacts. This should have affected each volume acquired similarly because the volumes were averaged. Factors affecting detector resolution are electronic noise, diffusion of photons in the scintillator coating, and potentially imperfect coupling with the scintillator, the fiber optic screen, and the photodetector. Clinical spatial resolution depends upon the detector and the focal spot size, the source-to-object distance, and the object-to-image distance.

Focal spot size impacts spatial resolution. The larger the focal spot size, the lower the spatial resolution and vice versa. The focal spot size for CBCT units is usually fixed; the smaller the focal spot size, the greater the cost of the CBCT unit. The focal spot size for the CS9300 unit is 7 um.

The source-to-object and object-to-receptor distance impacts spatial resolution. Generally the longer the source-to-object and shorter object-to-receptor distances are, the higher the spatial resolution. In CBCT imaging, there are limitations in manipulating these distances due to the size of the CBCT unit and because of patient positioning.

Patient movement was not a factor affecting spatial resolution in the study because all image quality phantoms and the anthropomorphic phantom did not move during image acquisition.

Underexposure of an image can result in a noisy appearance. Adjusting the mAs while maintaining the kVp may show the difference in noise without the difference in beam quality. Quantum mottle is due to photon flux.

The quantity of x-rays produced is controlled by mAs. In order to achieve optimal image quality, a receptor needs to have the proper exposure. In film, an overexposed image would appear too dark, and an underexposed image would appear too light. With digital imaging, as long as there is enough exposure, the computer algorithms can produce an image of diagnostic quality. However, proper amperage and time settings are important to have the optimal image quality and least amount of exposure to the patient.

Diagnostic information depends upon image characteristics that include the density/brightness, contrast, spatial resolution, and noise. Of the image characteristics, the observers seemed to prefer images with higher spatial resolution over images with higher CNR. Smaller voxel sizes (under 200 um) have been associated with higher accuracy for volumetric measurements when compared to larger voxel sizes (over 300 um) [63]. However in this study, accuracy was the same regardless of voxel size due to the high contrast and large anatomic structures identified. Other studies have shown that for specific diagnostic tasks, such as identifying mesiobuccal canals in maxillary molars, a higher spatial resolution improves detection [45]. Designing a study with specific imaging tasks at different voxel sizes could lead to a more clinically relevant recommendation for certain voxel size recommendations. This may have been due to the imaging task of identifying high contrast structures in which noise would have less of an impact on contrast and more of an impact on spatial resolution.

CONCLUSION

CNR improved for a peripherally positioned tilted test tool (Mod3). Reduced kVp and larger voxels appear to counteract the effect of reduced mAs producing improved CNR at LDLR. Image quality parameters are different at the center of a CBCT volume when compared to the periphery, depend on the orientation of the object, and vary as a function of kVp and voxel size. A LDLR employing a larger voxel size resulted in a reduction in MTF and an increase in CNR. Significant dose reductions may result in loss of image quality. However, reductions in image quality may be acceptable for certain diagnostic tasks.

Observers preferred images with higher MTF rather than higher CNR. Structures at the periphery of the volume and at an angle with respect to the axial plane were associated with lower preference overall. The FOV that resulted in higher preference overall was the 17 x 6 cm FOV.

APPENDIX

CNR STATISTICAL ANALYSIS

fov 2 and 3 and 4 without significant interaction

Class Level Information		
Class	**Levels**	**Values**
Phantom	4	1 2 3 4
Dose	2	1 2
FOV	5	1 2 3 4 5

Number of Observations Read	120
Number of Observations Used	120

Dependent Variable: CNR CNR

Source	DF	Sum of Squares	Mean Square	F Value	Pr > F
Model	27	5470.092845	202.596031	19.90	<.0001
Error	92	936.630258	10.180764		
Corrected Total	119	6406.723102			

R-Square	Coeff Var	Root MSE	CNR Mean
0.853805	19.33190	3.190731	16.50500

Source	DF	Type I SS	Mean Square	F Value	Pr > F
FOV	4	137.641331	34.410333	3.38	0.0126
Phantom	3	3206.040818	1068.680273	104.97	<.0001
Dose	1	1756.845645	1756.845645	172.57	<.0001
Phantom*FOV	12	172.563736	14.380311	1.41	0.1744
Dose*FOV	4	134.437775	33.609444	3.30	0.0142
Phantom*Dose	3	62.563540	20.854513	2.05	0.1126

Source	DF	Type III SS	Mean Square	F Value	Pr > F
FOV	4	137.641331	34.410333	3.38	0.0126
Phantom	3	3206.040818	1068.680273	104.97	<.0001
Dose	1	1756.845645	1756.845645	172.57	<.0001
Phantom*FOV	12	172.563736	14.380311	1.41	0.1744
Dose*FOV	4	134.437775	33.609444	3.30	0.0142
Phantom*Dose	3	62.563540	20.854513	2.05	0.1126

2way interaction model

FOV=1

Class Level Information		
Class	**Levels**	**Values**
Phantom	4	1 2 3 4
Dose	2	1 2

Number of Observations Read	24
Number of Observations Used	24

Dependent Variable: CNR CNR

FOV=1

Source	DF	Sum of Squares	Mean Square	F Value	Pr > F
Model	7	1416.492343	202.356049	30.54	<.0001
Error	16	106.025830	6.626614		
Corrected Total	23	1522.518173			

R-Square	Coeff Var	Root MSE	CNR Mean
0.930362	14.56304	2.574221	17.67640

Source	DF	Type I SS	Mean Square	F Value	Pr > F
Phantom	3	526.7145461	175.5715154	26.49	<.0001
Dose	1	794.7079595	794.7079595	119.93	<.0001
Phantom*Dose	3	95.0698378	31.6899459	4.78	0.0145

Source	DF	Type III SS	Mean Square	F Value	Pr > F
Phantom	3	526.7145461	175.5715154	26.49	<.0001
Dose	1	794.7079595	794.7079595	119.93	<.0001

Source	DF	Type III SS	Mean Square	F Value	Pr > F
Phantom*Dose	3	95.0698378	31.6899459	4.78	0.0145

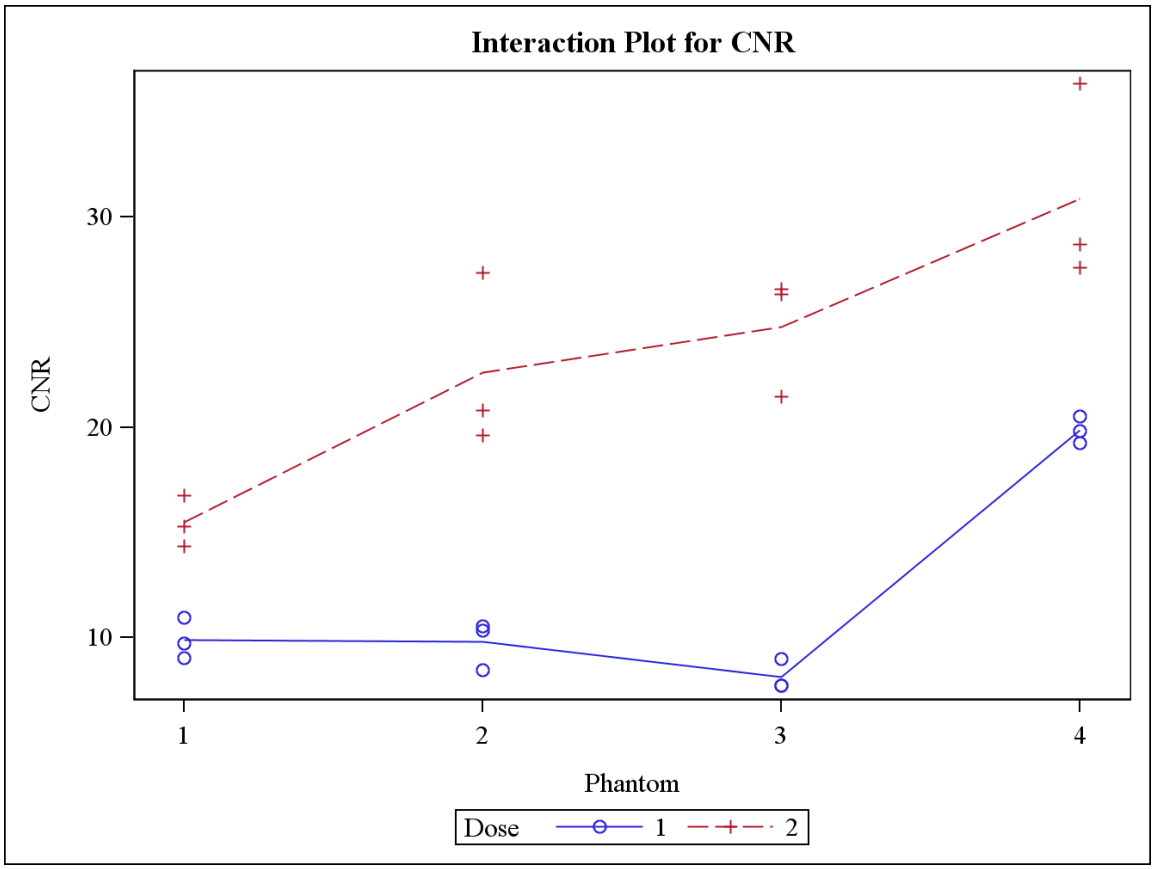

FOV=2

Class Level Information		
Class	Levels	Values
Phantom	4	1 2 3 4

Class Level Information		
Class	**Levels**	**Values**
Dose	2	1 2

Number of Observations Read	24
Number of Observations Used	24

Dependent Variable: CNR CNR

FOV=2

Source	DF	Sum of Squares	Mean Square	F Value	Pr > F
Model	7	842.2917196	120.3273885	17.18	<.0001
Error	16	112.0535324	7.0033458		
Corrected Total	23	954.3452519			

R-Square	Coeff Var	Root MSE	CNR Mean
0.882586	15.94494	2.646384	16.59701

Source	DF	Type I SS	Mean Square	F Value	Pr > F
Phantom	3	458.6538395	152.8846132	21.83	<.0001
Dose	1	342.8535634	342.8535634	48.96	<.0001
Phantom*Dose	3	40.7843166	13.5947722	1.94	0.1637

Source	DF	Type III SS	Mean Square	F Value	Pr > F
Phantom	3	458.6538395	152.8846132	21.83	<.0001
Dose	1	342.8535634	342.8535634	48.96	<.0001
Phantom*Dose	3	40.7843166	13.5947722	1.94	0.1637

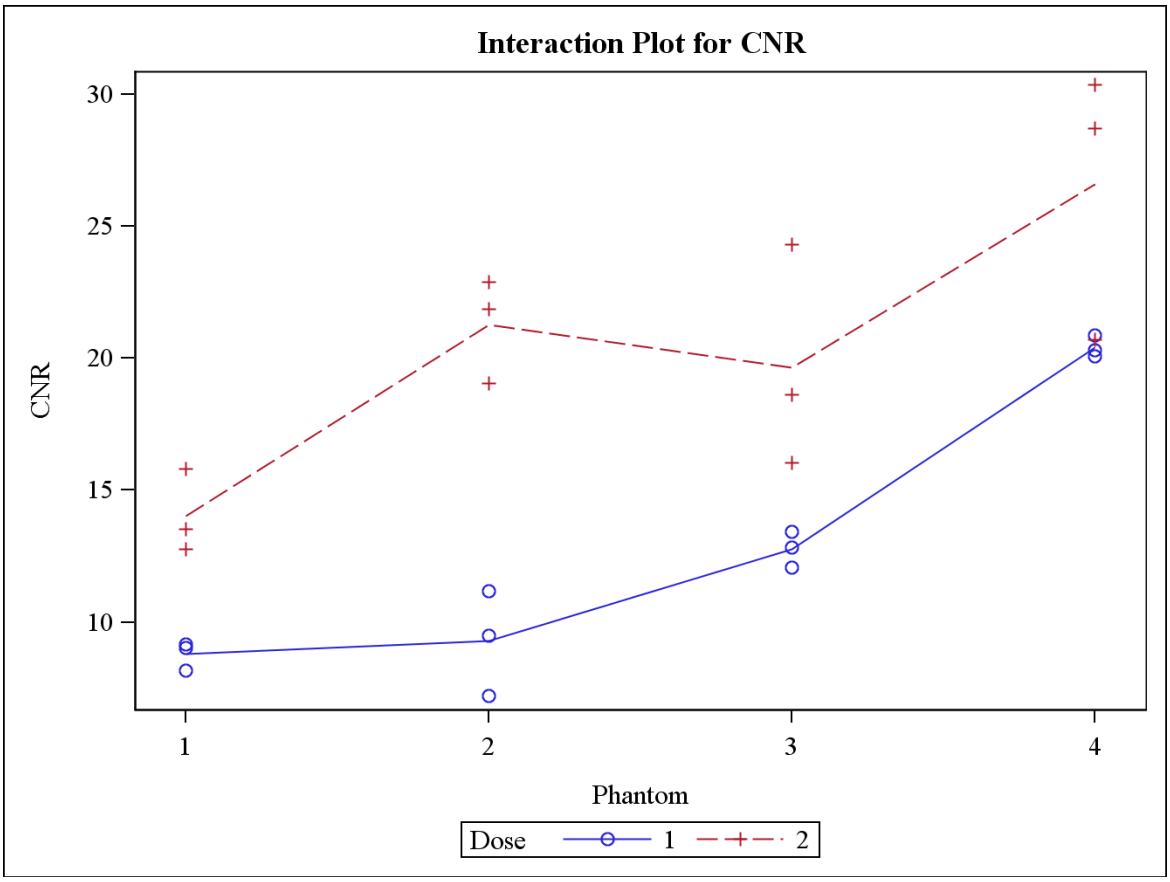

FOV=3

Class Level Information		
Class	**Levels**	**Values**
Phantom	4	1 2 3 4
Dose	2	1 2

Number of Observations Read	24

Number of Observations Used	24

Dependent Variable: CNR CNR

FOV=3

Source	DF	Sum of Squares	Mean Square	F Value	Pr > F
Model	7	1523.793228	217.684747	13.69	<.0001
Error	16	254.493823	15.905864		
Corrected Total	23	1778.287051			

R-Square	Coeff Var	Root MSE	CNR Mean
0.856888	22.76888	3.988216	17.51608

Source	DF	Type I SS	Mean Square	F Value	Pr > F
Phantom	3	1076.744355	358.914785	22.56	<.0001
Dose	1	361.807587	361.807587	22.75	0.0002
Phantom*Dose	3	85.241285	28.413762	1.79	0.1903

Source	DF	Type III SS	Mean Square	F Value	Pr > F
Phantom	3	1076.744355	358.914785	22.56	<.0001
Dose	1	361.807587	361.807587	22.75	0.0002
Phantom*Dose	3	85.241285	28.413762	1.79	0.1903

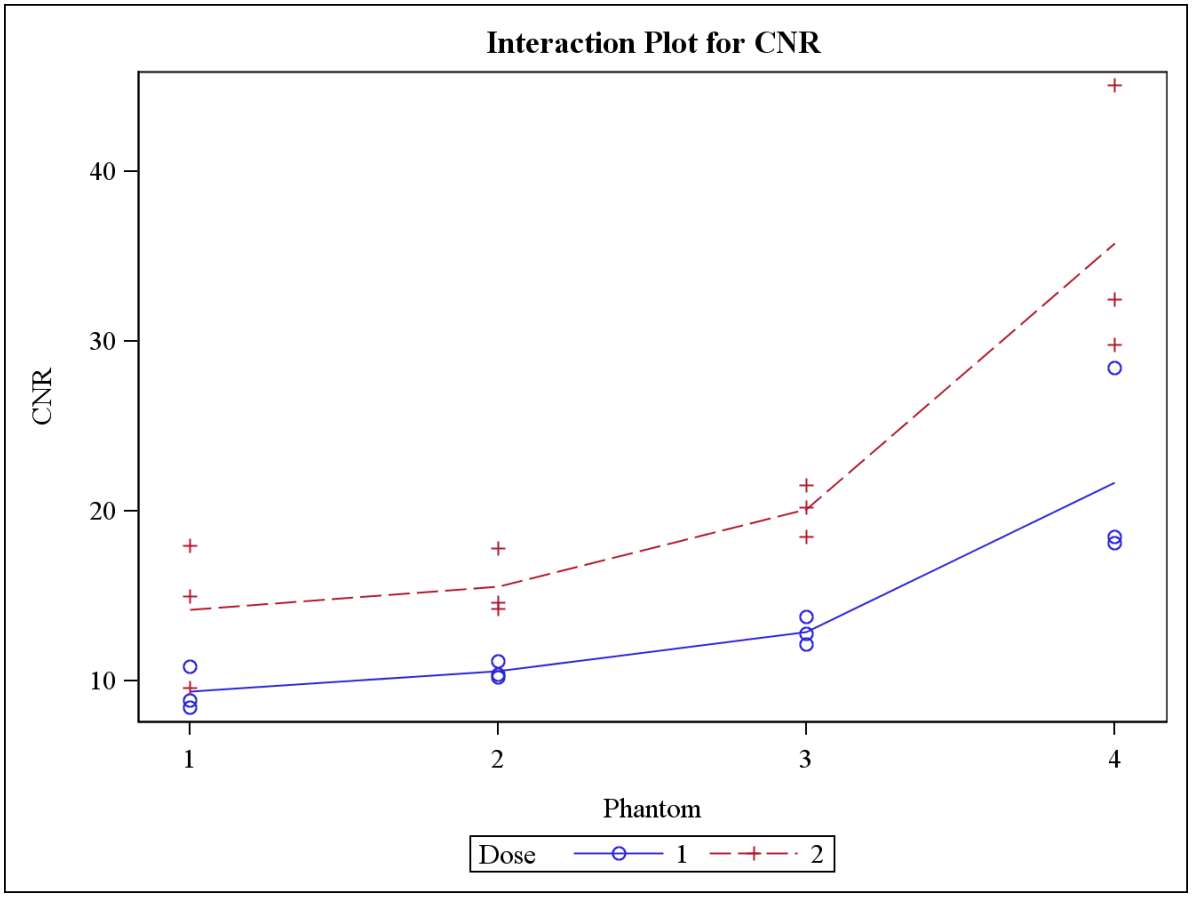

FOV=4

Class Level Information		
Class	**Levels**	**Values**
Phantom	4	1 2 3 4
Dose	2	1 2

Number of Observations Read	24
Number of Observations Used	24

Dependent Variable: CNR CNR

FOV=4

Source	DF	Sum of Squares	Mean Square	F Value	Pr > F
Model	7	579.4049520	82.7721360	9.89	<.0001
Error	16	133.8659153	8.3666197		
Corrected Total	23	713.2708673			

R-Square	Coeff Var	Root MSE	CNR Mean
0.812321	18.10277	2.892511	15.97828

Source	DF	Type I SS	Mean Square	F Value	Pr > F
Phantom	3	374.3074127	124.7691376	14.91	<.0001
Dose	1	192.9274214	192.9274214	23.06	0.0002
Phantom*Dose	3	12.1701179	4.0567060	0.48	0.6975

Source	DF	Type III SS	Mean Square	F Value	Pr > F
Phantom	3	374.3074127	124.7691376	14.91	<.0001
Dose	1	192.9274214	192.9274214	23.06	0.0002
Phantom*Dose	3	12.1701179	4.0567060	0.48	0.6975

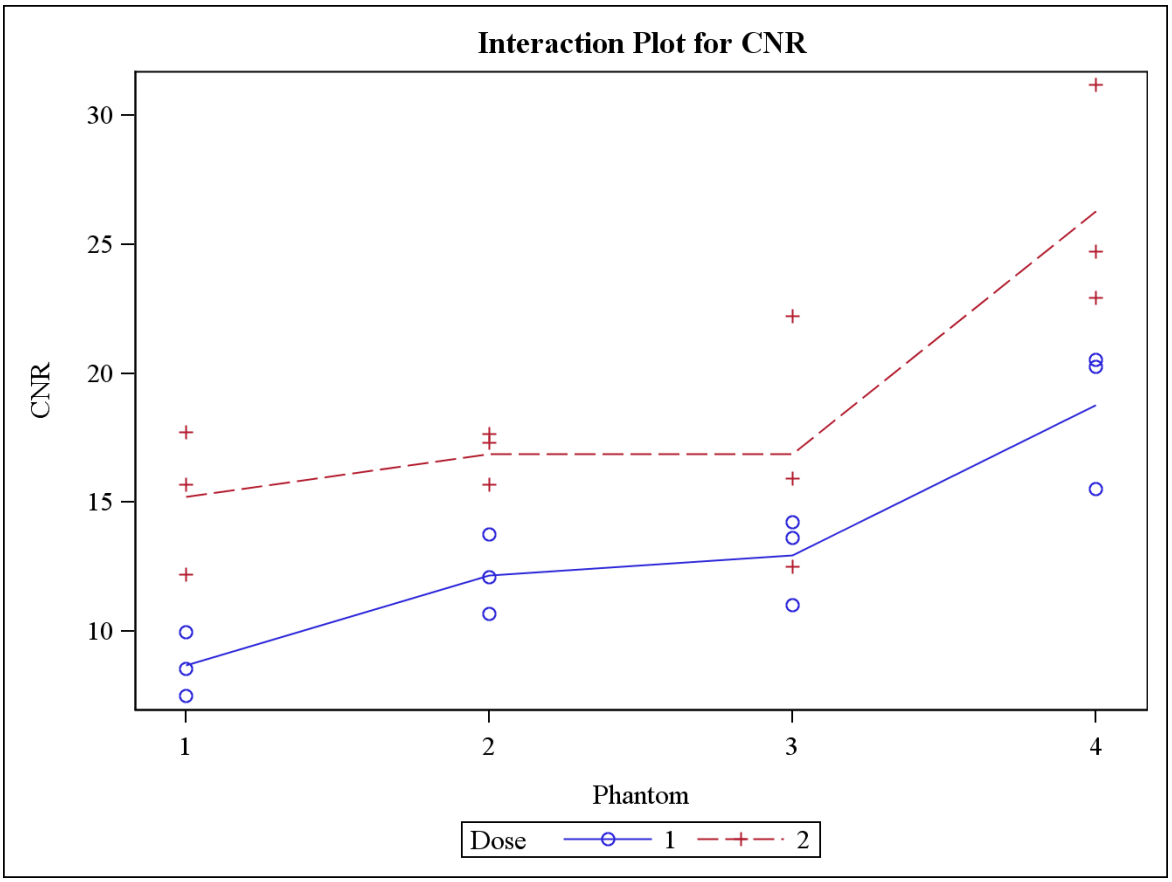

FOV=5

Class Level Information		
Class	**Levels**	**Values**
Phantom	4	1 2 3 4
Dose	2	1 2

Number of Observations Read	24

Number of Observations Used	24

Dependent Variable: CNR CNR

FOV=5

Source	DF	Sum of Squares	Mean Square	F Value	Pr > F
Model	7	1221.376661	174.482380	35.21	<.0001
Error	16	79.283768	4.955235		
Corrected Total	23	1300.660429			

R-Square	Coeff Var	Root MSE	CNR Mean
0.939043	15.08437	2.226036	14.75724

Source	DF	Type I SS	Mean Square	F Value	Pr > F
Phantom	3	942.1844014	314.0614671	63.38	<.0001
Dose	1	198.9868878	198.9868878	40.16	<.0001
Phantom*Dose	3	80.2053716	26.7351239	5.40	0.0093

Source	DF	Type III SS	Mean Square	F Value	Pr > F
Phantom	3	942.1844014	314.0614671	63.38	<.0001
Dose	1	198.9868878	198.9868878	40.16	<.0001
Phantom*Dose	3	80.2053716	26.7351239	5.40	0.0093

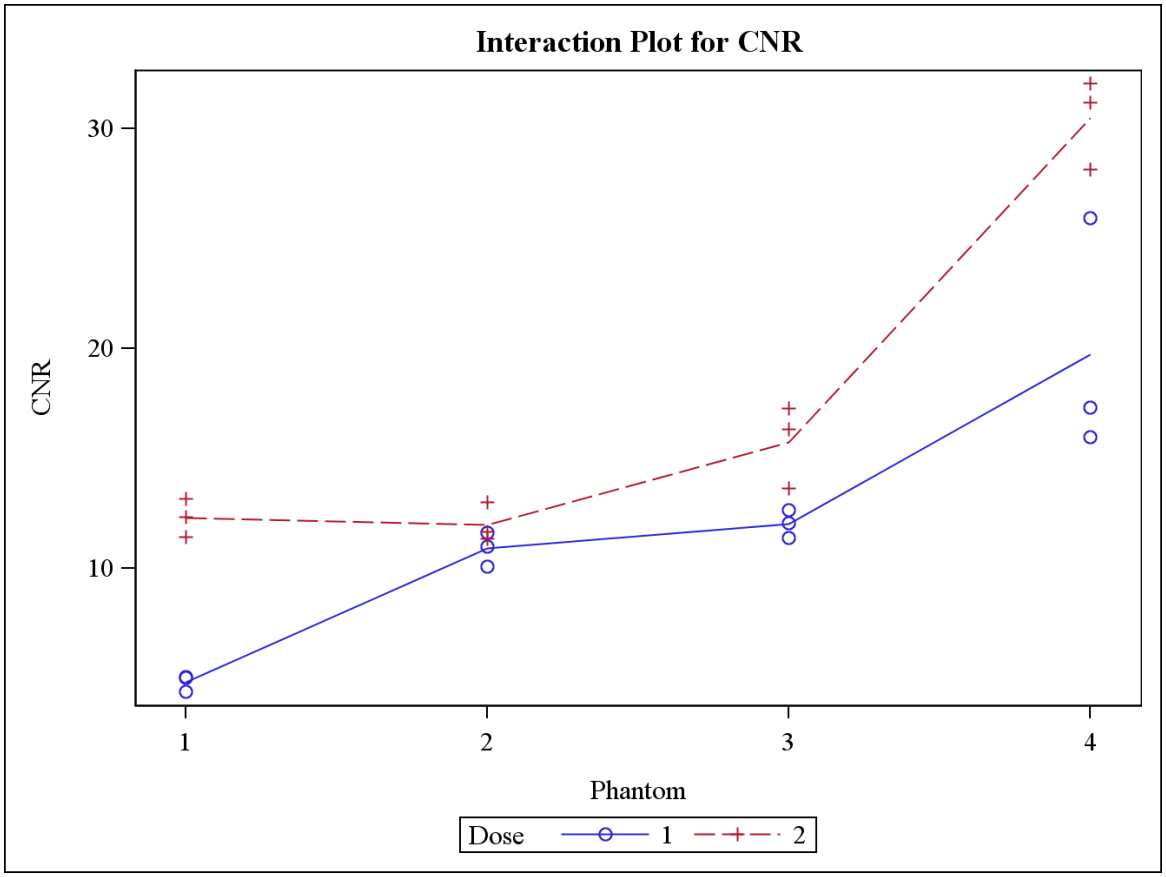

Fov 1 and 5 with significant interaction

FOV=1

Class Level Information		
Class	**Levels**	**Values**
Phantom	4	1 2 3 4
Dose	2	1 2

Number of Observations Read	24
Number of Observations Used	24

Dependent Variable: CNR CNR

FOV=1

Source	DF	Sum of Squares	Mean Square	F Value	Pr > F
Model	7	1416.492343	202.356049	30.54	<.0001
Error	16	106.025830	6.626614		
Corrected Total	23	1522.518173			

R-Square	Coeff Var	Root MSE	CNR Mean
0.930362	14.56304	2.574221	17.67640

Source	DF	Type I SS	Mean Square	F Value	Pr > F
Phantom	3	526.7145461	175.5715154	26.49	<.0001
Dose	1	794.7079595	794.7079595	119.93	<.0001
Phantom*Dose	3	95.0698378	31.6899459	4.78	0.0145

Source	DF	Type III SS	Mean Square	F Value	Pr > F
Phantom	3	526.7145461	175.5715154	26.49	<.0001
Dose	1	794.7079595	794.7079595	119.93	<.0001
Phantom*Dose	3	95.0698378	31.6899459	4.78	0.0145

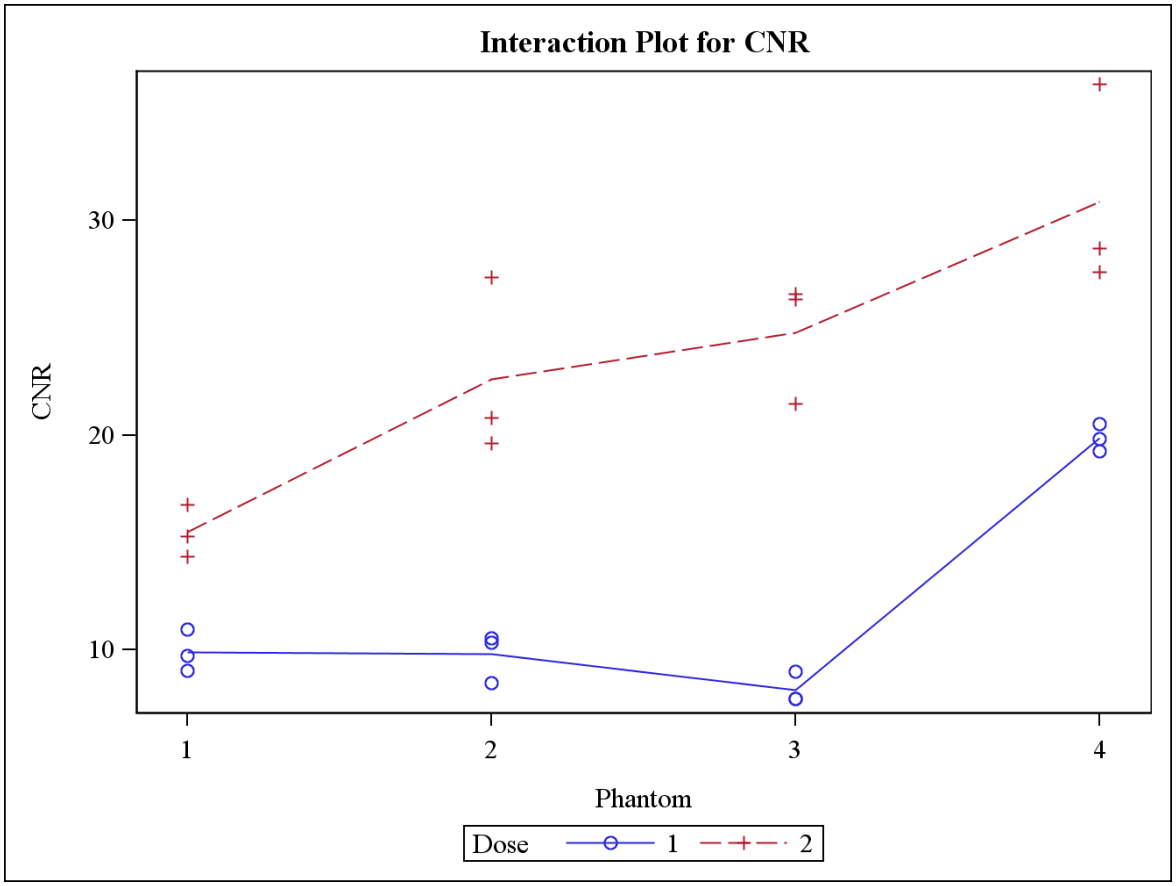

Least Squares Means

Adjustment for Multiple Comparisons: Tukey

FOV=1

Phantom	Dose	CNR LSMEAN	LSMEAN Number
1	**1**	9.8935556	1
1	**2**	15.4718889	2

Phantom	Dose	CNR LSMEAN	LSMEAN Number
2	**1**	9.7921111	3
2	**2**	22.5944444	4
3	**1**	8.1425556	5
3	**2**	24.7792222	6
4	**1**	19.8598889	7
4	**2**	30.8775556	8

Least Squares Means for effect Phantom*Dose

Pr > |t| for H0: LSMean(i)=LSMean(j)

Dependent Variable: CNR

i/j	1	2	3	4	5	6	7	8
1		0.2066	1.0000	0.0004	0.9882	<.0001	0.0042	<.0001
2	0.2066		0.1911	0.0573	0.0477	0.0078	0.4609	<.0001
3	1.0000	0.1911		0.0003	0.9916	<.0001	0.0038	<.0001
4	0.0004	0.0573	0.0003		<.0001	0.9606	0.8857	0.0201
5	0.9882	0.0477	0.9916	<.0001		<.0001	0.0009	<.0001
6	<.0001	0.0078	<.0001	0.9606	<.0001		0.3310	0.1372

Least Squares Means for effect Phantom*Dose Pr > |t| for H0: LSMean(i)=LSMean(j) Dependent Variable: CNR								
i/j	**1**	**2**	**3**	**4**	**5**	**6**	**7**	**8**
7	0.0042	0.4609	0.0038	0.8857	0.0009	0.3310		0.0016
8	<.0001	<.0001	<.0001	0.0201	<.0001	0.1372	0.0016	

Phantom	**Dose**	**CNR LSMEAN**	**95% Confidence Limits**	
1	**1**	9.893556	6.742895	13.044217
1	**2**	15.471889	12.321228	18.622550
2	**1**	9.792111	6.641450	12.942772
2	**2**	22.594444	19.443783	25.745105
3	**1**	8.142556	4.991895	11.293217
3	**2**	24.779222	21.628561	27.929883
4	**1**	19.859889	16.709228	23.010550
4	**2**	30.877556	27.726895	34.028217

Least Squares Means for Effect Phantom*Dose				
i	j	Difference Between Means	Simultaneous 95% Confidence Limits for LSMean(i)-LSMean(j)	
1	2	-5.578333	-12.855228	1.698562
1	3	0.101444	-7.175451	7.378340
1	4	-12.700889	-19.977784	-5.423994
1	5	1.751000	-5.525895	9.027895
1	6	-14.885667	-22.162562	-7.608772
1	7	-9.966333	-17.243228	-2.689438
1	8	-20.984000	-28.260895	-13.707105
2	3	5.679778	-1.597117	12.956673
2	4	-7.122556	-14.399451	0.154340
2	5	7.329333	0.052438	14.606228
2	6	-9.307333	-16.584228	-2.030438
2	7	-4.388000	-11.664895	2.888895
2	8	-15.405667	-22.682562	-8.128772
3	4	-12.802333	-20.079228	-5.525438
3	5	1.649556	-5.627340	8.926451
3	6	-14.987111	-22.264006	-7.710216

Least Squares Means for Effect Phantom*Dose				
i	j	Difference Between Means	Simultaneous 95% Confidence Limits for LSMean(i)-LSMean(j)	
3	**7**	-10.067778	-17.344673	-2.790883
3	**8**	-21.085444	-28.362340	-13.808549
4	**5**	14.451889	7.174994	21.728784
4	**6**	-2.184778	-9.461673	5.092117
4	**7**	2.734556	-4.542340	10.011451
4	**8**	-8.283111	-15.560006	-1.006216
5	**6**	-16.636667	-23.913562	-9.359772
5	**7**	-11.717333	-18.994228	-4.440438
5	**8**	-22.735000	-30.011895	-15.458105
6	**7**	4.919333	-2.357562	12.196228
6	**8**	-6.098333	-13.375228	1.178562
7	**8**	-11.017667	-18.294562	-3.740772

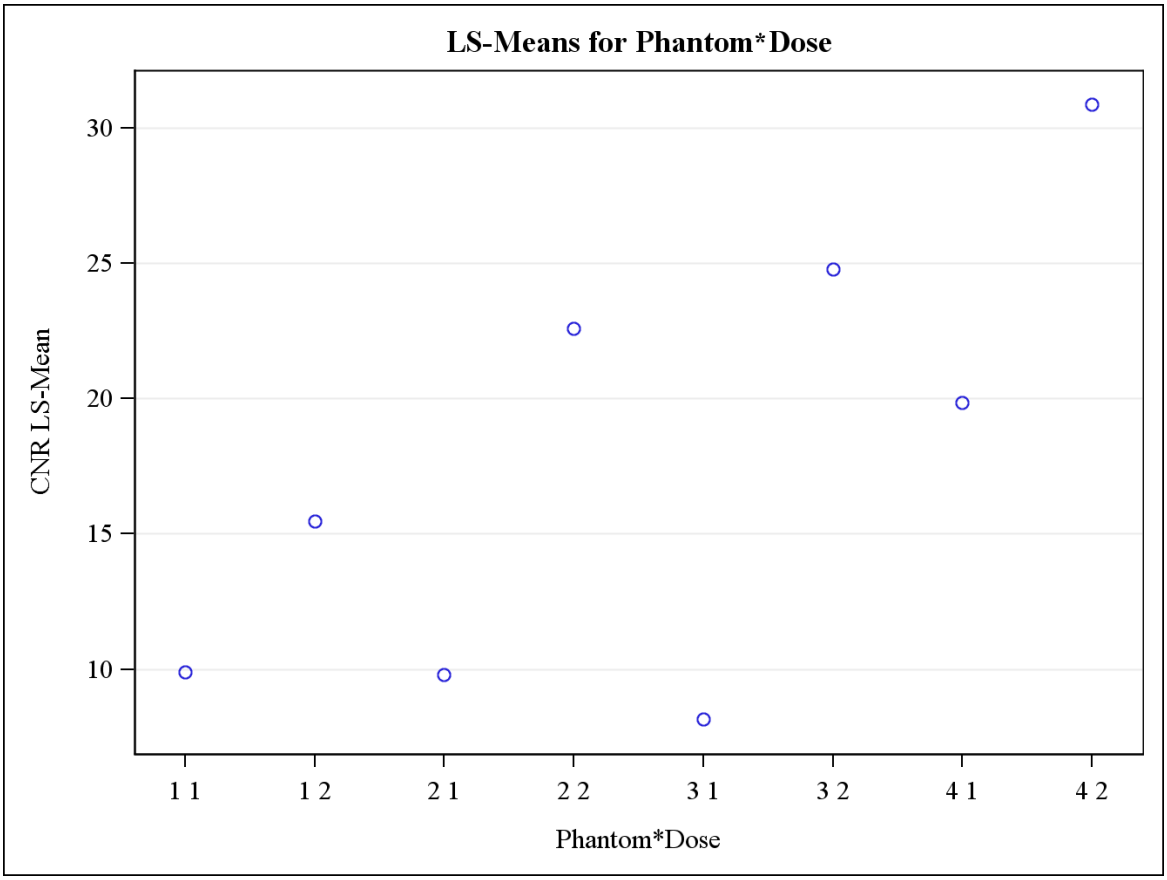
LS-Means for Phantom*Dose
CNR LS-Mean
30
25
20
15
10
1 1
1 2
2 1
2 2
3 1
3 2
4 1
4 2
Phantom*Dose

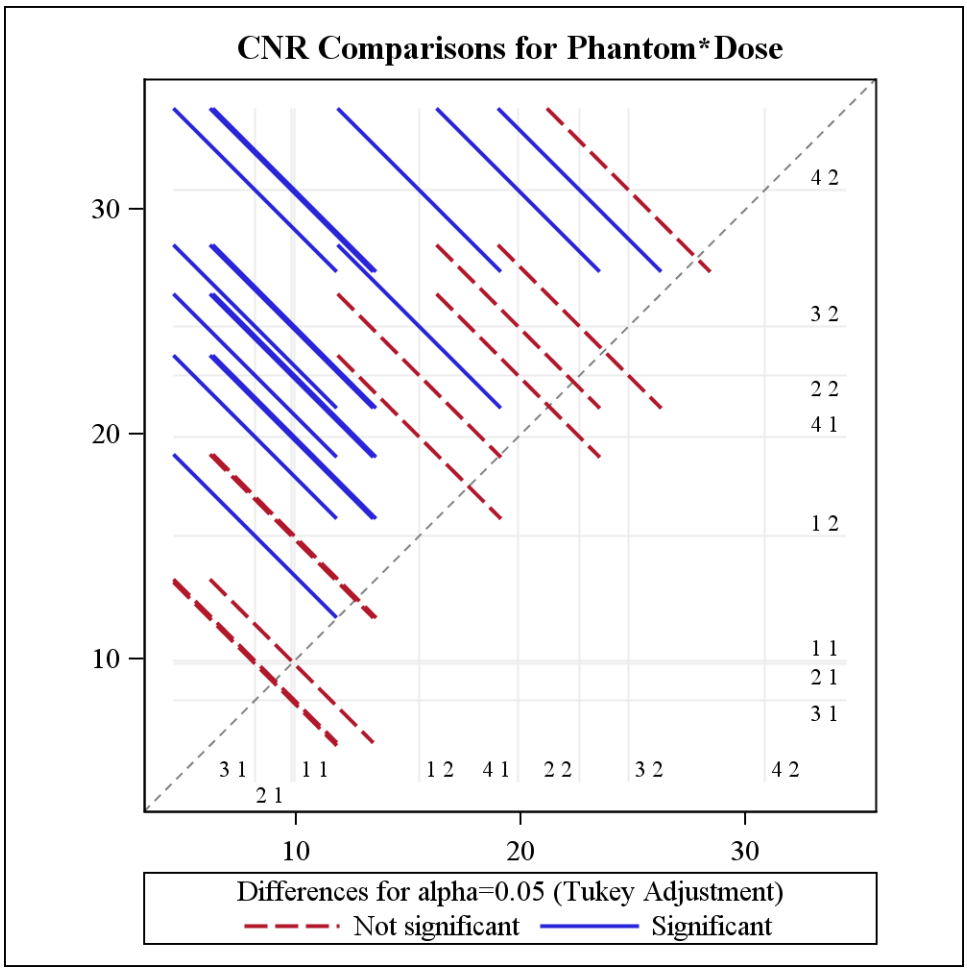

FOV=5

Class Level Information		
Class	**Levels**	**Values**
Phantom	4	1 2 3 4
Dose	2	1 2

Number of Observations Read	24
Number of Observations Used	24

Dependent Variable: CNR CNR

FOV=5

Source	DF	Sum of Squares	Mean Square	F Value	Pr > F
Model	7	1221.376661	174.482380	35.21	<.0001
Error	16	79.283768	4.955235		
Corrected Total	23	1300.660429			

R-Square	Coeff Var	Root MSE	CNR Mean
0.939043	15.08437	2.226036	14.75724

Source	DF	Type I SS	Mean Square	F Value	Pr > F
Phantom	3	942.1844014	314.0614671	63.38	<.0001
Dose	1	198.9868878	198.9868878	40.16	<.0001
Phantom*Dose	3	80.2053716	26.7351239	5.40	0.0093

Source	DF	Type III SS	Mean Square	F Value	Pr > F
Phantom	3	942.1844014	314.0614671	63.38	<.0001
Dose	1	198.9868878	198.9868878	40.16	<.0001
Phantom*Dose	3	80.2053716	26.7351239	5.40	0.0093

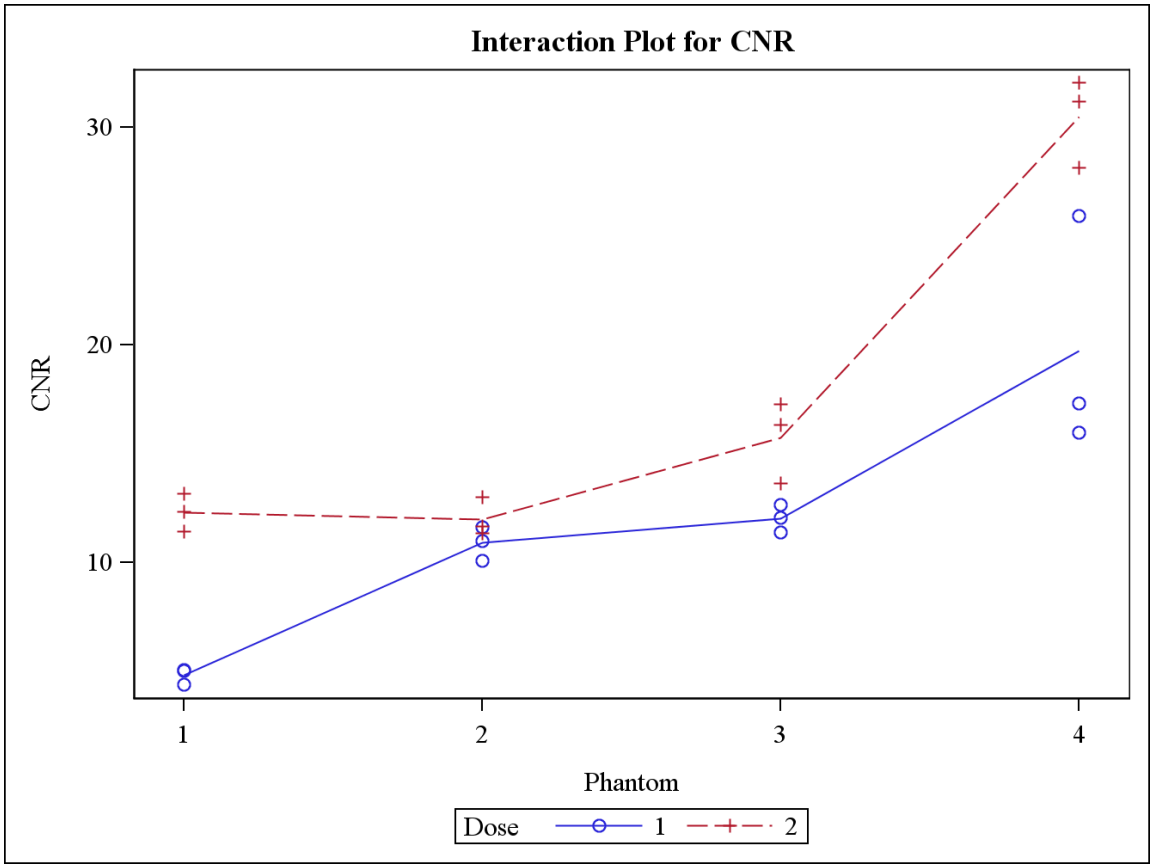

Least Squares Means

Adjustment for Multiple Comparisons: Tukey

FOV=5

Phantom	Dose	CNR LSMEAN	LSMEAN Number
1	**1**	4.8327778	1
1	**2**	12.3136667	2
2	**1**	10.8991111	3
2	**2**	12.0034444	4
3	**1**	12.0362222	5
3	**2**	15.7584444	6
4	**1**	19.7431111	7
4	**2**	30.4711111	8

Least Squares Means for effect Phantom*Dose

Pr > |t| for H0: LSMean(i)=LSMean(j)

Dependent Variable: CNR

i/j	1	2	3	4	5	6	7	8
1		0.0143	0.0630	0.0199	0.0192	0.0004	<.0001	<.0001
2	0.0143		0.9920	1.0000	1.0000	0.5721	0.0151	<.0001
3	0.0630	0.9920		0.9982	0.9979	0.2002	0.0033	<.0001

Least Squares Means for effect Phantom*Dose Pr > |t| for H0: LSMean(i)=LSMean(j) Dependent Variable: CNR								
i/j	**1**	**2**	**3**	**4**	**5**	**6**	**7**	**8**
4	0.0199	1.0000	0.9982		1.0000	0.4730	0.0108	<.0001
5	0.0192	1.0000	0.9979	1.0000		0.4832	0.0112	<.0001
6	0.0004	0.5721	0.2002	0.4730	0.4832		0.4043	<.0001
7	<.0001	0.0151	0.0033	0.0108	0.0112	0.4043		0.0005
8	<.0001	<.0001	<.0001	<.0001	<.0001	<.0001	0.0005	

Phantom	**Dose**	**CNR LSMEAN**	**95% Confidence Limits**	
1	**1**	4.832778	2.108270	7.557285
1	**2**	12.313667	9.589159	15.038174
2	**1**	10.899111	8.174604	13.623618
2	**2**	12.003444	9.278937	14.727952
3	**1**	12.036222	9.311715	14.760730
3	**2**	15.758444	13.033937	18.482952
4	**1**	19.743111	17.018604	22.467618

Phantom	Dose	CNR LSMEAN	95% Confidence Limits	
4	**2**	30.471111	27.746604	33.195618

Least Squares Means for Effect Phantom*Dose				
i	**j**	**Difference Between Means**	**Simultaneous 95% Confidence Limits for LSMean(i)-LSMean(j)**	
1	**2**	-7.480889	-13.773522	-1.188256
1	**3**	-6.066333	-12.358966	0.226300
1	**4**	-7.170667	-13.463300	-0.878034
1	**5**	-7.203444	-13.496078	-0.910811
1	**6**	-10.925667	-17.218300	-4.633034
1	**7**	-14.910333	-21.202966	-8.617700
1	**8**	-25.638333	-31.930966	-19.345700
2	**3**	1.414556	-4.878078	7.707189
2	**4**	0.310222	-5.982411	6.602855
2	**5**	0.277444	-6.015189	6.570078
2	**6**	-3.444778	-9.737411	2.847855

Least Squares Means for Effect Phantom*Dose				
i	j	Difference Between Means	Simultaneous 95% Confidence Limits for LSMean(i)-LSMean(j)	
2	7	-7.429444	-13.722078	-1.136811
2	8	-18.157444	-24.450078	-11.864811
3	4	-1.104333	-7.396966	5.188300
3	5	-1.137111	-7.429744	5.155522
3	6	-4.859333	-11.151966	1.433300
3	7	-8.844000	-15.136633	-2.551367
3	8	-19.572000	-25.864633	-13.279367
4	5	-0.032778	-6.325411	6.259855
4	6	-3.755000	-10.047633	2.537633
4	7	-7.739667	-14.032300	-1.447034
4	8	-18.467667	-24.760300	-12.175034
5	6	-3.722222	-10.014855	2.570411
5	7	-7.706889	-13.999522	-1.414256
5	8	-18.434889	-24.727522	-12.142256
6	7	-3.984667	-10.277300	2.307966
6	8	-14.712667	-21.005300	-8.420034

Least Squares Means for Effect Phantom*Dose				
i	j	Difference Between Means	Simultaneous 95% Confidence Limits for LSMean(i)-LSMean(j)	
7	8	-10.728000	-17.020633	-4.435367

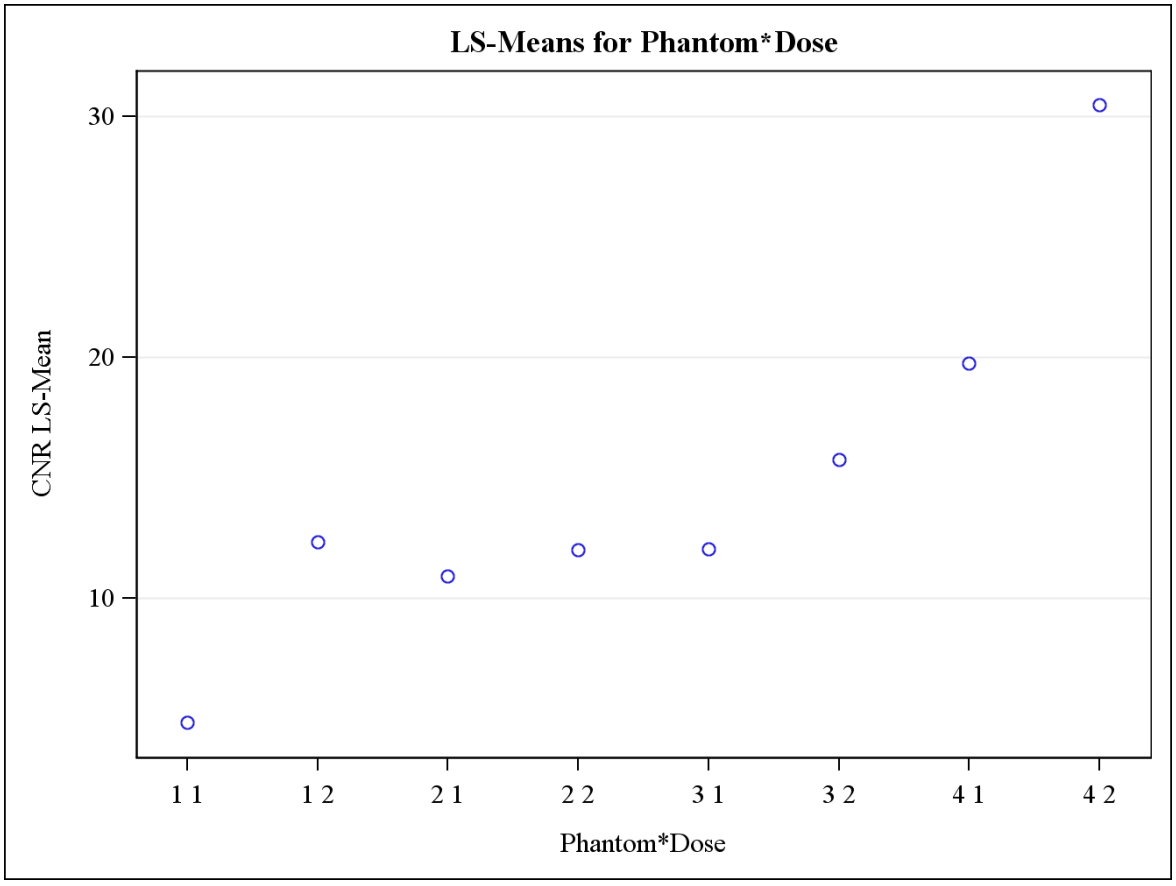

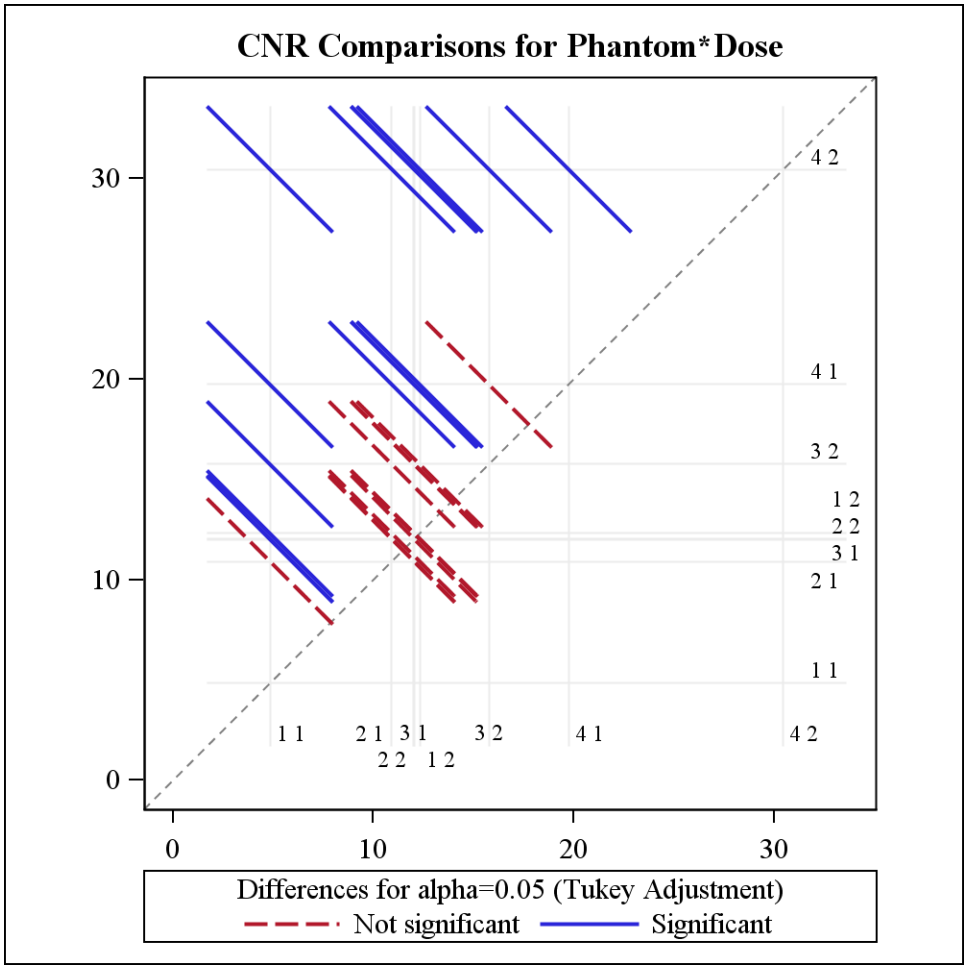
CNR Comparisons for Phantom*Dose
30
20
10
0
0
10
20
30
4 2
4 1
3 2
1 2
2 2
3 1
2 1
1 1
1 1
2 1
3 1
3 2
4 1
4 2
2 2
1 2
Differences for alpha=0.05 (Tukey Adjustment)
Not significant
Significant

fov 2 and 3 and 4 without significant interaction

FOV=2

Class Level Information		
Class	**Levels**	**Values**
Phantom	4	1 2 3 4
Dose	2	1 2

Number of Observations Read	24
Number of Observations Used	24

Dependent Variable: CNR CNR

FOV=2

Source	DF	Sum of Squares	Mean Square	F Value	Pr > F
Model	4	801.5074029	200.3768507	24.91	<.0001
Error	19	152.8378490	8.0440973		
Corrected Total	23	954.3452519			

R-Square	Coeff Var	Root MSE	CNR Mean
0.839851	17.08869	2.836212	16.59701

Source	DF	Type I SS	Mean Square	F Value	Pr > F
Phantom	3	458.6538395	152.8846132	19.01	<.0001
Dose	1	342.8535634	342.8535634	42.62	<.0001

Source	DF	Type III SS	Mean Square	F Value	Pr > F
Phantom	3	458.6538395	152.8846132	19.01	<.0001
Dose	1	342.8535634	342.8535634	42.62	<.0001

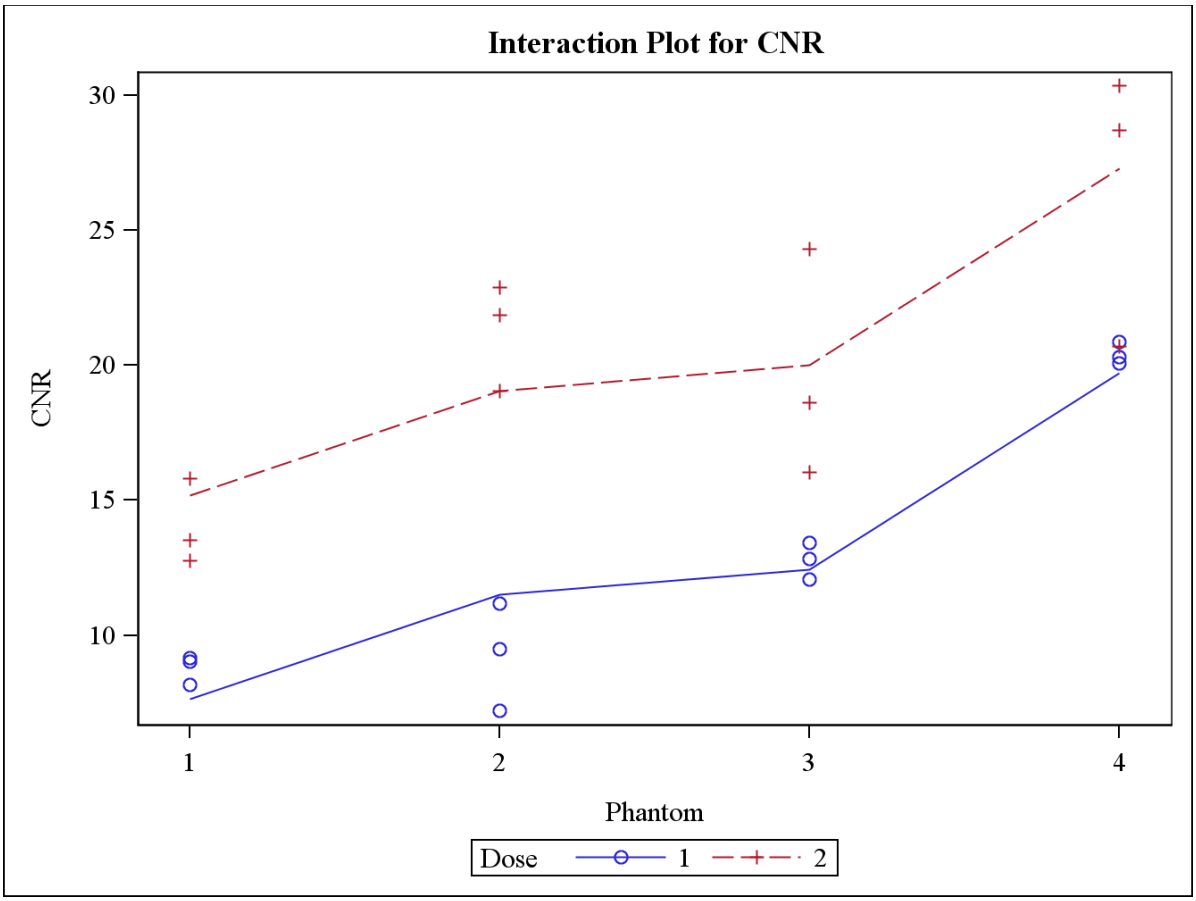

Least Squares Means

Adjustment for Multiple Comparisons: Tukey

FOV=2

Phantom	CNR LSMEAN	LSMEAN Number
1	11.4072778	1
2	15.2733333	2

Phantom	CNR LSMEAN	LSMEAN Number
3	16.2106111	3
4	23.4968333	4

Least Squares Means for effect Phantom Pr > |t| for H0: LSMean(i)=LSMean(j) Dependent Variable: CNR				
i/j	**1**	**2**	**3**	**4**
1		0.1193	0.0390	<.0001
2	0.1193		0.9391	0.0004
3	0.0390	0.9391		0.0014
4	<.0001	0.0004	0.0014	

Phantom	CNR LSMEAN	95% Confidence Limits	
1	11.407278	8.983810	13.830746
2	15.273333	12.849866	17.696801
3	16.210611	13.787143	18.634079

Phantom	CNR LSMEAN	95% Confidence Limits	
4	23.496833	21.073366	25.920301

Least Squares Means for Effect Phantom				
i	**j**	**Difference Between Means**	**Simultaneous 95% Confidence Limits for LSMean(i)-LSMean(j)**	
1	**2**	-3.866056	-8.470388	0.738277
1	**3**	-4.803333	-9.407666	-0.199001
1	**4**	-12.089556	-16.693888	-7.485223
2	**3**	-0.937278	-5.541610	3.667055
2	**4**	-8.223500	-12.827833	-3.619167
3	**4**	-7.286222	-11.890555	-2.681890

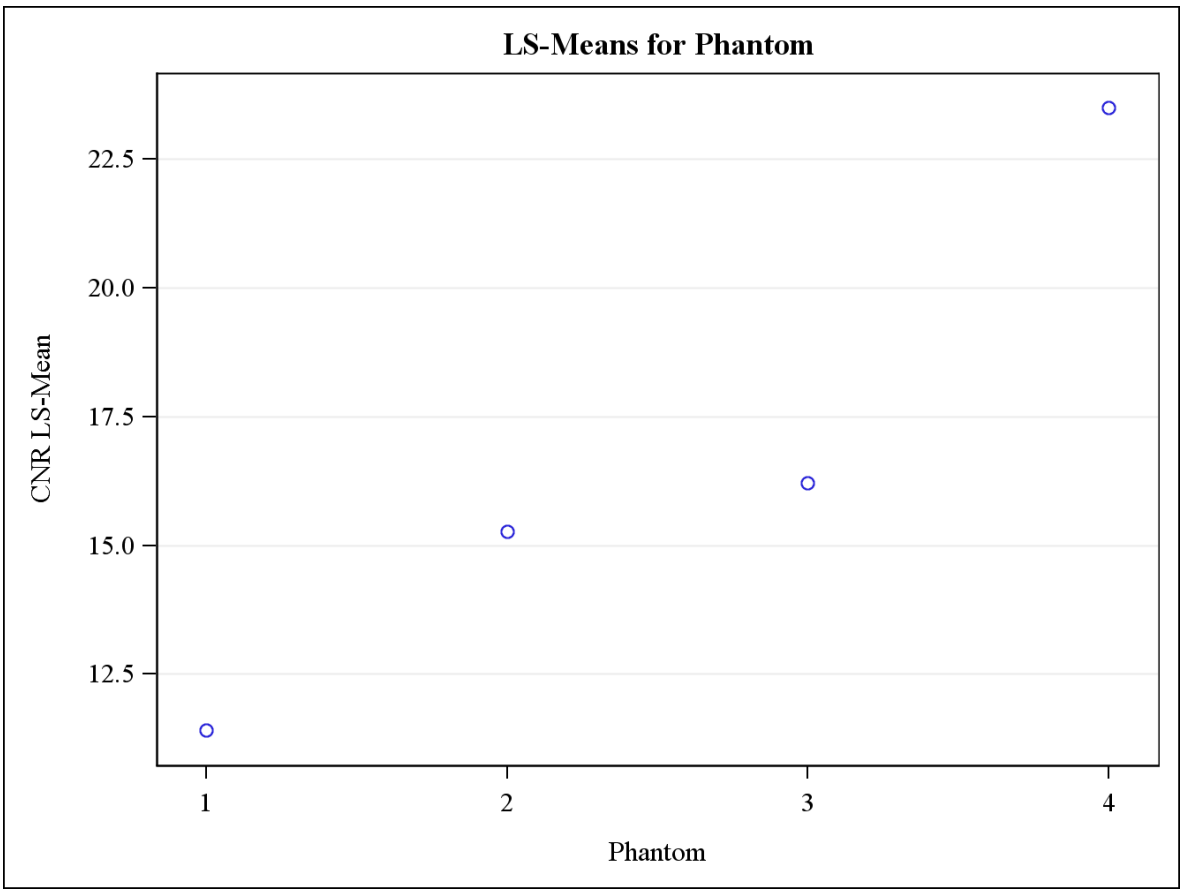
LS-Means for Phantom
CNR LS-Mean
22.5
20.0
17.5
15.0
12.5
1
2
3
4
Phantom

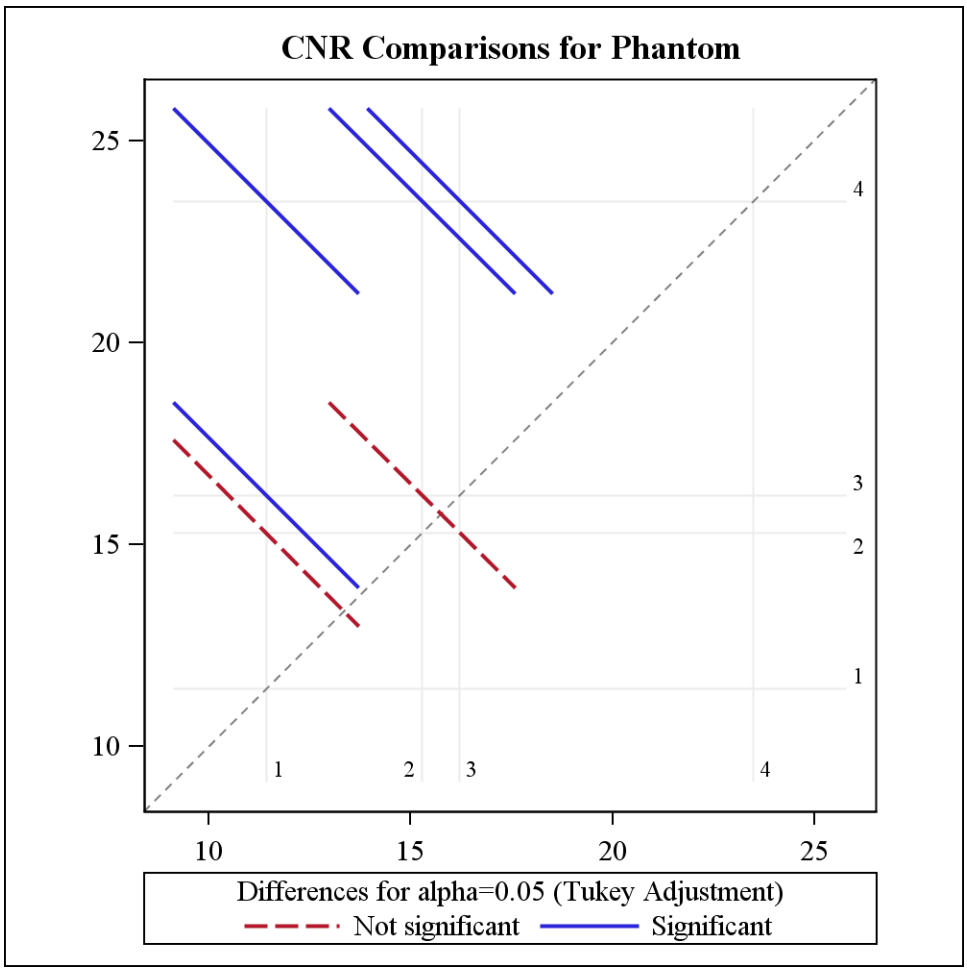

FOV=3

Class Level Information		
Class	**Levels**	**Values**
Phantom	4	1 2 3 4
Dose	2	1 2

Number of Observations Read	24
Number of Observations Used	24

Dependent Variable: CNR CNR

FOV=3

Source	DF	Sum of Squares	Mean Square	F Value	Pr > F
Model	4	1438.551943	359.637986	20.11	<.0001
Error	19	339.735108	17.880795		
Corrected Total	23	1778.287051			

R-Square	Coeff Var	Root MSE	CNR Mean
0.808954	24.14106	4.228569	17.51608

Source	DF	Type I SS	Mean Square	F Value	Pr > F
Phantom	3	1076.744355	358.914785	20.07	<.0001
Dose	1	361.807587	361.807587	20.23	0.0002

Source	DF	Type III SS	Mean Square	F Value	Pr > F
Phantom	3	1076.744355	358.914785	20.07	<.0001
Dose	1	361.807587	361.807587	20.23	0.0002

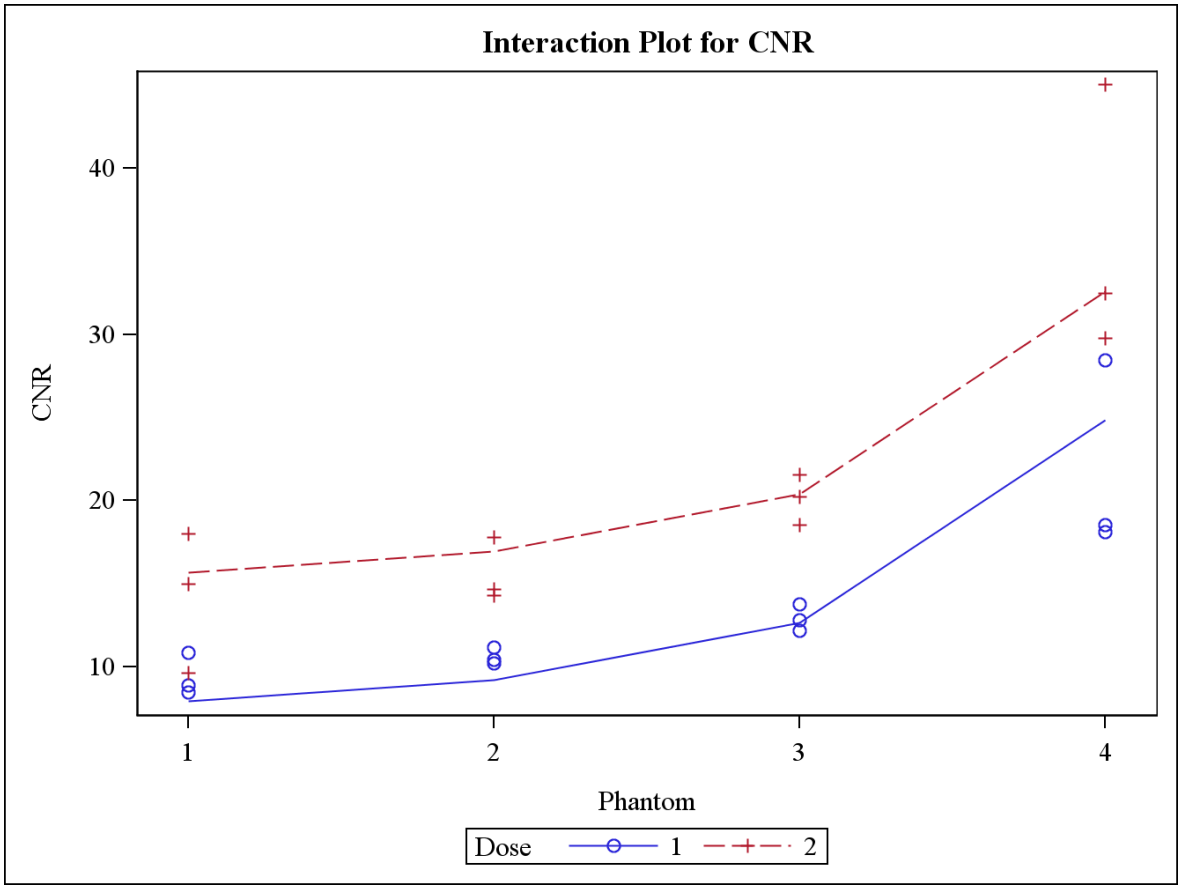

Least Squares Means

Adjustment for Multiple Comparisons: Tukey

FOV=3

Phantom	CNR LSMEAN	LSMEAN Number
1	11.7761667	1
2	13.0688333	2
3	16.4923333	3
4	28.7270000	4

Least Squares Means for effect Phantom Pr > |t| for H0: LSMean(i)=LSMean(j) Dependent Variable: CNR				
i/j	**1**	**2**	**3**	**4**
1		0.9508	0.2485	<.0001
2	0.9508		0.5132	<.0001
3	0.2485	0.5132		0.0004
4	<.0001	<.0001	0.0004	

Phantom	CNR LSMEAN	95% Confidence Limits	
1	11.776167	8.162967	15.389367
2	13.068833	9.455633	16.682033
3	16.492333	12.879133	20.105533
4	28.727000	25.113800	32.340200

Least Squares Means for Effect Phantom				
		Difference	Simultaneous 95% Confidence Limits for	
i	j	Between Means	LSMean(i)-LSMean(j)	
1	**2**	-1.292667	-8.157365	5.572032
1	**3**	-4.716167	-11.580865	2.148532
1	**4**	-16.950833	-23.815532	-10.086135
2	**3**	-3.423500	-10.288198	3.441198
2	**4**	-15.658167	-22.522865	-8.793468
3	**4**	-12.234667	-19.099365	-5.369968

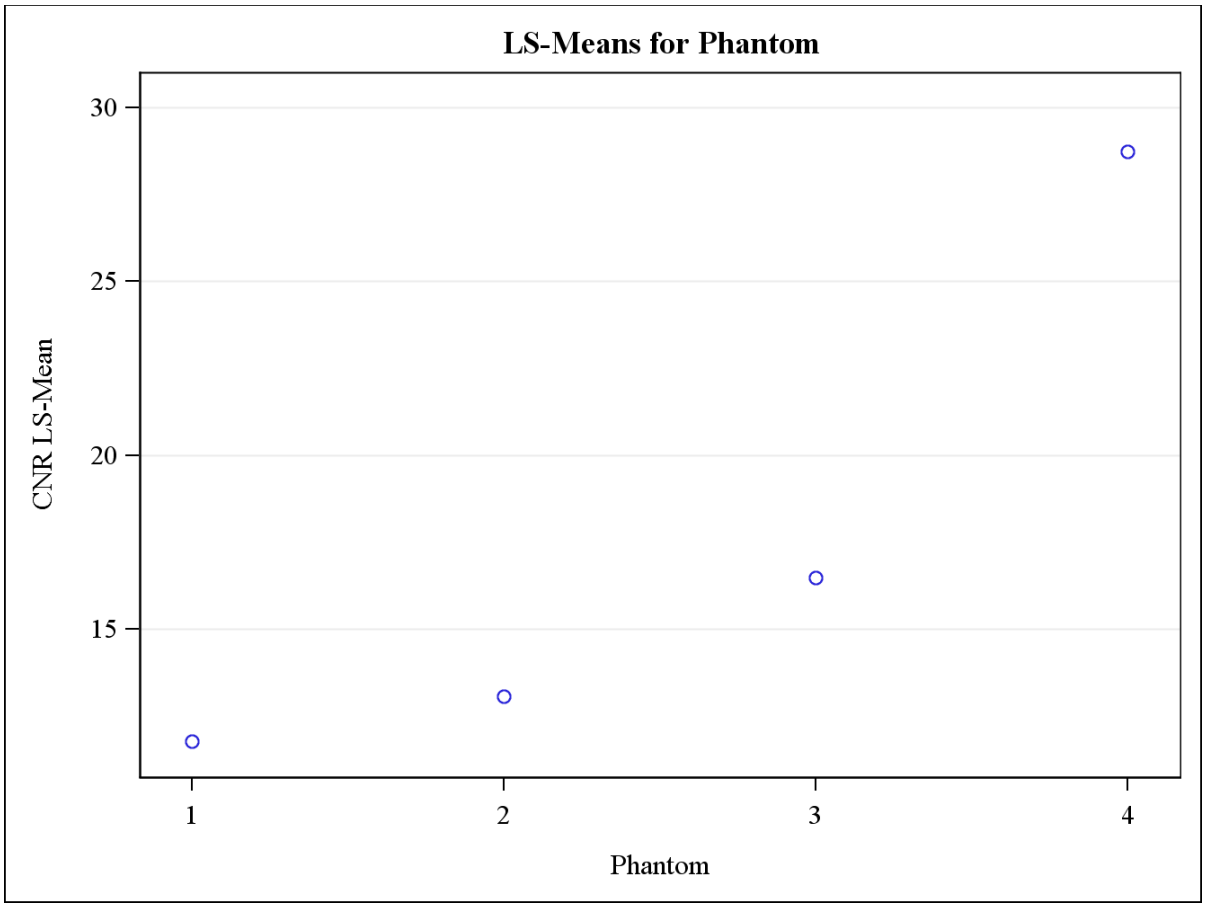
LS-Means for Phantom
CNR LS-Mean
30
25
20
15
1
2
3
4
Phantom

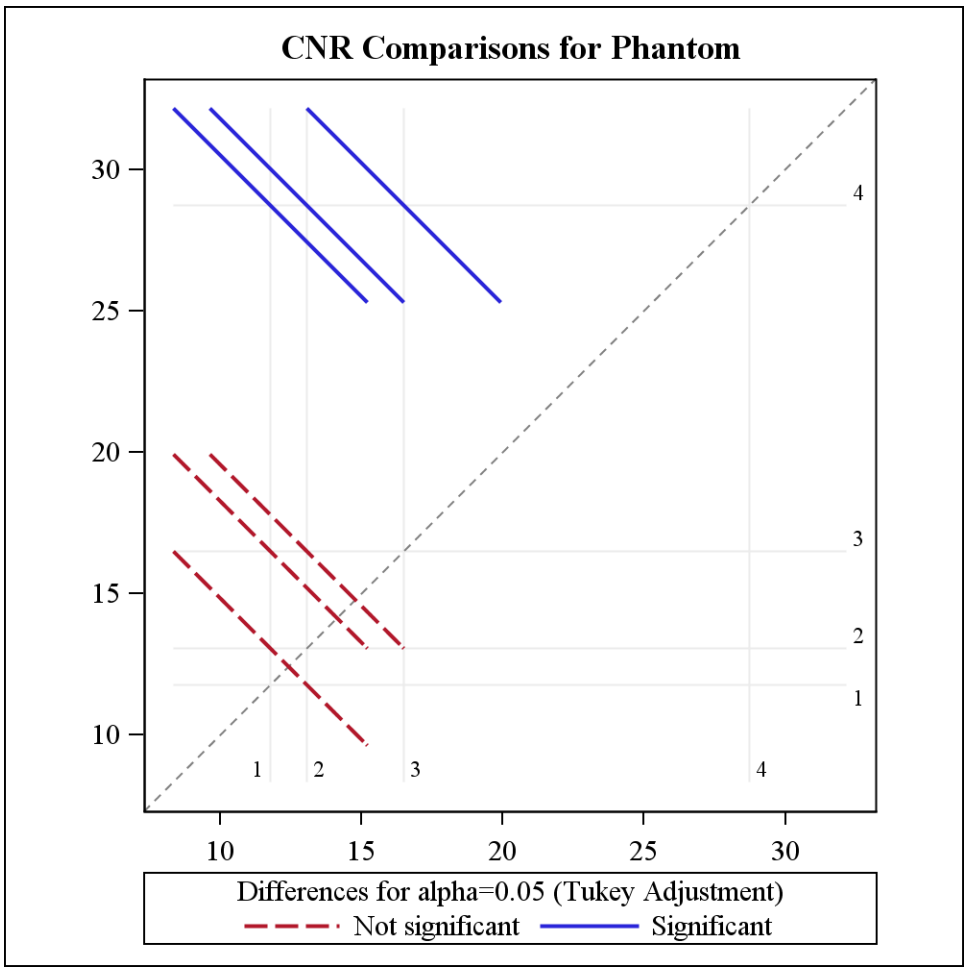

FOV=4

Class Level Information		
Class	**Levels**	**Values**
Phantom	4	1 2 3 4
Dose	2	1 2

Number of Observations Read	24
Number of Observations Used	24

Dependent Variable: CNR CNR

FOV=4

Source	DF	Sum of Squares	Mean Square	F Value	Pr > F
Model	4	567.2348341	141.8087085	18.45	<.0001
Error	19	146.0360332	7.6861070		
Corrected Total	23	713.2708673			

R-Square	Coeff Var	Root MSE	CNR Mean
0.795259	17.35095	2.772383	15.97828

Source	DF	Type I SS	Mean Square	F Value	Pr > F
Phantom	3	374.3074127	124.7691376	16.23	<.0001
Dose	1	192.9274214	192.9274214	25.10	<.0001

Source	DF	Type III SS	Mean Square	F Value	Pr > F
Phantom	3	374.3074127	124.7691376	16.23	<.0001
Dose	1	192.9274214	192.9274214	25.10	<.0001

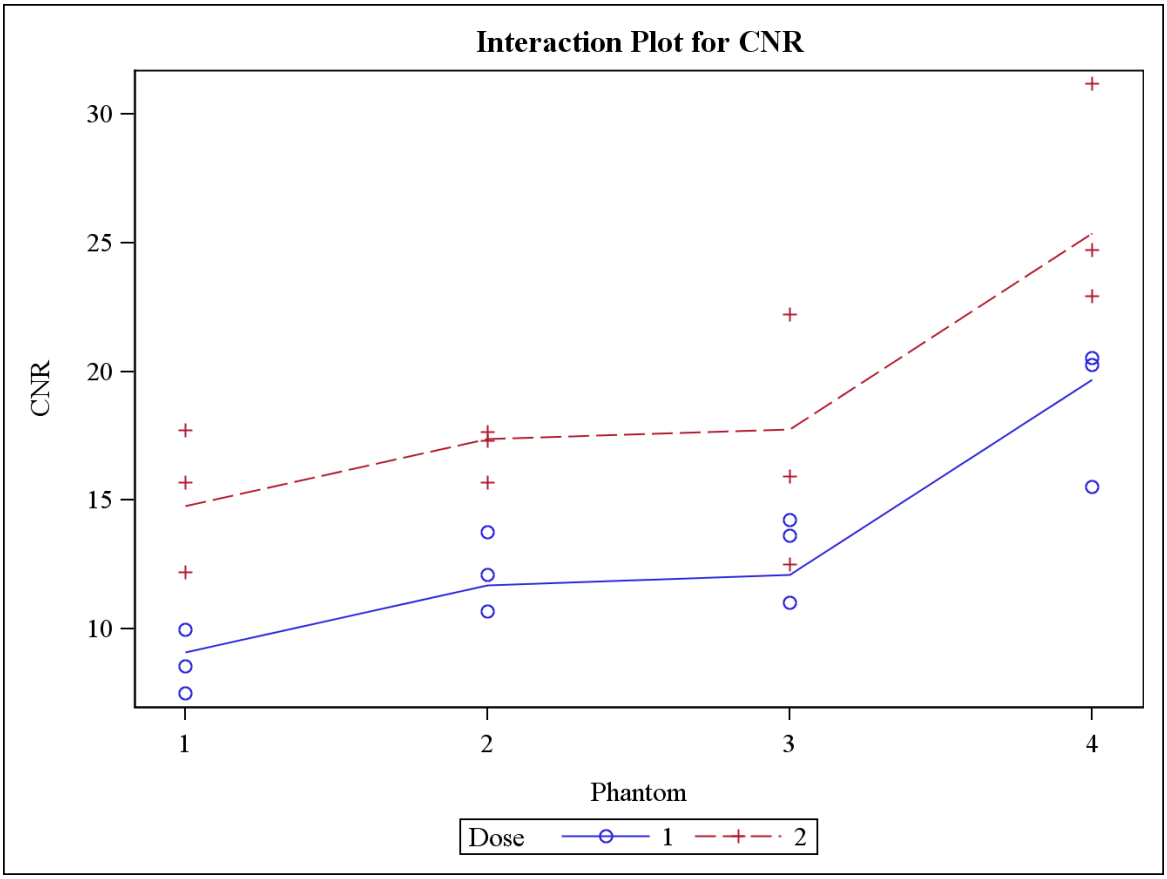

Least Squares Means

Adjustment for Multiple Comparisons: Tukey

FOV=4

Phantom	CNR LSMEAN	LSMEAN Number
1	11.9368889	1
2	14.5309444	2
3	14.9217222	3
4	22.5235556	4

Least Squares Means for effect Phantom Pr > |t| for H0: LSMean(i)=LSMean(j) Dependent Variable: CNR				
i/j	**1**	**2**	**3**	**4**
1		0.3913	0.2757	<.0001
2	0.3913		0.9947	0.0004
3	0.2757	0.9947		0.0007
4	<.0001	0.0004	0.0007	

Phantom	CNR LSMEAN	95% Confidence Limits	
1	11.936889	9.567961	14.305817
2	14.530944	12.162017	16.899872
3	14.921722	12.552795	17.290650
4	22.523556	20.154628	24.892483

Least Squares Means for Effect Phantom				
		Difference	Simultaneous 95% Confidence Limits for	
i	j	Between Means	LSMean(i)-LSMean(j)	
1	**2**	-2.594056	-7.094768	1.906657
1	**3**	-2.984833	-7.485546	1.515879
1	**4**	-10.586667	-15.087379	-6.085954
2	**3**	-0.390778	-4.891490	4.109934
2	**4**	-7.992611	-12.493323	-3.491899
3	**4**	-7.601833	-12.102546	-3.101121

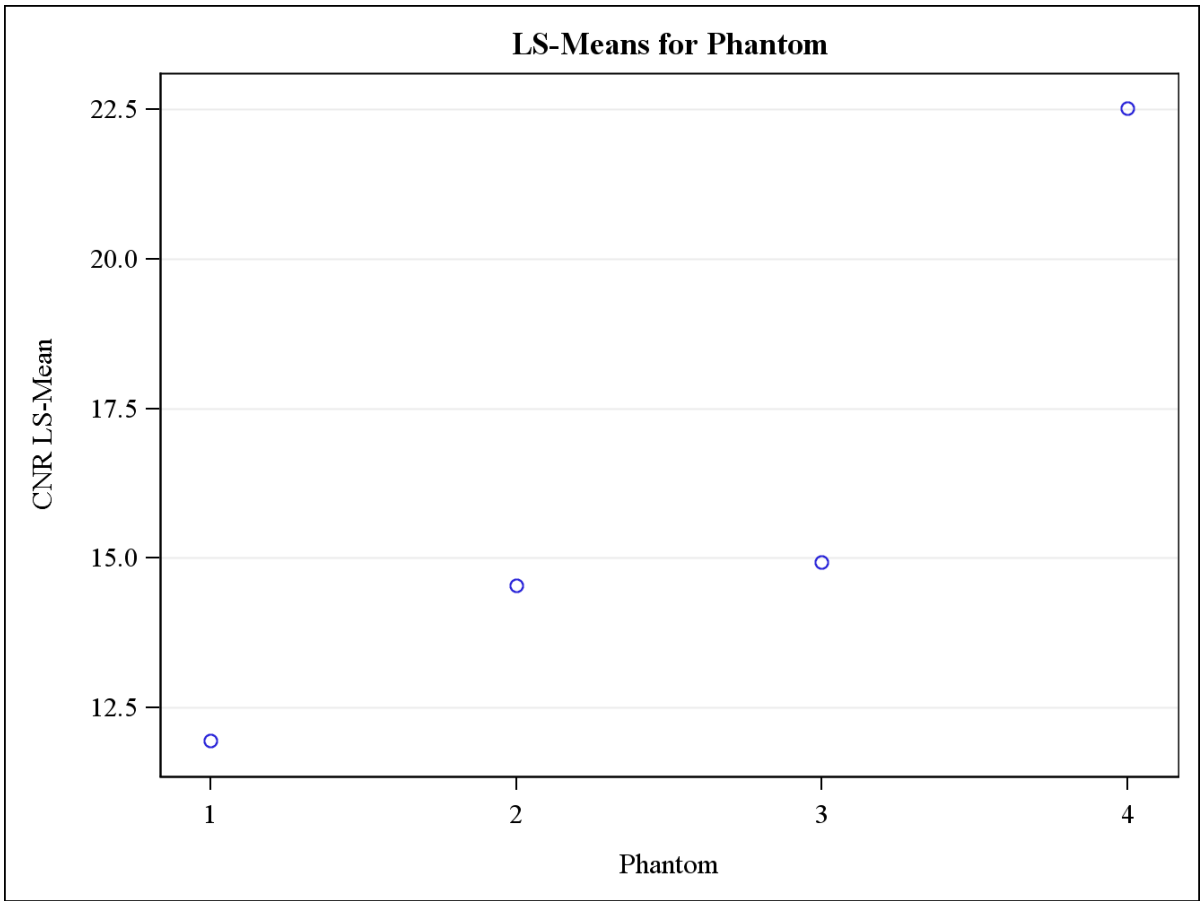
LS-Means for Phantom
CNR LS-Mean
22.5
20.0
17.5
15.0
12.5
1
2
3
4
Phantom

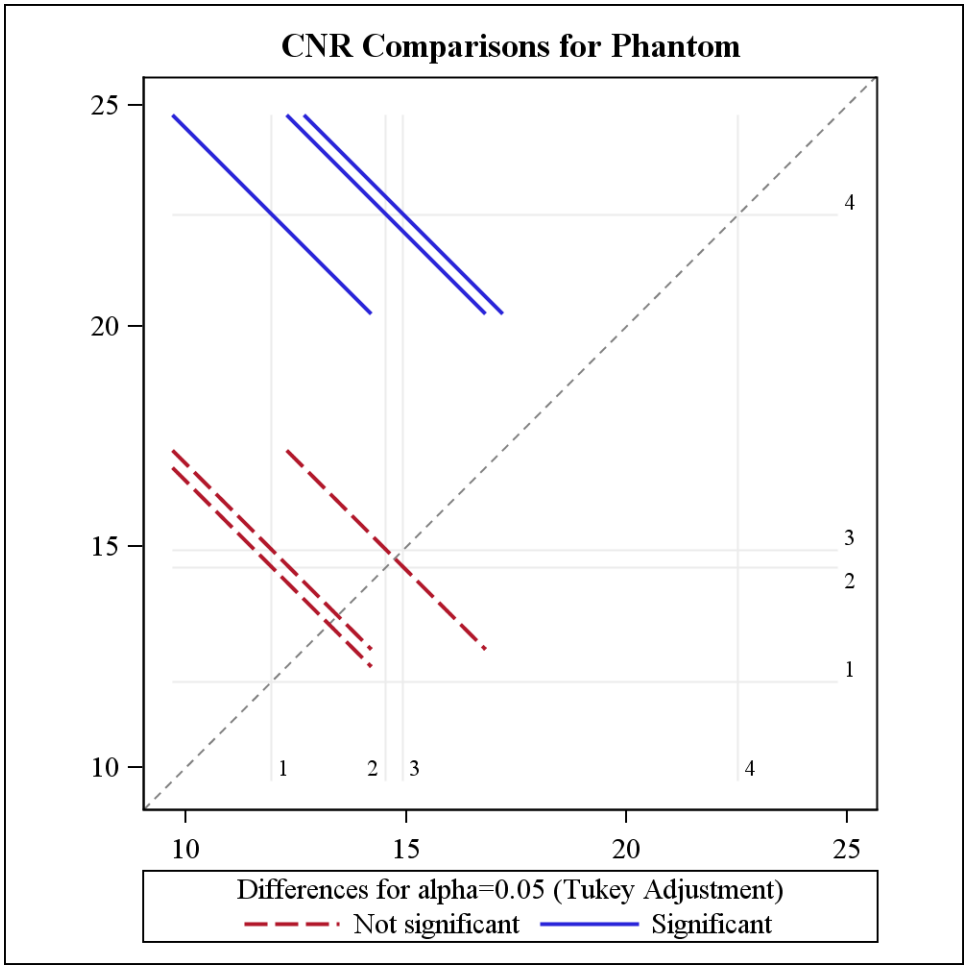

MTF STATISTICAL ANALYSIS

3way interaction model

Class Level Information

Class	Levels	Values
Phantom	4	1 2 3 4
FOV	5	1 2 3 4 5
Dose	2	1 2

Number of Observations Read	120
Number of Observations Used	120

Source	DF	Sum of Squares	Mean Square	F Value	Pr > F
Model	39	3.75308545	0.09623296	15.83	<.0001
Error	80	0.48626704	0.00607834		
Corrected Total	119	4.23935249			

R-Square	Coeff Var	Root MSE	MTF Mean
0.885297	6.698647	0.077964	1.163872

Source	DF	Type III SS	Mean Square	F Value	Pr > F
Phantom	3	0.11592691	0.03864230	6.36	0.0006

Dose	1	2.67764646	2.67764646	440.52	<.0001
Phantom*Dose	3	0.15434910	0.05144970	8.46	<.0001
FOV	4	0.30516841	0.07629210	12.55	<.0001
Phantom*FOV	12	0.28078031	0.02339836	3.85	0.0001
FOV*Dose	4	0.04186600	0.01046650	1.72	0.1533
Phantom*FOV*Dose	12	0.17734825	0.01477902	2.43	0.0095

2way interaction model

---------- FOV=1 ----------

Class Level Information

Class	Levels	Values
Phantom	4	1 2 3 4
Dose	2	1 2

Number of Observations Read	24
Number of Observations Used	24

Source	DF	Sum of Squares	Mean Square	F Value	Pr > F
Model	7	0.48098714	0.06871245	56.07	<.0001
Error	16	0.01960741	0.00122546		
Corrected Total	23	0.50059455			

R-Square	Coeff Var	Root MSE	MTF Mean

0.960832 3.174763 0.035007 1.102653

Source	DF	Type III SS	Mean Square	F Value	Pr > F
Phantom	3	0.00608350	0.00202783	1.65	0.2166
Dose	1	0.43353856	0.43353856	353.78	<.0001
Phantom*Dose	3	0.04136509	0.01378836	11.25	0.0003

---------- FOV=2 ----------

Class Level Information

Class	Levels	Values
Phantom	4	1 2 3 4
Dose	2	1 2

Number of Observations Read	24
Number of Observations Used	24

Source	DF	Sum of Squares	Mean Square	F Value	Pr > F
Model	7	0.81034346	0.11576335	41.42	<.0001
Error	16	0.04472052	0.00279503		

Corrected Total	23	0.85506398	

R-Square	Coeff Var	Root MSE	MTF Mean
0.947699	4.745195	0.052868	1.114139

Source	DF	Type III SS	Mean Square	F Value	Pr > F
Phantom	3	0.00365054	0.00121685	0.44	0.7307
Dose	1	0.78529896	0.78529896	280.96	<.0001
Phantom*Dose	3	0.02139396	0.00713132	2.55	0.0921

2way interaction model

---------- FOV=3 ----------

Class Level Information

Class	Levels	Values
Phantom	4	1 2 3 4
Dose	2	1 2

Number of Observations Read	24
Number of Observations Used	24

2way interaction model

---------- FOV=3 ----------

Source	DF	Sum of Squares	Mean Square	F Value	Pr > F
Model	7	0.62423114	0.08917588	4.86	0.0043
Error	16	0.29384807	0.01836550		
Corrected Total	23	0.91807922			

R-Square	Coeff Var	Root MSE	MTF Mean
0.679932	11.04490	0.135519	1.226986

Source	DF	Type III SS	Mean Square	F Value	Pr > F
Phantom	3	0.06256198	0.02085399	1.14	0.3646
Dose	1	0.45018204	0.45018204	24.51	0.0001
Phantom*Dose	3	0.11148712	0.03716237	2.02	0.1512

2way interaction model

---------- FOV=4 ----------

Class Level Information

Class	Levels	Values
Phantom	4	1 2 3 4
Dose	2	1 2

Number of Observations Read	24
Number of Observations Used	24

2way interaction model

---------- FOV=4 ----------

Dependent Variable: MTF MTF

Source	DF	Sum of Squares	Mean Square	F Value	Pr > F
Model	7	0.79602025	0.11371718	25.83	<.0001
Error	16	0.07045207	0.00440325		
Corrected Total	23	0.86647233			

R-Square	Coeff Var	Root MSE	MTF Mean
0.918691	5.712294	0.066357	1.161653

Source	DF	Type III SS	Mean Square	F Value	Pr > F
Phantom	3	0.29900338	0.09966779	22.64	<.0001
Dose	1	0.42978345	0.42978345	97.61	<.0001
Phantom*Dose	3	0.06723342	0.02241114	5.09	0.0116

2way interaction model

---------- FOV=5 ----------

Class Level Information

Class	Levels	Values
Phantom	4	1 2 3 4
Dose	2	1 2

Number of Observations Read	24
Number of Observations Used	24

2way interaction model

---------- FOV=5 ----------

Source	DF	Sum of Squares	Mean Square	F Value	Pr > F
Model	7	0.73633503	0.10519072	29.20	<.0001
Error	16	0.05763896	0.00360244		
Corrected Total	23	0.79397400			

R-Square	Coeff Var	Root MSE	MTF Mean
0.927404	4.944294	0.060020	1.213931

Source	DF	Type III SS	Mean Square	F Value	Pr > F
Phantom	3	0.02540783	0.00846928	2.35	0.1108
Dose	1	0.62070945	0.62070945	172.30	<.0001

Phantom*Dose	3	0.09021775	0.03007258	8.35	0.0014

Fov 1 and 4 and 5 with significant interaction

---------- FOV=1 ----------

Class Level Information

Class	Levels	Values
Phantom	4	1 2 3 4
Dose	2	1 2

Number of Observations Read	24
Number of Observations Used	24

Fov 1 and 4 and 5 with significant interaction

---------- FOV=1 ----------

Least Squares Means

Adjustment for Multiple Comparisons: Tukey

Phantom	Dose	MTF LSMEAN	LSMEAN Number
1	1	1.19966667	1
1	2	1.06055556	2
2	1	1.25422222	3
2	2	0.93477778	4
3	1	1.22388889	5

3	2	0.96588889	6
4	1	1.27044444	7
4	2	0.91177778	8

Least Squares Means for effect Phantom*Dose

Pr > |t| for H0: LSMean(i)=LSMean(j)

Dependent Variable: MTF

i/j	1	2	3	4	5	6	7	8
1		0.0033	0.5642	<.0001	0.9870	<.0001	0.2719	<.0001
2	0.0033		<.0001	0.0082	0.0007	0.0661	<.0001	0.0017
3	0.5642	<.0001		<.0001	0.9563	<.0001	0.9989	<.0001
4	<.0001	0.0082	<.0001		<.0001	0.9503	<.0001	0.9903
5	0.9870	0.0007	0.9563	<.0001		<.0001	0.7281	<.0001
6	<.0001	0.0661	<.0001	0.9503	<.0001		<.0001	0.5734
7	0.2719	<.0001	0.9989	<.0001	0.7281	<.0001		<.0001
8	<.0001	0.0017	<.0001	0.9903	<.0001	0.5734	<.0001	

Phantom	Dose	MTF LSMEAN	95% Confidence Limits	
1	1	1.199667	1.156821	1.242512
1	2	1.060556	1.017710	1.103401
2	1	1.254222	1.211377	1.297068
2	2	0.934778	0.891932	0.977623
3	1	1.223889	1.181043	1.266734
3	2	0.965889	0.923043	1.008734
4	1	1.270444	1.227599	1.313290
4	2	0.911778	0.868932	0.954623

Fov 1 and 4 and 5 with significant interaction

---------- FOV=1 ----------

Least Squares Means

Adjustment for Multiple Comparisons: Tukey

Least Squares Means for Effect Phantom*Dose

i	j	Difference Between Means	Simultaneous 95% Confidence Limits for LSMean(i)-LSMean(j)	
1	2	0.139111	0.040153	0.238069
1	3	-0.054556	-0.153513	0.044402
1	4	0.264889	0.165931	0.363847
1	5	-0.024222	-0.123180	0.074736
1	6	0.233778	0.134820	0.332736
1	7	-0.070778	-0.169736	0.028180
1	8	0.287889	0.188931	0.386847
2	3	-0.193667	-0.292625	-0.094709
2	4	0.125778	0.026820	0.224736
2	5	-0.163333	-0.262291	-0.064375
2	6	0.094667	-0.004291	0.193625
2	7	-0.209889	-0.308847	-0.110931
2	8	0.148778	0.049820	0.247736
3	4	0.319444	0.220487	0.418402
3	5	0.030333	-0.068625	0.129291
3	6	0.288333	0.189375	0.387291
3	7	-0.016222	-0.115180	0.082736
3	8	0.342444	0.243487	0.441402
4	5	-0.289111	-0.388069	-0.190153
4	6	-0.031111	-0.130069	0.067847
4	7	-0.335667	-0.434625	-0.236709

4	8	0.023000	-0.075958	0.121958
5	6	0.258000	0.159042	0.356958
5	7	-0.046556	-0.145513	0.052402
5	8	0.312111	0.213153	0.411069
6	7	-0.304556	-0.403513	-0.205598
6	8	0.054111	-0.044847	0.153069
7	8	0.358667	0.259709	0.457625

Fov 1 and 4 and 5 with significant interaction

---------- FOV=4 ----------

Least Squares Means

Adjustment for Multiple Comparisons: Tukey

Phantom	Dose	MTF LSMEAN	LSMEAN Number
1	1	1.27411111	1
1	2	1.03844444	2
2	1	1.16433333	3
2	2	0.79822222	4
3	1	1.30555556	5
3	2	1.19744444	6
4	1	1.43788889	7
4	2	1.07722222	8

Least Squares Means for effect Phantom*Dose

Pr > |t| for H0: LSMean(i)=LSMean(j)

Dependent Variable: MTF

i/j	1	2	3	4	5	6	7	8
1		0.0091	0.4956	<.0001	0.9987	0.8379	0.1112	0.0362
2	0.0091		0.3389	0.0077	0.0029	0.1296	<.0001	0.9952
3	0.4956	0.3389		<.0001	0.2227	0.9982	0.0023	0.7398
4	<.0001	0.0077	<.0001		<.0001	<.0001	<.0001	0.0019
5	0.9987	0.0029	0.2227	<.0001		0.5134	0.2858	0.0118
6	0.8379	0.1296	0.9982	<.0001	0.5134		0.0076	0.3905
7	0.1112	<.0001	0.0023	<.0001	0.2858	0.0076		0.0001

Phantom	Dose	MTF LSMEAN	95% Confidence Limits	
1	1	1.274111	1.192895	1.355327
1	2	1.038444	0.957228	1.119661
2	1	1.164333	1.083117	1.245550
2	2	0.798222	0.717006	0.879438
3	1	1.305556	1.224339	1.386772
3	2	1.197444	1.116228	1.278661
4	1	1.437889	1.356673	1.519105
4	2	1.077222	0.996006	1.158438

Fov 1 and 4 and 5 with significant interaction

---------- FOV=4 ----------

Least Squares Means

Adjustment for Multiple Comparisons: Tukey

Least Squares Means for Effect Phantom*Dose

i	j	Difference Between Means	Simultaneous 95% Confidence Limits for LSMean(i)-LSMean(j)	
1	2	0.235667	0.048086	0.423247
1	3	0.109778	-0.077802	0.297358
1	4	0.475889	0.288309	0.663469
1	5	-0.031444	-0.219025	0.156136
1	6	0.076667	-0.110914	0.264247
1	7	-0.163778	-0.351358	0.023802
1	8	0.196889	0.009309	0.384469
2	3	-0.125889	-0.313469	0.061691
2	4	0.240222	0.052642	0.427802
2	5	-0.267111	-0.454691	-0.079531
2	6	-0.159000	-0.346580	0.028580
2	7	-0.399444	-0.587025	-0.211864
2	8	-0.038778	-0.226358	0.148802
3	4	0.366111	0.178531	0.553691
3	5	-0.141222	-0.328802	0.046358
3	6	-0.033111	-0.220691	0.154469
3	7	-0.273556	-0.461136	-0.085975
3	8	0.087111	-0.100469	0.274691
4	5	-0.507333	-0.694914	-0.319753
4	6	-0.399222	-0.586802	-0.211642
4	7	-0.639667	-0.827247	-0.452086
4	8	-0.279000	-0.466580	-0.091420
5	6	0.108111	-0.079469	0.295691
5	7	-0.132333	-0.319914	0.055247
5	8	0.228333	0.040753	0.415914
6	7	-0.240444	-0.428025	-0.052864
6	8	0.120222	-0.067358	0.307802
7	8	0.360667	0.173086	0.548247

---------- FOV=5 ----------

Least Squares Means

Adjustment for Multiple Comparisons: Tukey

Phantom	Dose	MTF LSMEAN	LSMEAN Number
1	1	1.46322222	1
1	2	1.05277778	2
2	1	1.28144444	3
2	2	1.13166667	4
3	1	1.30011111	5
3	2	1.03511111	6
4	1	1.45422222	7
4	2	0.99288889	8

Least Squares Means for effect Phantom*Dose

Pr > |t| for H0: LSMean(i)=LSMean(j)

Dependent Variable: MTF

i/j	1	2	3	4	5	6	7	8
1		<.0001	0.0313	<.0001	0.0641	<.0001	1.0000	<.0001
2	<.0001		0.0049	0.7387	0.0023	0.9999	<.0001	0.9136
3	0.0313	0.0049		0.1048	0.9999	0.0024	0.0444	0.0005
4	<.0001	0.7387	0.1048		0.0524	0.5280	0.0001	0.1544
5	0.0641	0.0023	0.9999	0.0524		0.0012	0.0896	0.0002
6	<.0001	0.9999	0.0024	0.5280	0.0012		<.0001	0.9857
7	1.0000	<.0001	0.0444	0.0001	0.0896	<.0001		<.0001

Phantom	Dose	MTF LSMEAN	95% Confidence Limits	
1	1	1.463222	1.389762	1.536683
1	2	1.052778	0.979317	1.126238
2	1	1.281444	1.207984	1.354905
2	2	1.131667	1.058206	1.205127
3	1	1.300111	1.226651	1.373572
3	2	1.035111	0.961651	1.108572
4	1	1.454222	1.380762	1.527683
4	2	0.992889	0.919428	1.066349

Fov 1 and 4 and 5 with significant interaction

---------- FOV=5 ----------

Least Squares Means

Adjustment for Multiple Comparisons: Tukey

Least Squares Means for Effect Phantom*Dose

i	j	Difference Between Means	Simultaneous 95% Confidence Limits for LSMean(i)-LSMean(j)	
1	2	0.410444	0.240777	0.580112
1	3	0.181778	0.012110	0.351445
1	4	0.331556	0.161888	0.501223
1	5	0.163111	-0.006556	0.332778
1	6	0.428111	0.258444	0.597778
1	7	0.009000	-0.160667	0.178667
1	8	0.470333	0.300666	0.640001

2	3	-0.228667	-0.398334	-0.058999
2	4	-0.078889	-0.248556	0.090778
2	5	-0.247333	-0.417001	-0.077666
2	6	0.017667	-0.152001	0.187334
2	7	-0.401444	-0.571112	-0.231777
2	8	0.059889	-0.109778	0.229556
3	4	0.149778	-0.019890	0.319445
3	5	-0.018667	-0.188334	0.151001
3	6	0.246333	0.076666	0.416001
3	7	-0.172778	-0.342445	-0.003110
3	8	0.288556	0.118888	0.458223
4	5	-0.168444	-0.338112	0.001223
4	6	0.096556	-0.073112	0.266223
4	7	-0.322556	-0.492223	-0.152888
4	8	0.138778	-0.030890	0.308445
5	6	0.265000	0.095333	0.434667
5	7	-0.154111	-0.323778	0.015556
5	8	0.307222	0.137555	0.476890
6	7	-0.419111	-0.588778	-0.249444
6	8	0.042222	-0.127445	0.211890
7	8	0.461333	0.291666	0.631001

fov 2 and 3 without significant interaction

---------- FOV=2 ----------

Class Level Information

Class	Levels	Values
Phantom	4	1 2 3 4
Dose	2	1 2

Number of Observations Read	24
Number of Observations Used	24

fov 2 and 3 without significant interaction

---------- FOV=2 ----------

Source	DF	Sum of Squares	Mean Square	F Value	Pr > F
Model	4	0.78894950	0.19723738	56.68	<.0001
Error	19	0.06611448	0.00347971		
Corrected Total	23	0.85506398			

R-Square	Coeff Var	Root MSE	MTF Mean
0.922679	5.294588	0.058989	1.114139

Source	DF	Type III SS	Mean Square	F Value	Pr > F
Phantom	3	0.00365054	0.00121685	0.35	0.7898
Dose	1	0.78529896	0.78529896	225.68	<.0001

fov 2 and 3 without significant interaction

---------- FOV=3 ----------

Class Level Information

Class	Levels	Values

Phantom	4	1 2 3 4
Dose	2	1 2

Number of Observations Read	24
Number of Observations Used	24

fov 2 and 3 without significant interaction

Source	DF	Sum of Squares	Mean Square	F Value	Pr > F
Model	4	0.51274402	0.12818600	6.01	0.0027
Error	19	0.40533520	0.02133343		
Corrected Total	23	0.91807922			

R-Square	Coeff Var	Root MSE	MTF Mean
0.558496	11.90394	0.146060	1.226986

Source	DF	Type I SS	Mean Square	F Value	Pr > F
Phantom	3	0.06256198	0.02085399	0.98	0.4241
Dose	1	0.45018204	0.45018204	21.10	0.0002

Source	DF	Type III SS	Mean Square	F Value	Pr > F

Phantom	3	0.06256198	0.02085399	0.98	0.4241
Dose	1	0.45018204	0.45018204	21.10	0.0002

SUBJECTIVE IMAGE QUALITY ANALYSIS

Observer preference scores

Image Name	Phantom Comparison	FOV (cm)	Dose Protocol	Preference Score (points)	CNR Score (points)	MTF Score (points)
R2_1	Standard	17x11	Regular	23	1	23
R2_2	Mod 1	17x11	Regular	15	5	13
R2_3	Mod 2	17x11	Regular	22	4	20
R2_4	Mod 3	17x11	Regular	22	2	22
R3_1	Standard	17x11	Low	27	15	9
R3_2	Mod 1	17x11	Low	12	6	6
R3_3	Mod 2	17x11	Low	11	5	7
R3_4	Mod 3	17x11	Low	9	7	9
R4_1	Standard	17x6	Regular	28	4	24
R4_2	Mod 1	17x6	Regular	31	17	19
R4_3	Mod 2	17x6	Regular	24	6	22
R4_4	Mod 3	17x6	Regular	22	0	20
R5_1	Standard	17x6	Low	18	18	10

R5_2	Mod 1	17x6	Low	28	20	0
R5_3	Mod 2	17x6	Low	20	12	12
R5_4	Mod 3	17x6	Low	11	9	11
R6_1	Standard	10x10	Regular	18	6	18
R6_2	Mod 1	10x10	Regular	24	3	15
R6_3	Mod 2	10x10	Regular	27	7	27
R6_4	Mod 3	10x10	Regular	29	9	29
R7_1	Standard	10x10	Low	19	15	13
R7_2	Mod 1	10x10	Low	3	3	1
R7_3	Mod 2	10x10	Low	14	10	4
R7_4	Mod 3	10x10	Low	5	5	5
R8_1	Standard	10x5	Regular	13	9	13
R8_2	Mod 1	10x5	Regular	24	0	24
R8_3	Mod 2	10x5	Regular	35	9	25
R8_4	Mod 3	10x5	Regular	33	9	21
R9_1	Standard	10x5	Low	6	4	2
R9_2	Mod 1	10x5	Low	11	9	3
R9_3	Mod 2	10x5	Low	20	14	2
R9_4	Mod 3	10x5	Low	3	1	3
R10_1	Standard	8x8	Regular	21	9	12
R10_2	Mod 1	8x8	Regular	23	3	15
R10_3	Mod 2	8x8	Regular	6	0	6
R10_4	Mod 3	8x8	Regular	34	10	24

R11_1	Standard	8x8	Low	7	6	6
R11_2	Mod 1	8x8	Low	9	9	1
R11_3	Mod 2	8x8	Low	1	1	1
R11_4	Mod 3	8x8	Low	12	10	6

Table #: Observer preference for phantom, FOV, and dose protocol association with CNR and MTF. A or C in the observer columns = observer preferred image A or C. B in the observer columns = no preference. A or C in the CNR or MTF columns = A if CNR or MTF higher of preferred image, C if CNR or MTF lower of preferred image. B in CNR or MTF columns = no significant difference in CNR or MTF between compared images.

Phantom A & C	FOV (cm) A	FOV (cm) C	Dose Protocol A	Dose Protocol C	Observer 1	Observer 2	CNR	MTF
Standard	17x11	17x11	Regular	Low	C	C	C	A
Standard	17x11	17x6	Regular	Regular	C	A	C	A
Standard	17x11	17x6	Regular	Low	C	A	C	A
Standard	17x11	10x10	Regular	Regular	A	A	C	A
Standard	17x11	10x10	Regular	Low	A	C	C	A
Standard	17x11	10x5	Regular	Regular	B	A	C	A
Standard	17x11	10x5	Regular	Low	A	A	C	A
Standard	17x11	8x8	Regular	Regular	A	C	C	A
Standard	17x11	8x8	Regular	Low	A	A	C	A
Standard	17x11	17x6	Low	Regular	C	C	A	C
Standard	17x11	17x6	Low	Low	B	A	C	B

Standard	17x11	10x10	Low	Regular	A	A	A	C
Standard	17x11	10x10	Low	Low	A	C	C	C
Standard	17x11	10x5	Low	Regular	A	C	A	C
Standard	17x11	10x5	Low	Low	A	A	C	A
Standard	17x11	8x8	Low	Regular	A	A	A	C
Standard	17x11	8x8	Low	Low	A	A	C	B
Standard	17x6	17x6	Regular	Low	B	A	C	A
Standard	17x6	10x10	Regular	Regular	B	A	C	C
Standard	17x6	10x10	Regular	Low	A	C	C	A
Standard	17x6	10x5	Regular	Regular	A	C	C	B
Standard	17x6	10x5	Regular	Low	A	A	C	A
Standard	17x6	8x8	Regular	Regular	A	A	C	A
Standard	17x6	8x8	Regular	Low	A	A	C	A
Standard	17x6	10x10	Low	Regular	A	C	A	C
Standard	17x6	10x10	Low	Low	A	B	A	C
Standard	17x6	10x5	Low	Regular	A	B	A	C
Standard	17x6	10x5	Low	Low	A	B	A	A
Standard	17x6	8x8	Low	Regular	B	B	A	C
Standard	17x6	8x8	Low	Low	B	C	C	B
Standard	10X10	10x10	Regular	Low	A	B	C	A
Standard	10X10	10x5	Regular	Regular	B	A	A	B
Standard	10X10	10x5	Regular	Low	A	A	C	A
Standard	10X10	8x8	Regular	Regular	B	C	C	A

Standard	10X10	8x8	Regular	Low	A	A	C	A
Standard	10X10	10x5	Low	Regular	B	A	A	C
Standard	10X10	10x5	Low	Low	C	A	B	A
Standard	10X10	8x8	Low	Regular	C	A	A	B
Standard	10X10	8x8	Low	Low	A	A	C	A
Standard	10X5	10x5	Regular	Low	A	C	A	A
Standard	10X5	8x8	Regular	Regular	C	C	C	A
Standard	10X5	8x8	Regular	Low	A	B	C	A
Standard	10X5	8x8	Low	Regular	C	C	A	C
Standard	10X5	8x8	Low	Low	B	C	C	C
Standard	8X8	8X8	Regular	Low	A	A	C	A
Mod 1	17x11	17x11	Regular	Low	C	A	C	A
Mod 1	17x11	17x6	Regular	Regular	C	C	C	A
Mod 1	17x11	17x6	Regular	Low	C	A	C	A
Mod 1	17x11	10x10	Regular	Regular	C	A	A	A
Mod 1	17x11	10x10	Regular	Low	A	B	C	A
Mod 1	17x11	10x5	Regular	Regular	A	C	A	C
Mod 1	17x11	10x5	Regular	Low	A	C	C	A
Mod 1	17x11	8x8	Regular	Regular	C	C	A	A
Mod 1	17x11	8x8	Regular	Low	A	C	C	A
Mod 1	17x11	17x6	Low	Regular	C	C	C	C
Mod 1	17x11	17x6	Low	Low	C	C	C	A
Mod 1	17x11	10x10	Low	Regular	C	C	A	C

Mod 1	17x11	10x10	Low	Low	A	C	C	A
Mod 1	17x11	10x5	Low	Regular	A	C	A	C
Mod 1	17x11	10x5	Low	Low	A	C	C	A
Mod 1	17x12	8x8	Low	Regular	A	C	A	C
Mod 1	17x13	8x8	Low	Low	A	C	C	A
Mod 1	17x6	17x6	Regular	Low	C	A	C	A
Mod 1	17x6	10x10	Regular	Regular	B	A	A	C
Mod 1	17x6	10x10	Regular	Low	A	A	C	A
Mod 1	17x6	10x5	Regular	Regular	A	C	A	C
Mod 1	17x6	10x5	Regular	Low	A	A	C	A
Mod 1	17x6	8x8	Regular	Regular	A	A	A	C
Mod 1	17x6	8x8	Regular	Low	A	A	C	A
Mod 1	17x6	10x10	Low	Regular	A	C	A	C
Mod 1	17x6	10x10	Low	Low	A	A	A	C
Mod 1	17x6	10x5	Low	Regular	A	C	A	C
Mod 1	17x6	10x5	Low	Low	A	A	C	C
Mod 1	17x6	8x8	Low	Regular	A	A	A	C
Mod 1	17x6	8x8	Low	Low	A	A	C	C
Mod 1	10X10	10x10	Regular	Low	A	A	C	A
Mod 1	10X10	10x5	Regular	Regular	C	A	A	C
Mod 1	10X10	10x5	Regular	Low	A	A	C	A
Mod 1	10X10	8x8	Regular	Regular	B	C	A	B
Mod 1	10X10	8x8	Regular	Low	A	A	C	A

Mod 1	10X10	10x5	Low	Regular	C	C	A	C
Mod 1	10X10	10x5	Low	Low	C	C	C	A
Mod 1	10X10	8x8	Low	Regular	C	C	A	C
Mod 1	10X10	8x8	Low	Low	C	C	C	A
Mod 1	10X5	10x5	Regular	Low	A	A	C	A
Mod 1	10X5	8x8	Regular	Regular	A	C	C	A
Mod 1	10X5	8x8	Regular	Low	A	A	C	A
Mod 1	10X5	8x8	Low	Regular	C	C	A	C
Mod 1	10X5	8x8	Low	Low	B	A	C	B
Mod 1	8X8	8X8	Regular	Low	A	A	C	A
Mod 2	17x11	17x11	Regular	Low	A	A	C	A
Mod 2	17x11	17x6	Regular	Regular	C	A	C	B
Mod 2	17x11	17x6	Regular	Low	C	A	C	A
Mod 2	17x11	10x10	Regular	Regular	A	C	C	B
Mod 2	17x11	10x10	Regular	Low	A	C	C	A
Mod 2	17x11	10x5	Regular	Regular	C	C	C	A
Mod 2	17x11	10x5	Regular	Low	A	C	C	A
Mod 2	17x11	8x8	Regular	Regular	A	A	A	A
Mod 2	17x11	8x8	Regular	Low	A	A	C	A
Mod 2	17x11	17x6	Low	Regular	C	C	A	C
Mod 2	17x11	17x6	Low	Low	C	C	C	C
Mod 2	17x11	10x10	Low	Regular	C	C	A	C
Mod 2	17x11	10x10	Low	Low	A	C	C	A

Mod 2	17x11	10x5	Low	Regular	C	C	A	C
Mod 2	17x11	10x5	Low	Low	B	C	C	A
Mod 2	17x11	8x8	Low	Regular	A	A	A	C
Mod 2	17x11	8x8	Low	Low	A	A	C	A
Mod 2	17x6	17x6	Regular	Low	A	A	C	A
Mod 2	17x6	10x10	Regular	Regular	A	C	B	B
Mod 2	17x6	10x10	Regular	Low	A	C	C	A
Mod 2	17x6	10x5	Regular	Regular	C	C	A	A
Mod 2	17x6	10x5	Regular	Low	A	C	C	A
Mod 2	17x6	8x8	Regular	Regular	A	A	A	A
Mod 2	17x6	8x8	Regular	Low	A	A	C	A
Mod 2	17x6	10x10	Low	Regular	A	C	A	C
Mod 2	17x6	10x10	Low	Low	A	C	C	A
Mod 2	17x6	10x5	Low	Regular	C	C	A	C
Mod 2	17x6	10x5	Low	Low	A	C	C	A
Mod 2	17x6	8x8	Low	Regular	A	A	A	C
Mod 2	17x6	8x8	Low	Low	A	A	C	A
Mod 2	10X10	10x10	Regular	Low	A	A	C	A
Mod 2	10X10	10x5	Regular	Regular	C	B	A	A
Mod 2	10X10	10x5	Regular	Low	A	A	C	A
Mod 2	10X10	8x8	Regular	Regular	A	A	A	A
Mod 2	10X10	8x8	Regular	Low	A	A	C	A
Mod 2	10X10	10x5	Low	Regular	C	C	A	C

Mod 2	10X10	10x5	Low	Low	C	B	A	A
Mod 2	10X10	8x8	Low	Regular	C	A	A	C
Mod 2	10X10	8x8	Low	Low	B	A	A	A
Mod 2	10X5	8x8	Regular	Regular	A	A	C	A
Mod 2	10X5	8x8	Regular	Low	A	A	A	A
Mod 2	10X5	8x8	Low	Regular	A	A	C	A
Mod 2	10X5	8x8	Low	Low	A	A	A	C
Mod 2	10X5	8X8	Regular	Low	A	A	C	B
Mod 2	8X8	8X8	Regular	Low	A	A	C	A
Mod 3	17x11	17x11	Regular	Low	A	A	C	A
Mod 3	17x11	17x6	Regular	Regular	C	A	A	A
Mod 3	17x11	17x6	Regular	Low	A	A	C	A
Mod 3	17x11	10x10	Regular	Regular	C	C	C	C
Mod 3	17x11	10x10	Regular	Low	A	A	C	A
Mod 3	17x11	10x5	Regular	Regular	C	C	C	A
Mod 3	17x11	10x5	Regular	Low	A	A	C	A
Mod 3	17x11	8x8	Regular	Regular	C	C	B	A
Mod 3	17x11	8x8	Regular	Low	A	A	C	A
Mod 3	17x11	17x6	Low	Regular	C	C	A	C
Mod 3	17x11	17x6	Low	Low	B	C	A	C
Mod 3	17x11	10x10	Low	Regular	C	C	A	C
Mod 3	17x11	10x10	Low	Low	B	A	C	A
Mod 3	17x11	10x5	Low	Regular	C	C	A	C

Mod 3	17x11	10x5	Low	Low	A	A	A	A
Mod 3	17x11	8x8	Low	Regular	C	C	A	C
Mod 3	17x11	8x8	Low	Low	B	C	B	A
Mod 3	17x6	17x6	Regular	Low	A	A	C	A
Mod 3	17x6	10x10	Regular	Regular	C	C	C	C
Mod 3	17x6	10x10	Regular	Low	A	A	C	A
Mod 3	17x6	10x5	Regular	Regular	C	C	C	A
Mod 3	17x6	10x5	Regular	Low	A	A	C	A
Mod 3	17x6	8x8	Regular	Regular	C	C	C	A
Mod 3	17x6	8x8	Regular	Low	A	A	C	A
Mod 3	17x6	10x10	Low	Regular	C	C	A	C
Mod 3	17x6	10x10	Low	Low	B	B	C	A
Mod 3	17x6	10x5	Low	Regular	C	C	A	C
Mod 3	17x6	10x5	Low	Low	A	A	A	A
Mod 3	17x6	8x8	Low	Regular	C	C	A	C
Mod 3	17x6	8x8	Low	Low	B	B	B	A
Mod 3	10X10	10x10	Regular	Low	A	A	C	A
Mod 3	10X10	10x5	Regular	Regular	C	C	A	A
Mod 3	10X10	10x5	Regular	Low	A	A	C	A
Mod 3	10X10	8x8	Regular	Regular	C	B	A	A
Mod 3	10X10	8x8	Regular	Low	A	A	C	A
Mod 3	10X10	10x5	Low	Regular	C	C	A	C
Mod 3	10X10	10x5	Low	Low	B	C	A	C

Mod 3	10X10	8x8	Low	Regular	C	C	A	C
Mod 3	10X10	8x8	Low	Low	B	C	A	C
Mod 3	10X5	8x8	Regular	Regular	A	A	C	A
Mod 3	10X5	8x8	Regular	Low	C	B	A	A
Mod 3	10X5	8x8	Low	Regular	A	A	C	A
Mod 3	10X5	8x8	Low	Low	C	C	A	C
Mod 3	10X5	8X8	Regular	Low	C	C	C	B
Mod 3	8X8	8X8	Regular	Low	A	A	C	A

Aim Two (Observer Session) Analysis

1. Analyze what drives the agreement between two observers

Response variable: the agreement between observer 1 and observer 2

Predictor variable: - Phantom (either phantom_a or phantom_c since they remain the same)

- FOV_a
- FOV_c
- Dose_a
- Dose_c

Model Selection:

Before fitting a logistic regression model, the stepwise selection method is applied to remove any insignificant variables from the model before adding a significant variable to the model.

Prior to the first step, the intercept-only model is fit and individual score statistics for the potential variables are evaluated (Table 1).

In step 1, the variable phantom is selected into the model since it is the most significant variable among those to be chosen (p-value = 0.0011).

In step 2, the variable FOV_c is added to the model since both Phantom and FOV_c remains significant.

There is no evidence that FOV_A, Dose_A and Dose_C is related to the agreement.

Table 1: Individual score statistics for all predictors

Stepwise Model Selection

The LOGISTIC Procedure

Analysis of Effects Eligible for Entry

Effect	*DF*	*Score Chi-Square*	*Pr > ChiSq*
phantom	3	16.1111	0.0011
FOV_A	4	4.4778	0.3452
FOV_C	4	11.5403	0.0211
Dose_A	1	0.0937	0.7595
Dose_C	1	0.0938	0.7595

Table 2: A summary of the stepwise selection model

Summary of Stepwise Selection								
	Effect			Number	Score	Wald		Variable
Step	Entered	Removed	DF	In	Chi-Square	Chi-Square	Pr > ChiSq	Label
1	phantom		3	1	16.1111		0.0011	Phantom A
2	FOV_C		4	2	12.2533		0.0156	FOV C

Logistic Regression:

The null hypothesis of a logistic regression is that there is no association between the predictor variables and the response variable.

The type 3 analysis below shows that both phantom and FOV_c is significant. Therefore, we reject H_0. Phantom has a strong association with the agreement, FOV_c has some association with agreement.

Table 3: Type 3 Analysis of Effects

The LOGISTIC Procedure

Type 3 Analysis of Effects

Effect	*DF*	*Wald Chi-Square*	*Pr > ChiSq*
phantom	3	15.3195	0.0016
FOV_C	4	11.7329	0.0195

The Parameter Estimates show that Mod 3 is the most significant predictor on Agreement.

Table 4: Parameter estimates

Analysis of Maximum Likelihood Estimates

Parameter		*DF*	*Estimate*	*Standard Error*	*Wald Chi-Square*	*Pr > ChiSq*
Intercept		1	0.4800	0.2819	2.8990	0.0886
phantom	*Mod 1*	1	-0.3401	0.2776	1.5015	0.2204
phantom	*Mod 2*	1	0.0340	0.2821	0.0145	0.9041
phantom	*Mod 3*	1	1.1315	0.3309	11.6900	0.0006

Analysis of Maximum Likelihood Estimates						
Parameter		*DF*	*Estimate*	*Standard Error*	*Wald Chi-Square*	*Pr > ChiSq*
FOV_C	*10x10*	1	-0.7146	0.3944	3.2829	0.0700
FOV_C	*10x5*	1	-0.2592	0.3636	0.5082	0.4759
FOV_C	*17x11*	1	0.7468	0.9690	0.5939	0.4409
FOV_C	*17x6*	1	-0.4632	0.4621	1.0047	0.3162

From table 5, we can see that the estimated proportion for the agreement (Agree) is increasing with the Phantom. Modification 3 has the highest proportion, there is a 82.2% agreement between 2 observers.

Table 5: Phantom by agreement contingency table

	Agreement		
Phantom	*Agree (N=108)*	*Disagree (N=72)*	*Total (N=180)*
Standard	19 (42.2)	26 (57.8)	45 (25.0)
Mod 1	24 (53.3)	21 (46.7)	45 (25.0)
Mod 2	28 (62.2)	17 (37.8)	45 (25.0)
Mod 3	37 (82.2)	8 (17.8)	45 (25.0)

Note: Values expressed as N(%)

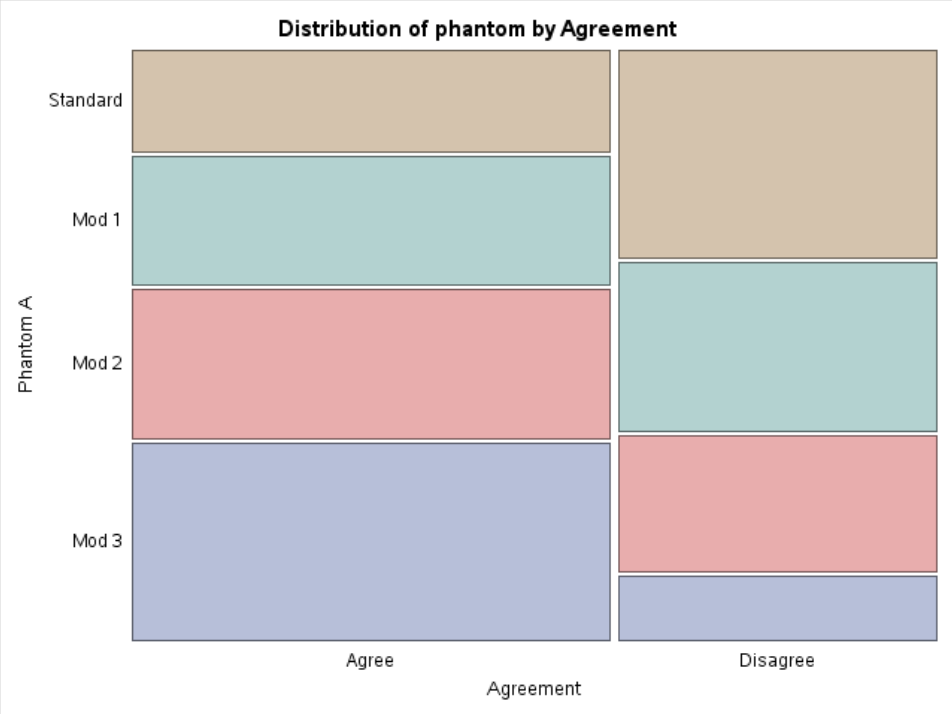
Distribution of phantom by Agreement
Standard
Mod 1
Mod 2
Mod 3
Phantom A
Agree
Disagree
Agreement

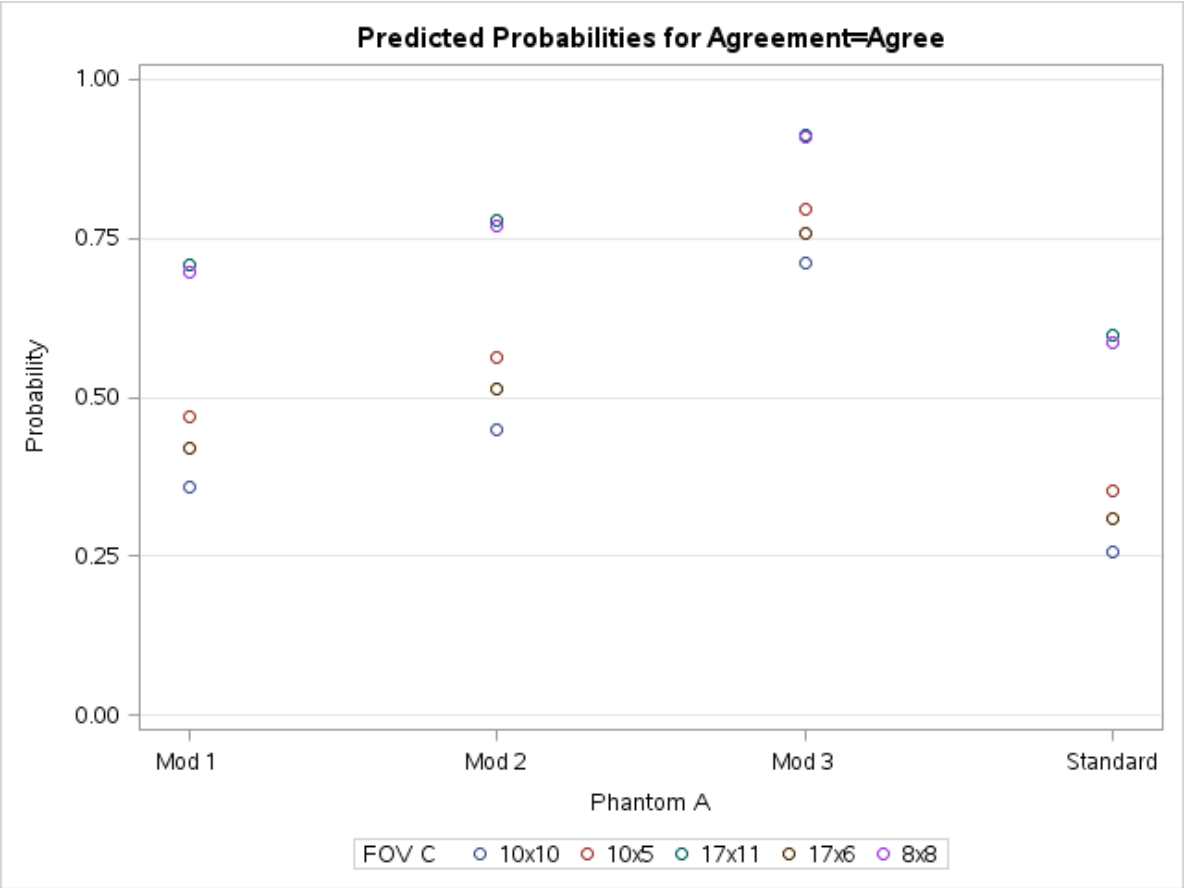

For the rest of the part, I am just repeating all the steps I did above.

2. Analyze what drives the agreement between CNR and MTF

Analysis of Effects Eligible for Entry

Effect	*DF*	*Score Chi-Square*	*Pr > ChiSq*
phantom	3	3.0451	0.3847
FOV_A	4	1.4717	0.8317
FOV_C	4	1.0887	0.8961

Analysis of Effects Eligible for Entry			
		Score	
Effect	*DF*	*Chi-Square*	*Pr > ChiSq*
Dose_A	1	0.3574	0.5500
Dose_C	1	1.1187	0.2902

Note: No (additional) effects met the 0.05 significance level for entry into the model.

None of the predictors seems to fit in the logistic model. The *p*-values shows that they are no significant. It may cause by the agree rate of CNR and MRF is so low. Only 28 out of 152 pairs agree.

Agreement	*Frequency*	*Percent*	*Cumulative Frequency*	*Cumulative Percent*
Agree	28	15.56	28	15.56
Disagree	152	84.44	180	100.00

3. Analyze what drives the agreement between observer1 and CNR

4. Analyze what drives the agreement between observer1 and MTF

The result shows that Dose_C has some kind of relation with the agreement of Observer1 and MTF. None of the other predictors matters.

5. Analyze what drives the agreement between observers 2 and CNR

6. Analyze what drives the agreement between observers 2 and MTF

Both of the results from part 5 and 6 show that none of the predictors is associated with the agreement. I will dig more

REFERENCES

1. GmbH, Q.M.G., *QUART DVT_kp Routine CBCT Test Phantom*, Q.A.i.R. Technologies, Editor. 2009.

2. Dula, K., et al., *SADMFR Guidelines for the Use of Cone-Beam Computed Tomography/ Digital Volume Tomography.* Swiss Dent J, 2014. **124**(11): p. 1169-83.

3. Ludlow, J.B., L.E. Davies-Ludlow, and S.L. Brooks, *Dosimetry of two extraoral direct digital imaging devices: NewTom cone beam CT and Orthophos Plus DS panoramic unit.* Dentomaxillofac Radiol, 2003. **32**(4): p. 229-34.

4. Alamri, H.M., et al., *Applications of CBCT in dental practice: a review of the literature.* Gen Dent, 2012. **60**(5): p. 390-400; quiz 401-2.

5. Howerton, W.B., Jr. and M.A. Mora, *Advancements in digital imaging: what is new and on the horizon?* J Am Dent Assoc, 2008. **139 Suppl**: p. 20s-24s.

6. Pauwels, R., et al., *Development and applicability of a quality control phantom for dental cone-beam CT.* Journal of applied clinical medical physics / American College of Medical Physics, 2011. **12**(4): p. 3478.

7. Pauwels, R., et al., *Comparison of spatial and contrast resolution for cone-beam computed tomography scanners.* Oral surgery, oral medicine, oral pathology and oral radiology, 2012. **114**(1): p. 127-135.

8. Bryant, J.A., N.A. Drage, and S. Richmond, *Study of the scan uniformity from an i-CAT cone beam computed tomography dental imaging system.* Dentomaxillofac Radiol, 2008. **37**(7): p. 365-74.

9. Al-Okshi, A., et al., *Effective dose of cone beam CT (CBCT) of the facial skeleton: a systematic review.* Br J Radiol, 2015. **88**(1045): p. 20140658.

10. Palomo, J.M., P.S. Rao, and M.G. Hans, *Influence of CBCT exposure conditions on radiation dose.* Oral Surg Oral Med Oral Pathol Oral Radiol Endod, 2008. **105**(6): p. 773-82.

11. Lofthag-Hansen, S., *Cone beam computed tomography radiation dose and image quality assessments.* Swed Dent J Suppl, 2010(209): p. 4-55.

12. *Recommendations for quality assurance in dental radiography.* Oral Surg Oral Med Oral Pathol, 1983. **55**(4): p. 421-26.

13. Bamba, J., et al., *Image quality assessment of three cone beam CT machines using the SEDENTEXCT CT phantom.* Dento maxillo facial radiology, 2013. **42**(8): p. 20120445.

14. Xu, J., et al., *Technical assessment of a cone-beam CT scanner for otolaryngology imaging: image quality, dose, and technique protocols.* Medical physics, 2012. **39**(8): p. 4932-4942.

15. *SIDENTEXCT Report Evidence Based Guidelines CBCT.* 2012: p. 1-156.

16. Miracle, A.C. and S.K. Mukherji, *Conebeam CT of the head and neck, part 1: physical principles.* AJNR Am J Neuroradiol, 2009. **30**(6): p. 1088-95.

17. Wang, A.S., et al., *Low-dose preview for patient-specific, task-specific technique selection in cone-beam CT.* Med Phys, 2014. **41**(7): p. 071915.

18. Elstrom, U.V., et al., *Evaluation of image quality for different kV cone-beam CT acquisition and reconstruction methods in the head and neck region.* Acta Oncol, 2011. **50**(6): p. 908-17.

19. Carlton, R.A., Adler, *Principles of Radiographic imaging: An Art and A Science.* 2012. **5th Edition**: p. 864.

20. Keenan, J.R. and A.V. Keenan, *Accuracy of dental radiographs for caries detection.* Evid Based Dent, 2016. **17**(2): p. 43.

21. Bader, J.D., D.A. Shugars, and A.J. Bonito, *Systematic reviews of selected dental caries diagnostic and management methods.* J Dent Educ, 2001. **65**(10): p. 960-8.

22. Muramtsu, C., et al., *Quantitative evaluation of alveolar bone resorption on dental panoramic radiographs by standardized dentition image transformation and probability estimation.* Conf Proc IEEE Eng Med Biol Soc, 2016. **2016**: p. 1038-1041.

23. Grimard, B.A., et al., *Comparison of clinical, periapical radiograph, and cone-beam volume tomography measurement techniques for assessing bone level changes following regenerative periodontal therapy.* J Periodontol, 2009. **80**(1): p. 48-55.

24. Frederiksen, N.L. and P.W. Goaz, *Parameters affecting radiographic contrast.* Dentomaxillofac Radiol, 1990. **19**(4): p. 173-7.

25. Solomon, J., et al., *Effect of Radiation Dose Reduction and Reconstruction Algorithm on Image Noise, Contrast, Resolution, and Detectability of Subtle Hypoattenuating Liver Lesions at Multidetector CT: Filtered Back Projection versus a Commercial Model-based Iterative Reconstruction Algorithm.* Radiology, 2017: p. 161736.

26. Kwong, J.C., et al., *Image quality produced by different cone-beam computed tomography settings.* Am J Orthod Dentofacial Orthop, 2008. **133**(2): p. 317-27.

27. Siewerdsen, J.H. and D.A. Jaffray, *Cone-beam computed tomography with a flat-panel imager: magnitude and effects of x-ray scatter.* Med Phys, 2001. **28**(2): p. 220-31.

28. Torgersen, G.R., et al., *A phantom for simplified image quality control of dental cone beam computed tomography units.* Oral Surg Oral Med Oral Pathol Oral Radiol, 2014. **118**(5): p. 603-11.

29. Scarfe, W.C., et al., *Maxillofacial cone beam computed tomography: essence, elements and steps to interpretation.* Aust Dent J, 2012. **57 Suppl 1**: p. 46-60.

30. Schulze, R., et al., *Artefacts in CBCT: a review.* Dentomaxillofac Radiol, 2011. **40**(5): p. 265-73.

31. Scarfe, W.C., A.G. Farman, and P. Sukovic, *Clinical applications of cone-beam computed tomography in dental practice.* J Can Dent Assoc, 2006. **72**(1): p. 75-80.

32. Swennen, G.R. and F. Schutyser, *Three-dimensional cephalometry: spiral multi-slice vs cone-beam computed tomography.* Am J Orthod Dentofacial Orthop, 2006. **130**(3): p. 410-6.

33. Scarfe, W.C. and A.G. Farman, *What is cone-beam CT and how does it work?* Dent Clin North Am, 2008. **52**(4): p. 707-30, v.

34. Hatcher, D.C. and C.L. Aboudara, *Diagnosis goes digital.* Am J Orthod Dentofacial Orthop, 2004. **125**(4): p. 512-5.

35. Molen, A.D., *Considerations in the use of cone-beam computed tomography for buccal bone measurements.* Am J Orthod Dentofacial Orthop, 2010. **137**(4 Suppl): p. S130-5.

36. Nikneshan, S., et al., *Accuracy of linear measurement using cone-beam computed tomography at different reconstruction angles.* Imaging Sci Dent, 2014. **44**(4): p. 257-62.

37. Vasconcelos, T.V., et al., *Evaluation of artifacts generated by zirconium implants in cone-beam computed tomography images.* Oral Surg Oral Med Oral Pathol Oral Radiol, 2017. **123**(2): p. 265-272.

38. Ludlow, J.B., et al., *Effective dose of dental CBCT-a meta analysis of published data and additional data for nine CBCT units.* Dentomaxillofac Radiol, 2015. **44**(1): p. 20140197.

39. Fujita, H., et al., *A simple method for determining the modulation transfer function in digital radiography.* IEEE Trans Med Imaging, 1992. **11**(1): p. 34-9.

40. Elkhateeb, S.M., G.R. Torgersen, and E.A. Arnout, *Image quality assessment of clinically-applied CBCT protocols using a QAT phantom.* Dentomaxillofac Radiol, 2016. **45**(5): p. 20160075.

41. Pauwels, R., et al., *A pragmatic approach to determine the optimal kVp in cone beam CT: balancing contrast-to-noise ratio and radiation dose.* Dentomaxillofac Radiol, 2014. **43**(5): p. 20140059.

42. Ballrick, J.W., et al., *Image distortion and spatial resolution of a commercially available cone-beam computed tomography machine.* Am J Orthod Dentofacial Orthop, 2008. **134**(4): p. 573-82.

43. Maloul, A., J. Fialkov, and C. Whyne, *The impact of voxel size-based inaccuracies on the mechanical behavior of thin bone structures.* Ann Biomed Eng, 2011. **39**(3): p. 1092-100.

44. Abouei, E., S. Lee, and N.L. Ford, *Quantitative performance characterization of image quality and radiation dose for a CS 9300 dental cone beam computed tomography machine.* J Med Imaging (Bellingham), 2015. **2**(4): p. 044002.

45. Bauman, R., et al., *Ex vivo detection of mesiobuccal canals in maxillary molars using CBCT at four different isotropic voxel dimensions.* Int Endod J, 2011. **44**(8): p. 752-8.

46. Endo, M., et al., *Effect of scattered radiation on image noise in cone beam CT.* Med Phys, 2001. **28**(4): p. 469-74.

47. Chen, Y., et al., *Characterization of scatter in cone-beam CT breast imaging: comparison of experimental measurements and Monte Carlo simulation.* Med Phys, 2009. **36**(3): p. 857-69.

48. de Oliveira, M.V., et al., *Quality assurance phantoms for cone beam computed tomography: a systematic literature review.* Dentomaxillofac Radiol, 2017: p. 20160329.

49. Seeram, E., *Digital image processing.* Radiol Technol, 2004. **75**(6): p. 435-52; quiz 453-5.

50. Curry TS, D., JE, Murry RC, *Christensen's physics of diagnostic radiology*. 4th ed. 1990, Philadelphia: Lippincott, Williams and Wilkins.

51. Kamburoglu, K. and S. Kursun, *A comparison of the diagnostic accuracy of CBCT images of different voxel resolutions used to detect simulated small internal resorption cavities.* Int Endod J, 2010. **43**(9): p. 798-807.

52. Holberg, C., et al., *Cone-beam computed tomography in orthodontics: benefits and limitations.* J Orofac Orthop, 2005. **66**(6): p. 434-44.

53. Sawchuk, D., et al., *Comparison of two three-dimensional cephalometric analysis computer software.* J Orthod Sci, 2014. **3**(4): p. 111-7.

54. Sohaib, S.A., et al., *The effect of decreasing mAs on image quality and patient dose in sinus CT.* Br J Radiol, 2001. **74**(878): p. 157-61.

55. Al-Okshi, A., C. Theodorakou, and C. Lindh, *Dose optimization for assessment of periodontal structures in cone beam CT examinations.* Dentomaxillofac Radiol, 2017: p. 20160311.

56. Chakeres, D.W., *Clinical significance of partial volume averaging of the temporal bone.* AJNR Am J Neuroradiol, 1984. **5**(3): p. 297-302.

57. Da Silveira, P.F., et al., *CBCT-based volume of simulated root resorption - influence of FOV and voxel size.* Int Endod J, 2015. **48**(10): p. 959-65.

58. Melo, S.L., et al., *Diagnostic ability of a cone-beam computed tomography scan to assess longitudinal root fractures in prosthetically treated teeth.* J Endod, 2010. **36**(11): p. 1879-82.

59. Wenzel, A., et al., *Variable-resolution cone-beam computerized tomography with enhancement filtration compared with intraoral photostimulable phosphor radiography in detection of transverse root fractures in an in vitro model.* Oral Surg Oral Med Oral Pathol Oral Radiol Endod, 2009. **108**(6): p. 939-45.

60. Watanabe, H., et al., *A comparative study for spatial resolution and subjective image characteristics of a multi-slice CT and a cone-beam CT for dental use.* Eur J Radiol, 2011. **77**(3): p. 397-402.

61. Lofthag-Hansen, S., A. Thilander-Klang, and K. Grondahl, *Evaluation of subjective image quality in relation to diagnostic task for cone beam computed tomography with different fields of view.* Eur J Radiol, 2011. **80**(2): p. 483-8.

62. Jaffray, D.A. and J.H. Siewerdsen, *Cone-beam computed tomography with a flat-panel imager: initial performance characterization.* Med Phys, 2000. **27**(6): p. 1311-23.

63. Maret, D., et al., *Effect of voxel size on the accuracy of 3D reconstructions with cone beam CT.* Dentomaxillofac Radiol, 2012. **41**(8): p. 649-55.